Comparative analysis of the mitochondrial proteome in a mouse model of Rett syndrome

Dissertation

for the award of the degree

"Doctor rerum naturalium"

(Dr.rer.nat.) of the Georg-August-Universität Göttingen

Within the doctoral program - Molecular Medicine of the Georg-August University School of Science (GAUSS)

Submitted by

Gocha Golubiani

from

Georgia, Tbilisi

Göttingen, 2023

Thesis Committee

Prof. Dr. Michael Müller
University Medical Center Göttingen
Department of Neurophysiology and Sensory Physiology

Prof. Dr. Peter Rehling
University Medical Center Göttingen
Department of Cellular Biochemistry

Prof. Dr. Revaz Solomonia
Ilia State University School of natural sciences and medicine
Institute of Chemical Biology

Members of the Examination Board

Prof. Dr. Thomas Bayer (Reviewer)
University Medical Center Göttingen
Division of Molecular Psychiatry

Prof. Dr. Elene Zhuravliova (Reviewer)
Ilia State University School of natural sciences and medicine
Institute of Chemical Biology

Prof. Dr. David Mikeladze (Second Reviewer)
Ilia State University School of natural sciences and medicine
Institute of Chemical Biology

Prof. Dr. Lali Shanshiashvili (Additional Reviewer)
Ilia State University School of natural sciences and medicine
Institute of Neurochemistry

Date of the oral examination: 31.03.2023

Declaration:

I hereby declare that my doctoral thesis entitled:

"Comparative analysis of the mitochondrial proteome in a mouse model of Rett syndrome" is the result of my personal effort and was prepared with no other sources than quoted.

Tbilisi 29.01.2023

Gocha Golubiani

Table of Contents

List of abbreviations

5-HT7R	5-hydroxytryptamine receptor 7
aCSF	Artificial cerebrospinal fluid
ADP	Adenosine diphosphate
AMP	Adenosine monophosphate
AMPK	Adenosine monophosphate-dependent protein kinase
ASB-14	Amidosulfobetaine-14
AT-hook	Adenosine and thymine hook
ATP	Adenosine triphosphate
BAA	Branched amino acids
BSA	Bovine serum albumin
CA1	Hippocampus pyramidal cells
CAMKIIa	Ca^{2+}/calmodulin-dependent protein kinase II
cAMP	Cyclic Adenosine monophosphate
CHAPS	3-[(3-cholamidopropyl)dimethylammonio]-1-propanesulfonate
C-MRC	Mitochondrial respiratory chain c
CNS	Central nervous system
COX7A	Cytochrome c oxidase subunit 7A
COX7A1	Cytochrome c oxidase subunit 7A1
COX7A2	Cytochrome C oxidase Subunit 7A2
CpG	Cytosine and guanine separated by a phosphate
CSA	Citrates synthase activity
CSF	Cerebrospinal fluid
DMSO	Dimethyl sulfoxide
DNA	Deoxyribonucleic Acid
DRP1	Dynamin-related protein 1
DTT	Dithiothreitol
EDTA	Ethylenediaminetetraacetic acid
EGTA	Egtazic acid
ETC	Electron transport chain

FAD	Flavin adenine dinucleotide
FADH$_2$	Reduced flavin adenine dinucleotide
FDG	18-Ffluorodeoxyglucose
FDR	False discovery rate
FMN	Flavin mononucleotide
F$_O$F1-ATPase	FoF1-ATPase/synthase
GABA	γ-Aminobutyric acid
GAPDH	Glyceraldehyde 3-phosphate dehydrogenase
GCaMP6f	Genetically-encoded calcium indicator
GC-MS	Gas chromatography–mass spectrometry
H$_2$DCFDA	Dichlorofluorescin diacetate
HEPES	(4-(2-hydroxyethyl)-1-piperazineethanesulfonic acid)
HIF	Hypoxia inducible factor
HPLC	High performance liquid chromatography
HSP60	60-kDa heat shock protein and related protein
ID	Intervening domain
IO	Isolation buffer
IS	Internal standard
KCC2	Potassium chloride cotransporter 2
KEGG	Kyoto encyclopedia of genes and genomes
FLEET	Liquid chromatography
LP-211	Receptor agonist drug
MAS	Mitochondrial assay buffe
MBD	Methylated DNA (methyl CpG) binding protein
MBD	Methyl-CpG binding domain
MeCP2	Methyl-CpG binding protein 2
MS	Mass spectrometer
MTCO1	Mitochondrially encoded cytochrome c oxidase I
MTF	Mitofusin
NADH	Nicotinamide adenine dinucleotide

NADPH	Nicotinamide adenine dinucleotide phosphate
NCoR	Nuclear receptor corepressor
NDUFB8	NADH:ubiquinone oxidoreductase subunit B8
NDUFS1	NADH:ubiquinone oxidoreductase core subunit S1
NDUFS8	NADH:ubiquinone oxidoreductase core subunit S8
NDUFV2	NADH:ubiquinone oxidoreductase core subunit V2
NDUSF4	NADH:ubiquinone oxidoreductase subunit S4
NID	NCoR/SMRT interaction domain
NLS	Nuclear localization signal
NTD	N-terminal domain
OXPHOS	Oxidative phosphorylation
PBS	Phosphate buffered saline
PCA	Principal component analysis
PCR	Polymerase chain reaction
PET	Positron emission tomography
PINK1	PTEN Induced Kinase 1
PMSF	Phenylmethylsulfonyl fluoride
PTEN	Phosphatase and tensin homolog gene
RNA	Ribonucleic acid
ROAST	Rotation gene set tests for complex microarray experiments
roGFP1	Reduction/oxidation sensitive green fluorescent protein
ROS	Reactive oxygen species
RP-UPLC	Rapid and sensitive reversed phase ultra-performance liquid chromatography
RTT	Rett syndrome
SCAFI	Supercomplex assembly factor I,
SDHB	Succinate dehydrogenase complex iron sulfur subunit B
SDS	Sodium dodecyl sulfate
SEM	Standard error of the mean
SLC14A1	Solute carrier family 14 member 1 urea transporter 1
SLC14A1	Solute carrier family 14 member 1

SLC2A4	Solute carrier family 2 member 4
S-MRC	Mitochondrial respiratory chain s
SMRT	Silencing mediator for retinoid and thyroid hormone receptor
SMRT	Silencing mediator of retinoic acid and thyroid hormone receptor
TCA	Tricarboxylic acid
TOF	Time of flight
TRD	Transcription repression domain
tRK1	Lysine transfer RNA acceptor 1
tRK2	Lysine transfer RNA acceptor 2
tRNA	Transfer Ribonucleic acid
UPLC	Ultra-performance liquid chromatography
UQCRC1	Ubiquinol-cytochrome c reductase core protein 1
UQCRC1	Ubiquinol-cytochrome c reductase core protein 1
UQCRC2	Ubiquinol-cytochrome c reductase core protein 2
UQCRC2	Ubiquinol-cytochrome C reductase core protein 2
VDAC3	Voltage dependent anion channel 3
WB	Western blot
WT	Wild type

List of figures

List of tables

Summary

Rett syndrome is a neural development disorder. The gene, for culprit protein, MeCP2 (methylated CpG binding protein) is located on chromosome X and the majority of patients are young girls. Rett syndrome patients do not suffer from neurodegenerative processes, instead, due to the neurons´ abnormal small size and denser packaging, the brain´s general volume is reduced and synapses as well as dendrite structure are weakened.

Rett syndrome patient's postnatal development appears normal during the first 6 to 16 month of life. After that, phenotype signs such as mental problems and lack of communication are observed, which are followed by a number of additional severe symptoms: irregular sleep and breathing, labored motor movements, frequent epileptic seizures, body weight loss, scoliosis, and stereotypic hand movements.

Post mortem tissue analyses of Rett syndrome patients show that mitochondrial ultra-structure is damaged and organelle functions are hindered. Cells suffer from higher concentrations of free radicals, oxidative stress, lack of ATP, and increased susceptibility to hypoxia. Mitochondrial changes were first discovered in muscle tissue. Damaged mitochondria contain vacuoles, small granular inclusions, distorted inner membranes, are leaky to protons, and general mitochondrial mass is increased. Mitochondrial impairments obviously lead to insufficient respiratory chain protein activity, cellular ATP deficits, and increased oxidative stress on the systemic level. Frequent apneas in Rett syndrome patients give rise to transient drops in blood oxygen levels, and cells with malfunctioning mitochondria were proposed to suffer from an oxidative burden.

Main goals of this thesis were (i) broad-range comparative proteomic analyses of mitochondria obtained from the brains of wild type and *Mecp2* gene knockout mice, specifically focusing on neocortex and hippocampus and (ii) untargeted metabolomic studies of the neocortex on the same group of animals. So far such a research approach was not carried out on the brains of *Mecp2* knockout Rett syndrome mouse models.

For the experiments, flash frozen brain tissues of 50 days old *Mecp2*-deficent and wild type variant male mice were used. The broad range proteomic study involved analyzing samples with two-dimensional electrophoresis and identifying peptide contents of differently expressed spots by mass spectrometry. The observed differences for some proteins were further confirmed by western blotting and specific antibodies. Findings show an upregulation of cytochrome b-c1 complex subunit 1 and prohibitin-1, as well as a downregulation of gamma-enolase and cAMP-dependent protein

kinase catalytic subunit alpha in both, *Mecp2$^{-/y}$* neocortex and hippocampus. The other series of mitochondrial proteome experiments involved an *ad hoc* approach and were aiming at mitochondrial fission and fusion regulatory proteins and mitochondrial oxidative phosphorylation chain components. Here it became apparent that mitochondrial dynamics regulation proteins were decreased in RTT mice, specifically mitofusin 1 was found at lower levels in cortical tissue and DRP-1 was expressed less in hippocampus.

For the rating of physiological aspects of Rett syndrome and wild type mice, general phenotypic parameters – such as body weight, size and blood parameters – were assessed. Also, brain mitochondria purification was performed on freshly extirpated brain tissues and biochemical assays were conducted on live and still functioning mitochondria to measure their reactive oxygen species accumulation by recording the emitted fluorescence signal of an oxidation sensitive dye in a spectrometer-based cuvette assay.

Untargeted metabolomic analysis required higher amounts of tissue material and was therefore limited to the cortices of *Mecp2*-deficent and wild type male mice. Flash frozen cortices were sent to a service provider, who performed the analyses and provided a large amount of valuable raw data for further in-depths bioinformatics analyses. Metabolomic data reveals 101 significantly altered metabolites in the MeCP2-deficient neocortex of adult male mice; 68 of them were increased whilst 33 were decreased compared to wild types. These differences cover more than 31 metabolic pathways, including pivotal aspects of cellular metabolism, such as pyruvate metabolism, glycolysis, citrate cycle and oxidative phosphorylation.

Data collected from different experiments show various molecular and metabolic abnormalities in the brains of Rett syndrome mice. The mitochondrial proteome of RTT mice clearly differs from wild type mice and this difference is also brain-region specific. Mitochondrial fusion/fission dynamics as well as their physiological performance seem negatively affected. *Mecp2*-knockout mice are suffering from increased oxidative stress, which in part might be due to poor mitochondrial function, and these alterations might have additional tolling influence on the already impaired conditions of metabolic and mitochondrial activities as well as key features of cellular metabolism.

All these results shed further light onto the mitochondrial and the metabolic alterations that appear as part of the pathogenesis of Rett syndrome in MeCP2 deficient brain tissue. Accordingly, these aspects should be taken into account when therapeutic approaches in RTT are developed and/or when further treatment concepts are formulated.

1. Introduction

1.1 History of Rett syndrome discovery

In 1966, the Austrian pediatric neurologist, Andreas Rett made first scientific entry for the Rett syndrome (further mentioned as RTT) by describing and documenting identical behavioral and mental disorder in a group of young female patients at his clinic (Rett, 1966). As the study was published only in German language, it addressed a limited auditorium, and his first work did not gain wide popularity among the international scientific communities. Andreas Rett misleadingly thought that the disorder was caused by hyper-ammonemia, which later proved to be wrong. After Andreas Rett published his second work in English language in 1977, the topic was picked up by a wider circle of researchers from different European countries such as France, Portugal and Sweden, and promoted relatively intensive studies soon enough. Because of established awareness, the number of clinically reported cases started to grow, granting further worldwide attention towards RTT, scientist of respecting fields acknowledged the existence of newly emerged neurological disorder, and an increased interest resulted in the flux of funds for further studies (Clarke, 1996). As public and scientific awareness grew, the various international Rett syndrome associations were established, which helped both, affected families and scientist to share the common experiences. Since that day numerous clinical studies and observations enriched the study field with more details, consecutively leading to creation of databases and further narrowing down potential biological causes of RTT, refining means of therapeutic control and expanding possible research directions (Leonard et al., 2017). Long before it was proven by systematic gene screening approach, it had been predicted that RTT could be linked to the X chromosome, since it was prominent almost exclusively in females, while male patients were born much rarely or died soon after the birth (Clarke, 1996).

One of the pivotal breakthroughs in researching the biological mechanisms of RTT was to identify the *MECP2* (Methyl-CpG Binding Protein 2) gene on chromosome X, which is the major culprit for developing the disorder (Amir et al., 1999). But even today, heaving that much information about RTT, unfortunately there is still no clinical treatment available for patients other than managing symptoms and ameliorating several of the disorder-related issues (Leonard et al., 2017).

1.2 RTT and clinical traits

RTT is a progressive neurodevelopmental disorder. The typical pathology does not activate necrotic pathways in the neurons; instead it disrupts normal growth of central neural systems and causes to form pathologically compacted and condensed brains. This severely affects neural activities, signal transduction and brain function. RTT is caused by spontaneous/sporadic mutations in the *MECP2* gene which is situated in X chromosome. These *MECP2* mutations have most devastating effects on the brain, especially at early postnatal development stages. Other tissues such as muscles are generally suffering from various metabolic problems (Gold et al., 2018).

About 95% of RTT cases are caused by spontaneous de novo mutations in the early stage of embryogenesis or in parental gametes (Bienvenu et al., 2000). Despite the fact, that the main reason is a genetic mutation, RTT is not an inherited disease, as the parents do not necessary have to be a carrier of the mutated gene, not to mention, that affected persons are less capable of reproduction. RTT is the second most commonly diagnosed disorder after Down syndrome. Every 1:10000 to 15000 live female births are reported to be affected by RTT (Leonard et al., 1997),which makes it a fairly common disorder in the female population (Ellaway and Christodoulou, 2001). After birth, female individuals with RTT appear to grow and develop normally for about 6 to 18 month, and usually the family does not suspect any adverse signs (Hagberg, 2002). After that time, first mild signs start to manifest, which then get progressively severe, ranging from mental retardation, communication problems, stereotypical hand movements, ataxia, severe physiological, physical, neurological signs, epilepsy and sleep pattern disturbances with breath apneas, which eventually culminates in patient´s death caused by different organs failure. Also sudden unexpected death may occur due to cardio-respiratory irregularities. Life expectance for female patients varies, but may span up to 70 years (Gold et al., 2018). Because the nature of RTT, the disease progression over time, can be separated in four stages: First, the early stagnation - from six to eighteen months - is characterized by a delayed general development of the child. Reduced eye contact, a weakened skeletal muscle performance and decreased head circumference growth are being observed. Second, the rapid regression stage from one to four years further worsens the degradation of learned motoric and communication skills. Microcephaly is more tolling. Stereotypic repetitive hands movement - such as meaningless wriggling and clapping - are established, frequent breath apneas start to develop and seizures might be present as well. Third, the pseudostationary stage,

(also known as plateau period) from two to ten years is characterized by prominent ataxia. Despite previous autism-like behaviors and less communication, the child might start to exhibit an increased desire to interact with the surrounding environment and people by means of eye-pointing. Seizures become more common. Fourth, the late motor deterioration stage brings patients to total and severe physical disability. Involuntary muscle movements are stronger, keeping body posture is challenged and may require wheelchair assistance. In addition to regular seizures and breathing problems, sleep becomes irregular and the digestion system might get affected as well (Motil et al., 2012). This condition usually last decades until eventual death of the patient is caused by respiratory infection, cardiac arrest, kidney- and respiratory failure (Anderson et al., 2014). However, not every female patient experiences severe stages. Speed and degree at which the disorder is presenting in each individual, very much depends on the actual mutation of *MECP2* gene (which will be discussed later) and probability of effected X chromosome activated in cell (Zhang et al., 2017). The expressed clinical characteristics may vary so much from classic clinical observation, that even though heaving broad and detailed lists of clinical characteristics of RTT, a genetic diagnosis is favored over an empirical one.

Unfortunately, up to this day, there is no direct and specific cure available for RTT patients. Therefore, multidisciplinary medical symptomatic care and management are highly practiced and encouraged. If special care is intensively applied shortly after diagnosis, some aspects of the general motor-, mental- and metabolic impairments can be managed to some degree, but they can never be fully cured or ameliorated (Warren et al., 2011). Most common drug treatments involve antiepileptic medicines for seizure control, selective serotonin reuptake inhibitors for anxiety management, strict nutritional management for gastrointestinal complication preventive measures, as well as maintaining vitamin D level (Kaufmann et al., 2016).

1.3 *MECP2* gene and MeCP2 protein

The *MECP2* gene, together with the encoded protein (MeCP2) was discovered during an experimental series searching for proteins that were capable of binding to methylated DNA. The *MECP2* gene consists of approximately 76 kilo nucleotide base (Quaderi et al., 1994). In humans, the *MeCP2* gene is located on the X chromosome (Xq28 site), whereas in mice it is encoded by the *Mecp2* gene located on the X A7.3 site (Liyanage and Rastegar, 2014). Several years later, after its

first discovery, the *MECP2* gene could be linked to RTT (Amir et al., 1999). The *MECP2* gene is expressed ubiquitously in every human tissue, but most redundant numbers have been found in central nervous system (CNS) neurons (Lewis et al., 1992) and glia (Ballas et al., 2009). Hence, in humans and rodents, *Mecp2* gene expression is closely regulated based on brain developmental stages. Expression is increased during active CNS growth and the synapse formation period; after maturation it stabilizes to certain maintained levels (Kishi and Macklis, 2004). In humans, *MECP2* expression starts to gradually increase after birth and it then reaches its peak maximum at an age of 10 years (Shahbazian et al., 2002). The MeCP2 protein is a nuclear protein, belongs to the methylated DNA (methyl CpG) binding protein (MBD) family, and it is considered to play a role in epigenetic gene expression regulation. MeCP2 is primarily known as global gene expression regulator, mostly transcription repressor, but it also has been noticed in transcription activation (Chahrour et al., 2008), messenger RNA splicing and chromatin remodeling (Lyst and Bird, 2015). Another member of the MBD proteins, MeCP1, which was discovered before MeCP2 in 1989 by same the group, requires at least 10 CpG sites to affectively bind to methylated DNA (Meehan et al., 1989). MeCP2 has the capability to recognize and bind to single 5` to 3` methylated CpG sites without any help of close proximate DNA sequences. This ability is the backbone of its expression regulatory mechanism (Lewis et al., 1992). Methylation of DNA plays a crucial role in gene expression. It is achieved by attracting special regulatory proteins to DNA methylation sites. By means of intricate interactions within recruited proteins, inhibition or transcription initiation levels are adjusted on demand (Moore et al., 2013). Later it was shown that MeCP2 also can bind to 5-hydroxy-methyl cytosine (5-hmC) and the affinities of binding to both types of methylated cytosines are the same (Mellén et al., 2012). During these experiments, MeCP2 protein was purified from rat brain due to its high levels and less susceptibility to proteolysis (Lewis et al., 1992). The rodent and human *MeCP2* gene share close structural and functional similarity, both include four exons and three introns (Kriaucionis and Bird, 2004). Non mammalian and plant organisms do not share this gene structure, as they have lower methylated genome contents and rely less on MBD proteins to regulate their gene expression. Although, they still have motifs of methylated DNA binding protein segments (Hendrich and Tweedie, 2003). The MeCP2 messenger RNA is subject of alternative translation start sites and splicing, which results in two isoforms of the MeCP2 protein: MeCP2_e1 and MeCP2_e2. In addition to this, mRNA alternative polyadenylation has also been described (Rodrigues et al., 2020). Exon one, three and four form protein E1, it consists of a total of 498 amino

acids, of which a 21 amino-acid spanning segment is unique for the E1 isoform. Exon two, three and four form E2, it consists of a total of 486 amino acids and has only a 9 amino acid containing unique sequence. Structurally, the E1 and E2 isoforms of MeCP2 differ only at their N-terminal domain (NTD) and the rest of the amino acid sequence is unchanged for both isoforms (Kriaucionis and Bird, 2004). Interestingly, exon four in human and rodents contains up to 8.5 kilo base of 3` untranslated region, which is the longest known tail in the human genome. This section contains four sites for polyadenylation and it helps to further fine-tune expressing transcripts (Pelka et al., 2005). Despite this difference, the two isoforms still share same functional responsibilities, but they differ by tissues where they are expressed. The E1 isoform is generally more abundant in the central neural system, while the E2 isoform has a more versatile expression pattern throughout the body (Kerr et al., 2012;Olson et al., 2014). The MeCP2 protein has two major domains with distinct amino acid composition and function: The methylated-DNA binding domain (MBD) towards the N terminal, and the transcription repression domain (TRD) at the opposite C terminal. In addition to those, MeCP2 also possesses three secondary domains: an intervening domain (ID) flanking the MBD, an AT hook, and the NCoR/SMRT interaction domain (NID) within the TRD (Baker et al., 2013)]. The MBD domain is designed to recognize and bind to methylated cytosine in a single CpG site (Lewis et al., 1992)]. TRD and NID domain recruit certain nuclear repression proteins such as NCoR1 (nuclear co-repressor 1) and SMRT – (silencing mediator of retinoic acid and thyroid hormone receptor). These proteins are part of the transcription repression proteins which can promote histone deacetylation and modify gene expression by rendering chromatin in a way that it is no longer accessible for transcription factors (Cui et al., 2011). TRD also houses AT hook and nuclear localization signal (NLS) segments, of which the AT hook enables MeCP2 to directly bind to double stranded DNA without any need of methylation or specific sequences (Baker et al., 2013). Proteins containing an NLS are designated to be transported inside nucleus. Although, MeCP2 mostly remains inside nucleus even without proper NLS as it already has an innate high affinity to DNA due to the AT hook and MBD domain (Lyst et al., 2018). The ID domain resides next to the MBD and facilitates its structural integrity and CpG binding potential (Claveria-Gimeno et al., 2017).

Despite having multiple functional domains, MeCP2 still remains a rather poorly structured protein. Approximately only 41% of protein show a secondary structure and the remaining 59% are under structured. This design allows MeCP2 to undergo multiple posttranslational modifications and to

interact with different proteins, which further complicates the already intricate regulatory mechanisms (Adams et al., 2007;Ghosh et al., 2010).

1.4 *MECP2* gene mutations

As mentioned before, RTT is caused by spontaneous de novo mutations in the *MECP2* gene and as for today, more than 550 mutations have been described (Neul et al., 2008). Huge part of them are cytosine to thymine transitions (Lee et al., 2001) and mutations can be classified as missense, nonsense or frame shift related (Amir et al., 1999). Surprisingly, from all of these mutations, only eight mutations are the major cause of 95 percent of reported RTT cases (Bienvenu et al., 2000). Four missense mutations (Arginine255X, Arginine270X, Arginine306Cysteine, and R294X) occur in the NID region, which includes the transcription repression domain (TRD) and four nonsense mutations affect the MBD (Arginine106Tryptophan, Arginine133Cysteine, Threonine158Methionine and Arginine168X) (Pejhan and Rastegar, 2021). Other minor part is deletion-related mutations and they affect the C terminal region. These mutations do not cause as severe clinical phenotype as the major eight mutations mentioned above (Neul et al., 2008). Mutations in the MBD and the NID interfere with proper protein functioning such as recognizing methylated CpG site and recruit transcription repression complexes, therefore disrupting one or both of the most important functions of MeCP2.

1.5 Animal models of RTT

The *Mecp2* gene shows fairly strong similarities among functional domains in vertebrate organisms (Kruusvee et al., 2017), and this greatly helped scientists in developing genetically modified animals to better understand the detailed functions of MeCP2. In particular, rodent models proved to be the most manageable, flexible and reliable source as research organisms for different approaches. Among rodents, rats and mice are major subjects, each with individual merits. Rats seem to perform better for physiological and preclinical trials but mice still remain organism of choice for many other researches, as they are relatively cheap to maintain and much needed genetic tools to generate desired genotypes are more accessible (Kyle et al., 2018). The Bird and the Jaenisch laboratories managed to engineer two most widely-used null allele genotypes for RTT researches: *ecp2*tm1.1Bird with erased exon 3 and 4, and *Mecp2*tm1.1Jae with erased exon 3(Guy et al., 2001;Baker et al., 2013). *Mecp2*tm1.1Jaeline is still capable to produce protein but with reduced size than normal but

this still leads to developing similar RTT signs as in full *Mecp2* knockout (Samaco et al., 2008). The fully knockout mouse line, *Mecp2* tm1.1Bird is unable to produce any functional MeCP2 protein, and was created by crossing the previously generated mouse line *Mecp2* tmlBird (exon 3 and 4 flanked with loxP) with mice carrying a germline deleting Cre driver (Guy et al., 2001;Liput, 2018). Despite the fact that RTT mostly affects females, the bulk of published mouse research employ male hemizygous *Mecp2* mutant mice because they exhibit a more consistent phenotype at a younger age. Despite the fact that female *Mecp2* mutant mice are more clinically comparable to human patients, random X activation in rodent females skews gene expression and results in a wide range of phenotype presentations, making it challenging to distinguish between phenotypes that arise through cell autonomous versus non-autonomous pathways (Katz et al., 2012). *Mecp2* tm1.1Bird and *Mecp2* tm1.1Jae, the two most often used male mouse models, typically exhibit overt abnormalities at four to six weeks of age and pass away between eight and twelve weeks of age (Chen et al., 2001;Guy et al., 2001). The *Mecp2* knockout mouse model [B6.129P2(C)-*Mecp2* tm1.1Bird] was used for this thesis. To ensure that the genetic circumstances were properly characterized and *Mecp2* was completely absent, all experiments and tissue analyses were conducted on the severe illness stage on postnatal day P50 and employed hemizygous male *Mecp2$^{-/y}$* mice (Guy et al., 2001).

1.6 Rett syndrome and synaptic plasticity

Several authors have studied neuronal activity in mouse models that underexpress MeCP2 (Zhang et al., 2008;Calfa et al., 2011;Janc and Müller, 2014;Lu et al., 2016;Kee et al., 2018). All of them suggested that learning and memory impairments result from disruptions in the excitation-to-inhibition balance. Reduced synaptic efficacy, less elaborated dendritic morphology and impaired long-term potentiation could be the basis of deficits in learning and memory of RTT mice (Chao et al., 2007;Guy et al., 2007;Belichenko et al., 2009;Na et al., 2013). To understand the source of disruptions in the excitation-to-inhibition balance, a recent study has applied large-scale in vivo calcium imaging in freely behaving animals and ex vivo slice recordings from identified cell types in the hippocampal CA1 subfield in RTT mice (He et al., 2022). Associative memory tasks were studied, and it was shown that during long-term memory retrieval, *MeCP2*-deficient CA1 cells poorly distinguish mnemonic context and form larger ensembles than wild-type mouse cells. Furthermore, simultaneous multiple whole-cell recordings revealed an involvement of somatostatin expressing interneurons in this defects. It was concluded that mutant somatostatin expressing interneurons

(*oriens-lacunosum moleculare* subset) cells are poorly recruited by CA1 pyramidal cells and are less active during long-term memory retrieval in vivo (He et al., 2022). The calcium indicator GCaMP6f was expressed under the CAMKIIa promoter in RTT and wild type mice, and it was revealed that reduced somatostatin expressing interneurons activity underlies poor long-term memory recall in RTT mice (He et al., 2022).

1.7 Mitochondrial abnormalities and Rett syndrome

For the very first time, the mitochondrial abnormalities in RTT patients were noticed by Eeg-Olofsson and colleagues, who have studied muscle biopsy samples by electron microscopy (Eeg-Olofsson et al., 1990). It was shown that mitochondria appeared abnormally swollen and were dumb-bell shaped. The next study of muscle mitochondria from 2 girls affected by RTT revealed a set of biochemical alterations and energy-metabolism related impairments (Dotti et al., 1993). Postmortem morphological studies of different brain regions of RTT patients also revealed obvious abnormalities of cerebral mitochondria. Thus electron microscopy studies of prefrontal neocortex neurons showed the presence of large, lucent-appearing mitochondria, whilst some mitochondria in other neurons contained electron-dense particles included within the mitochondrial matrix space (Cornford et al., 1994). In analogy to the changes observed in patients, the dendrites and axons of hippocampal neurons of a mouse RTT model were characterized with more elongated mitochondria as compared to wild type (WT) controls (Belichenko et al., 2009).

Based on these reports, whole series of follow-up studies were focused on molecular markers of mitochondrial abnormalities. In hippocampal slices of a RTT mouse model (*Mecp2$^{-/y}$*), an increased FAD/NADH baseline-ratio was detected in autofluorescence recordings on the tissue level, which indicates for increased mitochondrial/cellular oxidization (Großer et al., 2012). In the same series of experiments cytosolic redox balance was quantified with the genetically-encoded optical probe roGFP1. The obtained data once more confirmed that the hippocampus of *Mecp2$^{-/y}$* mice has higher oxidized baseline conditions, and a more vulnerable redox-balance than the hippocampus of WT mice (Großer et al., 2012).

In vivo magnetic resonance imaging and spectroscopy were applied for the study of *Mecp2*-null mice brains (Saywell et al., 2006). Morphometric study revealed a size reduction of the whole brain and in particular of those regions involved in cognitive and motor functions. These morphological

changes were paralleled also by significant metabolic anomalies. For example, decreased levels of N-acetylaspartate, myo-inositol, glutamine and glutamate, and increased levels of choline were confirmed (Saywell et al., 2006). Furthermore, in these experiments also a significant reduction of brain ATP levels was shown, once more indicating anomaly of energy metabolism that may reflect as well as contribute to the cerebral alterations and dysfunctions in RTT (Saywell et al., 2006).

A potential source of the oxidative stress and the redox imbalance, which obviously occur during the onset and progression RTT syndrome, could be an aberrant mitochondrial functionality. A dysfunctional complex II of the mitochondrial respiratory chain contributes to the marked increase in the levels of hydrogen peroxide production in the brains of female RTT mice (De Filippis et al., 2015b). When the complex II respiratory substrate- succinate, was applied as an energy source, decreased mitochondrial membrane potential generation and decreased mitochondrial ATP synthesis were detected in RTT mouse brains. This study also demonstrated a decreased phosphorylation of mitochondrial protein NDUFS4 in the cerebellum of RTT mice and suggested two possible underlying scenarios for this hypophosphorylation; either a deficit of cAMP phosphorylation system or a decreased protein level itself (De Filippis et al., 2015b).

The same group explored the possibility of beneficial effects brain serotonin receptor 7 (5-HT7R) stimulation under the conditions of the RTT pathology. As demonstrated, administration of the 5-HT7R selective agonist LP-211 substantially rescued the neurobehavioral phenotype of RTT mice (De Filippis et al., 2015b). Moreover the same type of treatment turned out to be protective by reverting the mitochondrial respiratory chain impairment and the oxidative phosphorylation deficiency. It is also important to note that LP-211 treatment decreased the radical species overproduction by brain mitochondria in the *Mecp2$^{-/y}$*-model (Valenti et al., 2017).

As mentioned above RTT is associated with an increased oxidative burden, and a higher fragility of the cellular redox equilibrium. These molecular changes could be involved in the worsening of certain symptoms and possibly also in disease progression in general. Accordingly any measures and treatments which are capable to counteract these processes could potentially mediate beneficial dampening effects on the time-course of disease progression. In line with this logic, the potency of the free radical scavenger and vitamin E derivative Trolox was studied in the hippocampal slices of male RTT mice (Janc and Müller, 2014). It was shown that in *Mecp2$^{-/y}$* hippocampal slices Trolox

treatment indeed reduced the neuronal hyperexcitability, enhanced the synaptic short-term plasticity, and fully restored the extent of synaptic long-term potentiation. However Trolox treatment did not have any effects on the severity of 4-aminopyridine induced seizure-like discharges (Janc and Müller, 2014).

Mitochondrial DNA (mtDNA) copy number has been considered as a potential biomarker of mitochondrial dysfunction in neurons and other tissues (Kilbaugh et al., 2015). In a recent study (Liu et al., 2022) mtDNA copy numbers were investigated in the peripheral blood of a large group of RTT patients (n = 142). MtDNA copy number was found to be significantly higher in the patients affected by RTT as compared with the control subjects. It is important to note that age, clinical severity, variant types, and hot-spot variants were not related to mtDNA copy number in RTT patients. Instead it was suggested by the authors that changes in mitochondrial function in RTT induce a compensatory increase in mtDNA copy number (Liu et al., 2022).

Gene expression differences occurring as part of the RTT pathology were studied in animal models and human patients. In this latter case peripheral tissues (blood cells, dermal fibroblasts) were usually investigated. One of the first studies of differential gene expression in the mouse model of RTT syndrome was carried out by differential display approach and it was conducted on whole mouse brains (Kriaucionis et al., 2006). This study revealed an overexpression of the nuclear gene for ubiquinol-cytochrome c reductase core protein 1 (Uqcrc1) (Kriaucionis et al., 2006). In the following study again a mouse model of RTT pathology was used and now cDNA microarray analysis was applied for the study of differential gene expression. In this case the hippocampal CA1 subfield was microdissected and microarray analysis revealed up to 10 differentially expressed genes, which did not include key players of mitochondrial respiration or scavenging enzymes (Großer et al., 2012). However, quantitative PCR confirmed a moderate upregulation [1.44 fold] of superoxide dismutase 1 mRNA in $Mecp2^{-/y}$ hippocampus, which can be considered as a potential compensatory response to the increased oxidative burden associated with RTT (Großer et al., 2012).

Changes in gene expression patterns associated with RTT syndrome were studied in the human peripheral lymphocytes, and isolated mRNA was used for microarray studies (Pecorelli et al., 2013). Obtained data indicated that RTT patients are characterized by an increased expression of quite a large number of genes involved in various aspects of mitochondrial organization, morphology, and

function (Pecorelli et al., 2013). Gene expression results were supported by whole cell proteomic studies of the dermal fibroblasts obtained from control subjects and RTT patients (Cicaloni et al., 2020). It was shown that main changes occur in the expression of proteins involved in the mitochondrial network (Cicaloni et al., 2020). In detail, the following mitochondrial proteins were confirmed to be upregulated in RTT patients: ATP synthase subunit g, mitochondrial cytochrome c oxidase subunit 6B1, NADH-cytochrome b5 reductase 3 and peroxiredoxin-5 (Cicaloni et al., 2020). These two series of studies involving gene expression on the one hand and whole cell proteome changes on the other hand, convincingly indicate that in RTT patients one of the most affected intracellular organelles in are the mitochondria. These datasets also prompt for further and more focused studies of the mitochondrial proteome, especially in brain mitochondria.

It should be mentioned that the mitochondrial proteome composition expresses very clear tissue specificity (Kappler et al., 2019). The brain regions are also different in view of mitochondrial content and mitochondrial activity; accordingly RTT pathology may affect them in a different way or at different severity (De Filippis et al., 2015b). An increase in mitochondrial mass could be anticipated as compensation for the impaired mitochondrial function in RTT. As a response, male wild type and *Mecp2$^{-/y}$* mice's various brain areas were subjected to spectrophotometric citrates synthase activity (CSA) assays. These investigations uncovered considerable spatial disparities. Cortical citrate synthase activity was consistently shown to be highest, while cerebellar citrate synthase activity was consistently lowest. The brainstem, midbrain, and hippocampal region all displayed intermediate levels. These brain regional differences can be expected to arise from the specific metabolic demands of the given tissues. *Mecp2$^{-/y}$* mice also displayed the corresponding order of activity. When Citrate synthase activity in WT and *Mecp2$^{-/y}$* mice were genotypically compared, only few noticeable changes were found. A considerably reduced citrate synthase activity was only found in *Mecp2$^{-/y}$* brainstems when compared to WT mice (van Agen & Müller, unpublished). This detected abnormality with the reduced mitochondrial content in the medulla might be interesting in relation to cardiorespiratory control, which is one of the characteristics of RTT (Weese-Mayer et al., 2006;Stettner et al., 2008). Relative protein expression levels of the mitochondrial marker VDAC3 (normalized to GAPDH) in the hippocampus and neocortex of adult male mice, are conceding with earlier observations that the *Mecp2$^{-/y}$* hippocampus and *Mecp2$^{-/y}$* neocortex reveal indifferent mitochondrial contents in comparison to WT mice (Can et al., 2018).

1.8 Metabolome and the Rett syndrome pathology

The metabolome can be defined as the ultimate product of gene, mRNA, and protein activities (Tosto and Reitz, 2016). In the previous chapters we have discussed a battery of cellular and molecular changes associated with RTT and obviously this neurodevelopmental pathology should include also very pronounced metabolome changes. Studies addressing these aspects were performed in the blood serum of humans and animals and in selected brain regions of mouse models of RTT. The experiments included approaches which were usually focused on certain metabolites, and only rarely whole metabolome studies have been applied.

In one of the first studies lactate, pyruvate, and citric acid cycle intermediates were measured in cerebrospinal fluid (CSF) obtained from RTT patients. The levels of lactate, pyruvate, alpha-ketoglutarate, and malate were significantly higher in RTT patients compared to the control subjects. In contrast, for citrate, cis-aconitate, succinate, fumarate, and oxaloacetate no differences were detected. Correlation analysis between the levels of these metabolites and clinical symptoms did not reveal any significant interaction (Matsuishi et al., 1994)

In another series of experiments lactate and pyruvate levels were measured in blood samples of 30 RTT patients, and repeated measurements were performed over time (Haas et al., 1995). On average, the lactate and pyruvate values determined were in the control range, however, individual patients presented reasonably elevations of both lactate and pyruvate contents with considerable fluctuation over time (Haas et al., 1995). The discrepancies between these two studies published (Matsuishi et al., 1994;Haas et al., 1995), most probably is due to the two difference sources of samples analyzed, i.e. CSF and blood. CSF-based measurements can be expected to more reliably reflect the conditions and changes occurring in the brain.

Positron emission tomography (PET) scanning of the brain supplied with 18-Ffluorodeoxyglucose (FDG) uptake was performed on 6 sedated female patients affected by RTT. The pattern of cerebral glucose uptake was clearly different from those described in Down syndrome, autism spectrum disorders or Alzheimer's disease and thus seemed unique for the conditions of RTT (Villemagne et al., 2002).

In *Mecp2⁻/ʸ* mice, blood analyses indicated a nearly 30% lower glucose level as compared to WT mice. Trolox treatment increased the blood glucose level in *Mecp2⁻/ʸ* mice up to the WT values (Janc et al., 2016b). All these data convincingly indicates for an altered carbohydrate metabolism in RTT. Altered sphingolipid metabolism is also the feature of the Rett syndrome. Over 900 metabolites in blood samples from 14 female subjects with RTT were measured in tandem mass spectrometry-based experiments (Cappuccio et al., 2019). The approach used by these authors was semi-quantitative, but alterations in lipids, mostly involved in sphingolipid metabolism, and sphinganine/sphingosine were convincingly demonstrated (Cappuccio et al., 2019). Cholesterol synthesis was found to be increased in the brain and body system of *Mecp2* null mice (Justice et al., 2013). Statin group drugs treatment, which decreases cholesterol levels improved the motor symptoms and increased the longevity in *Mecp2*-mutant mice (Justice et al., 2013).

High-resolution magnetic resonance spectroscopy was applied for the study of metabolome changes in the whole brains of *Mecp2* null mice (Viola et al., 2007). In detail, decreased levels of myo-inositol were detected in *Mecp2*-mutant mice as compared to WT. Also, reduced choline phospholipid turnover in *Mecp2*-null mice as compared to wild-type mice was reported (Viola et al., 2007). As one of the features of myo-inositol is osmoprotection, the authors suggested that perturbed osmoregulation may contribute to the pathology developing in mouse model of RTT (Viola et al., 2007).

Analysis of post-mortem brain tissue of female RTT patients have revealed significantly decreased number of cholinacetyltransferase-containing neurons in the basal forebrain as compared to age-matched healthy controls (Wenk and Hauss-Wegrzyniak, 1999). In the cerebrospinal fluid of RTT patients significantly higher levels of glutamate were detected (Lappalainen and Riikonen, 1996). Accordingly, various neurotransmitters such as acetylcholine and glutamate are markedly affected under the conditions of RTT.

One of the first, non-targeted wide-scale metabolomics studies of the plasma of RTT patients and corresponding controls was performed by Neul and colleagues (Neul et al., 2020). In total, plasma from 34 subjects affected by RTT were compared to 37 unaffected age- and gender-matched siblings. A total of significantly changed 36 metabolites were identified, that could be grouped broadly into amino acid metabolism, nitrogen handling, and exogenous substance pathways. As

expected, these changes observed point towards oxidative stress, mitochondrial dysfunction, and alterations in gut microflora (Neul et al., 2020).

More recently, it was indeed the gut bacterial microbiome and metabolome that was studied in RTT-affected females of various age and unaffected controls (Thapa et al., 2021). The composition of the gut microbiome did not differ between RTT patients and unaffected individuals. However, concentrations of protein end-products of the gut bacterial metabolome, which included GABA, tyrosine and glutamate were significantly lowered in the group of females affected by RTT (Thapa et al., 2021).

Without question, the different brain regions do have specificity according to metabolic processes and metabolome and most probably will be affected in a different manner during the course of RTT. According to this view we have performed an untargeted comparative metabolomics study by comparing the cortices of adult male wild type (WT) and male MeCP2-deficient mice (*Mecp2$^{-/y}$*). That was the second aim of the present thesis.

2. Research objectives

Because of several obvious mitochondrial complications in Rett syndrome human cases and animal models, major attention within this thesis was focused on the study of mitochondrial proteomics, in order to foster a better understanding of the molecular mechanism of mitochondrial impairment and energy flux disruptions in RTT. As the full mitochondrial proteome consists of more than 2000 proteins (Stauch et al., 2014), mitochondria cannot be considered completely autonomous organelles, and their proper functioning is codependent on general cell's wellbeing. Therefore, broader metabolomics and physiological parameters were also targeted in order to have a wider view on the complexity of this disorder on the cellular level. Since the negative effect of RTT is most prominently observed in brain, cortical and hippocampal brain tissues of *Mecp2$^{-/y}$* and WT mice were chosen to further narrow down organ- and tissue-specific processes.

3. Methods

3.1 Animal experiments – General aspects

Both the breeding of *Mecp2*-mutant mice as well as all mouse tissue analyzes for all described experiments below (metabolomics and proteomics) were carried out according to the European and German animal welfare guidelines and were authorized by the Office of Animal Welfare of the University Medical Center Göttingen and by the Lower Saxony State Office for Consumer Protection and Food Safety (file numbers G16/2177 and G17/2544).

3.2 Mouse model and brain tissue isolation

The experimental work of the present PhD thesis was performed on the *Mecp2* knockout mouse model [B6.129P2(C)-Mecp2$^{tm1.1Bird}$] (Guy et al., 2001). Hemizygous male (*Mecp2$^{-/y}$*) mice on postnatal day 50 (P50) were used in all of the described experiments. This period of postnatal development represents the severe disease stage. The control group of WT mice was matched by sex and age. The isolated cortices and hippocampi were processed individually. For all mice, phenotypic parameters were determined, blood collected and analyzed during dissection (Table1). Decapitation was carried out under deep ether anesthesia, cortices and hippocampi were dissected, frozen immediately in liquid nitrogen and stored at -80°C until analysis. The selection of male mice is based on the knowledge, that male mice exhibit Rett syndrome features more strongly and earlier than females (Guy et al., 2001).

Targeted and broad range proteomic studies were performed with brain tissues acquired from a total of 24 P50 male mice (10 wild type; 14 *Mecp2*-knockout). Both experimental approaches shared same sample sources but samples were equally aliquoted during mitochondrial extraction and then treated correspondingly for 1 and 2 dimensional electrophoresis down the line. Each individual targeted proteomic experiment consisted of 6 male wild type, 6 *Mecp2$^{-/y}$* mice and one internal standard sample prepared from wild type mouse hippocampus and cortical tissue. The 2 dimensional electrophoresis was limited to a total of only 6 samples due to technical capacity and it was equally split among 3 WT and 3 *Mecp2*-knockout mice. Reactive oxygen species generation measurements were recorded using fresh mitochondria extracted from 12 WT and 10 *Mecp2*-

Knockout male mice cortical tissue and for hippocampus – 8 WT and 6 *Mecp2*-knockout mice brain tissue was available.

Untargeted metabolomics analyses required exclusively cortical tissue from 6 *Mecp2*-knockouts and 6 WT male mice.

The data for hippocampus and neocortex were analyzed separately. As described above, the experiments typically involved only two groups of mice and therefore unpaired Student's t-test was applied to rate the statistical significance of the changes observed. All statistical tests were two-tailed and all significant differences ($P < 0.05$) are reported.

3.3 Isolation of mitochondria

A special mitochondrial isolation kit for tissue fractionation (89801; ThermoFisher Scientific) was used for mitochondrial fractions purification. The procedure was carried out according to the details given in manufacturer´s instructions. The same mitochondrial fraction was used for 2-dimensional (2-D) and 1-dimensional electrophoresis (1-D). The samples for these two types of electrophoresis required different treatments, therefore the mitochondrial samples were divided into two parts before the last step of the centrifugation protocol.

Samples for 1-dimensional electrophoresis were dissolved in 5% SDS (sodium dodecylsulphate) solution. Sample pellets intended for 2-dimensional gel electrophoresis were dissolved in a buffer which contained the following chemicals in a final concentration: 2% CHAPS, 2% TritonX-100, 7 M urea, 2 M thiourea, 0.1% ASB-14,2-mercaptoethanol, 2% pharmalyte 3–10. All sample buffers also contained bromophenol blue.

3.4 Isolation of native mitochondria for ROS measurements

Previously mentioned mouse genotypes were also used to measure mitochondrial reactive oxygen species (ROS) generation. Deeply anesthetized mice were decapitated. Their whole brain was removed within about 1 min. Before further micro-dissection to obtain hippocampal and cortical tissue, the brain was cooled in ice-cold aCSF (130 mM NaCl, 3.5 mM KCl, 1.25 mM NaH_2PO_4, 24 mM $NaHCO_3$, 1.2 mM $CaCl_2$, 1.2 mM $MgSO_4$ and 10 mM dextrose, constantly aerated with carbogen, i.e. 95% O_2 and 5% CO_2, pH 7.4).

After obtaining freshly extirpated hippocampal and cortical tissue, it was subjected to rapid manual homogenization with glass pestles containing 1 ml ice cold isolation buffer (IO: 20 mM Hepes, 220 mM mannitol, 70 mM sucrose, 1 mM EDTA, 0.5 mM PMSF, pH 7,6). The homogenate obtained was purified from cell debris and nuclear fraction by centrifuging 15 min 4°C at 800 G. After that, the supernatant was centrifuged with fresh vials for 30 min at 4°C 800 G. Final centrifugation of the supernatant was performed for 10 min at 4°C and 10,000 G. Supernatant was discarded and precipitate was resuspended in 100 µl of isolation buffer. Protein content was measured using a Bradford assay and 40 µg protein equivalent mitochondria were used for ROS generation measurements.

3.5 Protein determination

Protein concentrations in the samples meant for later electrophoresis (either 1-D or 2-D) were determined in quadruplicate assays using a micro bicinchoninic acid protein assay kit (23235; Pierce).

3.6 Metabolomic analyses

For metabolomics analyses a validated service provider – MetaSysX (Potsdam, Germany) was chosen. Initial bioinformatic analysis was conducted also by the same company. 100 mg of frozen brain tissue from each sample was grounded and further extracted according to the single-step protocol practiced by Salem's team at Max Planck Institute (Salem et al., 2016) with minor modification. Sample volumes were adjusted to equal amounts of material. Primary metabolites were analyzed by gas-chromatography coupled with mass-spectrometry (Gc-MS), whereas for the analysis of polar/semi-polar primary and secondary metabolites ultra-performance liquid chromatography (UPLC) -MS was applied. GC-MS was carried out on Agilent Technologies GC coupled to a MS (Leco Pegasus HT), consisting of an electron impact ionization source and a time-of-flight mass (TOF) analyzer. For polar/semi polar primary and secondary metabolites UPLC-MS measurements were conducted on a Waters ACQUITY Reversed Phase Ultra Performance Liquid Chromatography System (RP-UPLC), coupled to mass spectrometer (Orbitrap mass analyzer, electrospray ionization source, Thermo-Fisher). Chromatography was carried out with C18 columns and data were acquired in full scan MS mode (100-1500 mass range). Both positive and negative ionization modes spectra were recorded.

The spectra obtained were aligned and filtered. MetaSysX data base (for data obtained by UPLC-MS and GC-MC) and the Fiehn Library (for data obtained by GC-MS data) were used for the annotation of the extracted peaks. During the annotation and identification of the respective metabolites, the sample data generated on the different platforms was normalized to their respective group medians to obtain normalized intensities.

3.7 Bioinformatic analyses of metabolomic data

For the stabilization of variances all measurements were log-transformed. Missing values were set to the average of their respective measurements. Moderate t-test analysis was used for the identification of the differentially regulated metabolites. This test is implemented in the R package Limma (Smyth, 2005). ROAST rotation-based test was applied for the identification of upregulated and downregulated KEGG metabolism pathways (Wu et al., 2010). This ROAST test transforms Limma t-statistics into their equivalent z-scores from a standard normal distribution. For each pathway a single deregulation statistics is computed, taking the mean of the z-scores from the metabolites belonging to this pathway. Rotation test, a Monte Carlo technique is more suitable for small sample sizes than permutation. Hence p-value assessing the deregulation of each pathway is then obtained by this test. During pathways analysis we have considered only uniquely identified metabolites. Pathways which contained less than three identified metabolites were discarded. All p-values were adjusted for false discovery rate (Benjamini and Hochberg, 1995). BIOMEX software was applied for differential expression and ROAST analyses (Taverna et al., 2020).

3.8 Mitochondrial proteomic experiments

3.8.1 1-Dimensional gel electrophoresis and Western blotting.

Aliquots for 1-dimensional gel-electrophoresis contained 30 µg of protein. They were loaded in the same volume - 30 µl of buffer and subjected to SDS gel electrophoresis and Western blotting according to our earlier published lab-specific protocols (Meparishvili et al., 2015). The proteins from the gel were transferred onto nitrocellulose membranes, and the membranes were stained with Ponceau S solution 0.1% (w/v) to confirm transfer and uniform gel loading. The images were then analyzed with ImageJ (https://imagej.net/software/imagej). The nitrocellulose membranes were washed with phosphate buffer saline (PBS) with 0.05% Tween 20, and the standard

immunochemical procedures were carried out with peroxidase-labeled secondary antibodies and Super-Signal West Pico Chemiluminescent substrate (Pierce, 34580). To achieve the linearity of response, we have pre-flashed X-ray films with Sensitize (Amersham, RPN2051). Nitrocellulose membranes were then exposed to such pre-treated X-ray films. OXPHOS complexes were quantified with the Total OXPHOS rodent WB antibody cocktail (Abcam, ab110413). Levels of DRP1 – were evaluated with ab184247 (Abcam) antibodies. Mitofusin-1 was quantified with antibodies -ab57602 (Abcam), whereas protein 14-3-33 theta was detected by sc-59414 (Santa-Cruz) antibodies. Creatine kinase type B and HSP60 protein levels were evaluated with antibodies (Santa Cruz Biotechnology; sc-13115 and sc-13115, respectively).

LabWorks 4.0 (UVP) was applied for the measurement of the optical densities of the bands corresponding to the proteins of interest. Four internal protein standards containing 15, 30, 45 and 60 µg of total mitochondrial protein from the brain of WT mice were included in each gel. The same standards were used in all electrophoresis experiments performed and they served for the generation of calibration curves. Optical densities were significantly proportional to the amount of studied receptors. The data in Figures 2, 3, 5, 6 and 7 were obtained by dividing the value of optical density of each band from an experimental sample (e.g., neocortex of $Mecp2^{-/y}$ mice) by the optical density, which, from the calibration of the same autoradiograph, corresponded to 30 µg of standard total protein. The data expressed in this way will be termed "relative amount".

The densities of the protein bands were not normalized to any housekeeping protein, because it cannot be insured that such proteins will stay unaltered by our experimental conditions (Dittmer and Dittmer, 2006;Li and Shen, 2013;Ghosh et al., 2014). Uniformity and of each loaded sample was monitored using Ponceau S staining and band density calibration was based on protein standards.

3.8.2. SDS electrophoresis

0.75 mm thick, 12.5% polyacrylamide gels were used for SDS electrophoresis. All gels were run at 25°C with the following two sequential steps: (1)1–10 mA/gel, 80 V for 1 h and (2) 12 mA/gel, 150 V for 18 h.

3.8.3 2-D electrophoresis

First dimension isoelectric focusing was carried out on linear strips pH 3.0–10.0, 18 cm. They were first rehydrated overnight in the following solution: 0.1% DeStreak reagent 8 M urea, 0.5% pharmalyte3–10 and 0.5% TritonX-100. Then, isoelectric focusing was performed with the following regime: 500 V for 3 h and 3500 V for 18 h. On each strip 40 micrograms of mitochondrial fraction protein were loaded.

Following the isoelectric focusing step, the strips were equilibrated for 15 minutes in a buffer containing 0.05M Tris-HCl (pH 6.8), 6 M urea, 3% SDS, 1% DTT and 30% glycerol. Then, for the following 15 minutes, they were exposed to a buffer of the same composition, but in which DTT was substituted with 2.5% iodoacetamide.

3.8.4. Staining, scanning and image analysis.

2-D gels were stained with a silver staining kit (GE Healthcare). A glutaraldehyde processing step was omitted from our procedure. Scanning of the silver-stained gels was performed with an Labscan6.0 Image Scanner III (GE Healthcare). Obtained images were digitized and processed with ImageMaster 2-D platinum 7.0 software. For best equivalence of experimental conditions, six gels (three WT brain and three *Mecp2⁻/y* samples from neocortex and hippocampus) were run in parallel on a 2-D electrophoresis system. In sum, 6 brain samples of each region were analyzed for each genotype. The data are generated from the protein spots which were coinciding by isoelectric point and molecular weight (location) among different sets of experiments and were characterized by at least by 2 fold differences between *Mecp2⁻/y* and WT. Obtained data were analyzed by two-tailed t-test to assess potentially significant differences between the groups. In these statistical tests the significance level was set at 5%. Such confirmed, differentially expressed spots were excised out from gels and kept below –20ºC until MS analysis.

3.8.5. In-gel digestion and MS analysis

The excised spots were destained, reduced with DTT and alkylated by iodoacetamide. Then they were subjected to trypsin-mediated enzymatic digestion overnight at 37°C. After digestion, the supernatant was pipetted into a sample vial and loaded into an autosampler for automated LC-MS/MS analysis.

These mass spectrometry analyses were performed using by LCQ FLEET with nano HPLC system - Easy nLC-1000 (ThermoFisher Scientific, Waltham, MA). Peptides were separated by reverse-phase chromatography. MS/MS spectra data were analyzed by SEQUEST (Proteome Discoverer 1.4, ThermoFisher Scientific), searching against UniProt UniRef100 *Mus Musculus* species protein databases.

3.9 Spectrophotometric assay

ROS generation was measured using a multimode spectrophotometer flx-Xenius XM, SAFAS Monaco. It was tuned at 495 nm excitation wavelength and 525 nm emission wavelengths for the oxidation-sensitive dye H_2DCFDA (100 mM 2´,7´-dichlorodihydrofluorescein diacetate dissolved in DMSO - dimethyl sulfoxide). An amount of 40 μg isolated fresh mitochondria was transferred into a quartz cuvette with 1 ml mitochondrial assay buffer (MAS: 70 mM sucrose, 220 mM mannitol, 2 mM HEPES, 10 mM KH_2PO_4, 5 mM $MgCl_2$, 1 mM EGTA, and 0.2% BSA, pH 7.4) and a final H_2DCFDA concentration of 100 μM. The build-up of fluorescence was monitored for duration of 30 minutes and data was recorded with 1-minute intervals. Unpaired two tailed Student's t-test was used to determine significance of the observed differences. Mean ± standard deviation is used to represent analyses.

4. Results

Comparing the visually observable phenotypic appearance of WT and $Mecp2^{-/y}$ clearly shows clear differences in body size and length. Taking measurements of body and physiological parameters together with overall fitness tests (Janc et al., 2016a) support the visually observed phenotypic differences, thereby strongly suggesting that there have to be some alterations in the mitochondrial function and the cellular metabolism of the mice. $Mecp2^{-/y}$ animals were smaller, lighter, and had a trend toward slightly greater hematocrit and somewhat lower blood glucose levels, clearly distinguishing them from the control mice in terms of general phenotypic appearance (Table 1).

WT mice (n = 6)			
Body size [cm]	Body weight [g]	Blood glucose [mg/dL]	Hematocrit
8.23 ± 0.21	21.60 ± 1.06	242.50 ± 30.57	43.58 ± 2.05
8.2	22.7	211	46.3
8.6	22.6	247	45
8.1	20	243	41.3
8.4	22.5	235	45.3
8	21.2	215	41
8.1	20.6	304Z	42.6
$Mecp2^{-/y}$ mice (n = 6)			
7.17 ± 0.69 (p = 0.0078)	13.78 ± 3.70 (p = 0.0011)	200.00 ± 50.65 (p = 0.1393)	46.4 ± 2.46 (p = 0.0777)
6.9	11.5	177	50
6.5	11.4	147	47
8.3	20.5	306	47.7
7.9	17	208	46.7
6.9	12.1	185	42
6.5	10.2	177	45

Table 1. The examined WT and $Mecp2^{-/y}$ mice's phenotypic characteristics, including their respective means and standard deviations. A two-tailed, two-sided, unpaired t-test was used to compare genotypes (see p-values). Reproduced from Golubiani G, Lagani V, Solomonia R, Müller M. (2021). Metabolomic Fingerprint of *Mecp2*-Deficient Mouse Neocortex: Evidence for a Pronounced Multi-Facetted Metabolic Component in Rett Syndrome. Cells. 10: 2494. Table 1

4.1 The OXPHOS complexes

At the outset of experiments the OXPHOS complexes I, II, III, IV, and V's relative expression levels were investigated in the neocortex and hippocampus of *Mecp2$^{-/y}$* and WT mice.

Using 1-D electrophoresis and Western immunoblotting, the following proteins were quantitatively assessed:

- NADH: ubiquinone oxidoreductase subunit B8 (NDUFB8), complex I
- Succinate dehydrogenase complex iron sulfur subunit B (SDHB), complex II
- Ubiquinol-cytochrome C reductase core protein 2 (UQCRC2, alternate name cytochrome B-C1 complex subunit 2), complex III
- Cytochrome c oxidase subunit 1 (MTCO1), complex IV
- ATP synthase F1 subunit alpha, complex V

The targeted proteins are labile subunits of respected unassembled respiratory complexes. Consequently, quantitative evaluation of these subunits does give precise information about the relative amounts of the various complexes (Antibody mix used: Manufacturer – Abcam. Product ab110413). Our data do not indicates for genotype-related significant differences, as differing expression levels of the investigated proteins were found neither in the neocortex nor in the hippocampus (Figure 1, Table 2).

Protein	Hippocampus			Neocortex		
	Relative units (mean ± SEM)		P value	Relative units (mean ± SEM)		P value
	WT	$Mecp2^{-/y}$		WT	$Mecp2^{-/y}$	
NADH: ubiquinone oxidoreductase subunit B8 (NDUFB8), complex-I	1.35±0.05	1.17±0.09	0.12	0.78±0.06	0.85±0.09	0.51
Succinate dehydrogenase complex iron sulfur subunit B (SDHB), complex II	0.44±0.03	0.50±0.07	0.42	0.87±0.05	0.92±0.07	0.7
Ubiquinol-cytochrome C reductase core protein 2 (UQCRC2, alternate name cytochrome B-C1 complex subunit 2), complex III	0.44±0.06	0.53±0.06	0.32	1.05±0.05	1.06±0.06	0.9
Cytochrome c oxidase subunit 1 (MTCO1), complex IV	0.27±0.02	0.29±0.02	0.43	0.87±0.05	0.85±0.07	0.84
ATP synthase F1 subunit alpha, complex V	0.61±0.05	0.68±0.08	0.73	1.11±0.03	1.09±0.051	0.74

Table 2. Expression levels of selected subunits of OXPHOS complexes in the hippocampus and neocortex of $Mecp2^{-/y}$ and WT mice. Statistical analysis did not reveal any significant differences (see p values; degrees of freedom df=10 for all comparisons, S.E.M). Modified from Golubiani G, van Agen L, Tsverava L, Solomonia R, Müller M. (2023) Mitochondrial Proteome Changes in Rett Syndrome. Biology.; 12(7), 956. Table 1.

The composition of the complexes can alter in a variety of ways; therefore, relative proportions of the OXPHOS complexes do not exclusively reveal this hidden information. Furthermore, our findings do not rule out the possibility of additional variations in the entire mitochondrial proteome among WT and $Mecp2^{-/y}$ animals.
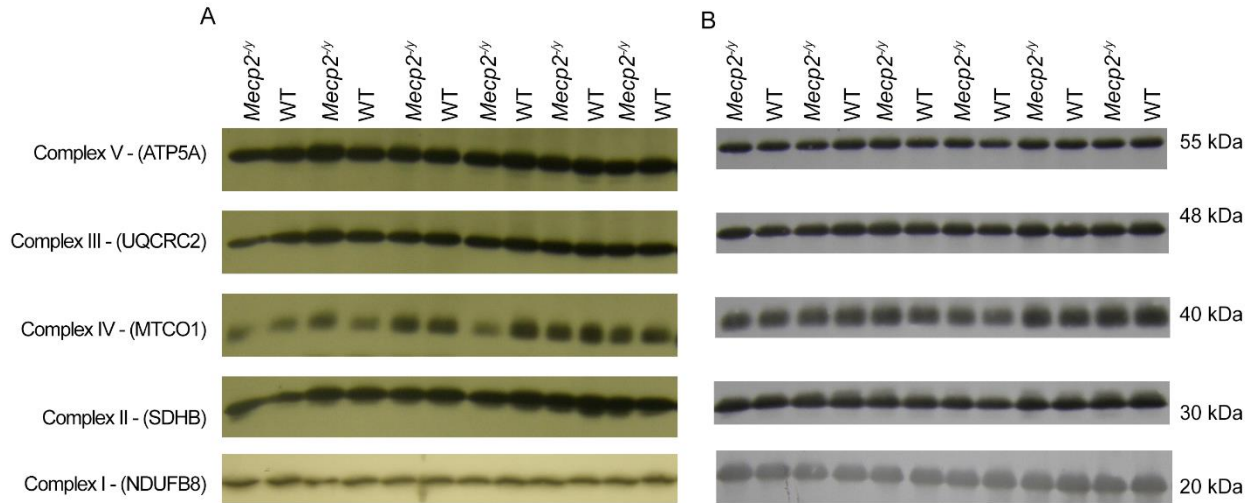
Figure 1. Western blot images of specific prominent subunits of the five mitochondrial OXPHOS complexes in the hippocampus (A) and neocortex (B) of *Mecp2*$^{-/y}$ and WT mice. Lanes were alternatingly loaded with *Mecp2*$^{-/y}$ and WT samples. No significant genotype-related differences were detected for the chosen subunits of the various respiratory chain complexes or the FoF1 ATP synthase complex *(see also Table-2).* Reproduced from Golubiani G, van Agen L, Tsverava L, Solomonia R, Müller M. (2023) Mitochondrial Proteome Changes in Rett Syndrome. *Biology*.; 12(7), 956. Figure 3.

4.2 Regulators of mitochondrial morphology

RTT appears to be intimately related to morphological changes in the mitochondria. Therefore, the expression levels of proteins that are essential for controlling the dynamics of mitochondrial fusion and fission, such as mitofusin 1 and dynamin-related protein 1, were evaluated. *Mecp2*$^{-/y}$ mice had considerably less mitofusin-1 in their neocortex compared to WT mice (t = 2.47, p = 0.033, df = 10). (Figure 2).
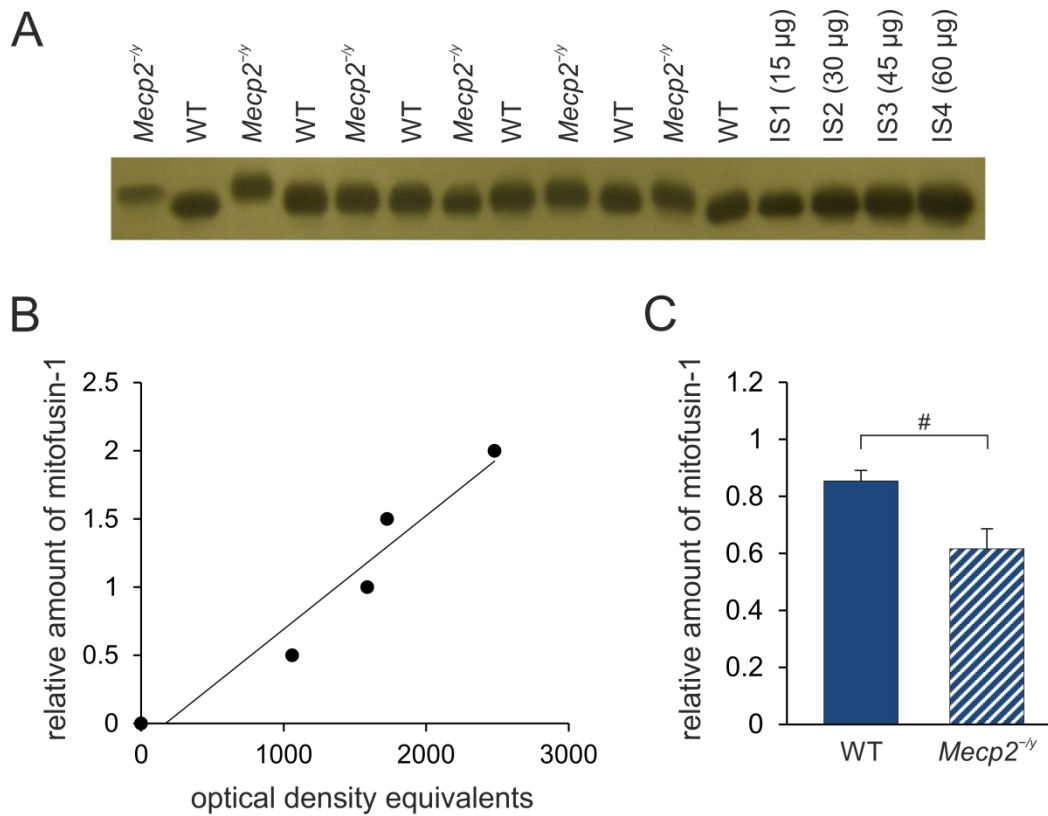
Figure 2. Western blot images of mitofusin 1 expression in the neocortex of WT and *Mecp2^-/y* mice. (A) Each lane represents a single sample. Internal standards, represented in lanes IS1–IS4, contain 15, 30, 45, and 60 µg of protein, respectively. (B) A calibration plot that has been fitted using linear least-squares regression. (C) Mitofusin-1 mean expression levels (mean ± standard error of the mean). RTT-related differences among genotypes are identified by crosshatches (# $p < 0.05$; unpaired 2-tailed Student´s t-test). Modified from Golubiani G, van Agen L, Tsverava L, Solomonia R, Müller M. (2023) Mitochondrial Proteome Changes in Rett Syndrome. *Biology*. 12, 956. Figure 4.

However in the neocortex, there were no discernible differences for DRP 1 (WT: 0.832 ± 0.076 *Mecp2^-/y*: 0.734 ± 0.140, n=6 each; p=0.549, values are given as mean ± SEM).

The hippocampus of *Mecp2^-/y* animals as compared to WT mice, expresses significantly reduced amounts of DRP1 (t = 2.39, p = 0.038, df = 10) (Figure 3). The detected levels of mitofusin-1 in the hippocampus were only slightly lower as compared to WT hippocampus (WT: 0.434 ± 0.026, *Mecp2^-/y*: 0.34 ± 0.065, n=5; p=0.234, values are given as mean ± SEM), but these alterations were not statistically significant.
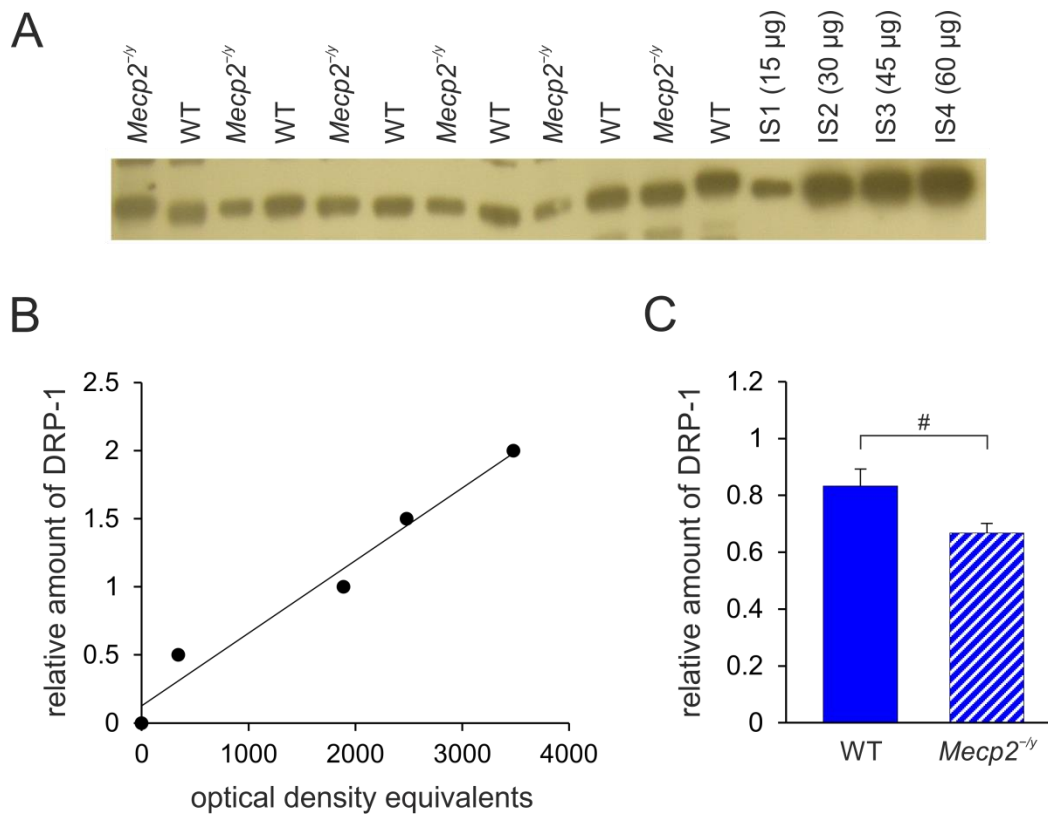
Figure 3. DRP1 expression in *Mecp2*$^{-/y}$ and WT mice's hippocampus. (A) A sample film: individual sample per lane. The internal standards, each comprising 15, 30, 45, and 60 µg of protein, are shown as lanes IS1–IS4. (B) A calibration plot that has been fitted using linear least-squares regression. (C) Mean DRP-1 concentrations in the hippocampus of the two separate groups of mice (mean ± standard error of the mean). Crosshatches are used to show genotype-related RTT differences (# $p < 0.05$; unpaired, two-tailed Student's t-test). Modified from Golubiani G, van Agen L, Tsverava L, Solomonia R, Müller M. (2023) Mitochondrial Proteome Changes in Rett Syndrome. *Biology.* 12(7), 956. Figure 5

4.3 The mitochondrial proteome differs among *Mecp2*$^{-/y}$ and WT mice

The 2D electrophoresis approach was applied to provide a more comprehensive picture of the differences between the mitochondrial proteomes of *Mecp2*$^{-/y}$ and control mice. Indeed, the 2D electrophoresis performed on the mitochondrial fractions that were purified from the neocortex and hippocampal regions of *Mecp2*$^{-/y}$ and WT mice revealed many protein bands with statistically significant changes, which included both upregulated and downregulated candidates (Figure 4).
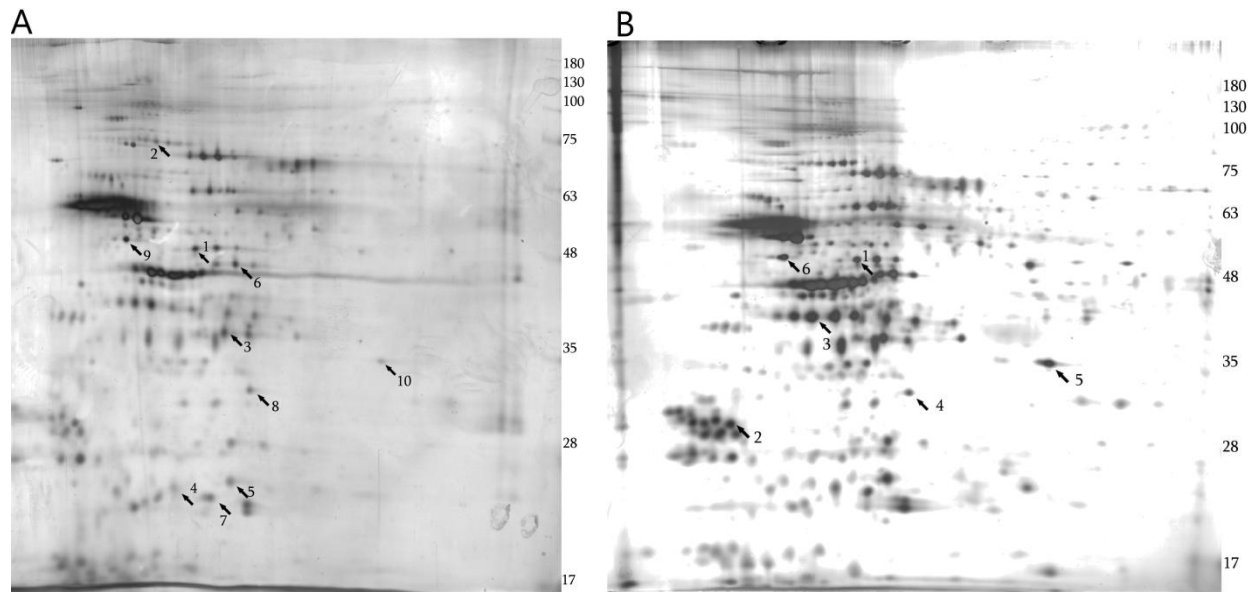
Figure 4. 2-Dimensional gel electrophoresis representative images of the mitochondrial fraction from the neocortex (B) and hippocampus (A) of *Mecp2$^{-/y}$* mice. Gels were stained with silver dye. Proteins found to be changed at least by 2-fold by "Image 2D platinum 7.0 software" are indicated by arrows. The arrows in the brackets shows the direction of changes in RTT (increase or decrease) as compared to WT mice. Reproduced from Golubiani G, van Agen L, Tsverava L, Solomonia R, Müller M. (2023) Mitochondrial Proteome Changes in Rett Syndrome. *Biology*.; 12(7), 956. Figure 6. The significantly changed proteins are as follows:

Hippocampus:

1 - Cytochrome b-c1 complex subunit 1, mitochondrial (↑)

2 - NADH-ubiquinone oxidoreductase 75 kDa subunit, mitochondrial (↑)

3 - Pyruvate dehydrogenase E1 component subunit beta, mitochondrial (↑)

4 - NADH dehydrogenase [ubiquinone] iron-sulfur protein 8, mitochondrial (↑)

5 - NADH dehydrogenase [ubiquinone] flavoprotein 2, mitochondrial (↑)

6 - Creatine kinase B-type (↑)

7 - ATP synthase subunit d (↑)

8 - Prohibitin 1 (↑)

9 - Gamma enolase (↓)

10 -cAMP-dependent protein kinase catalytic subunit alpha (↓)

Neocortex:

1 - Cytochromeb-c1 complex subunit 1, mitochondrial (↑)

2 - 14-3-3 protein theta (↓)

3 - Guanine nucleotide-binding protein G(o) subunitalpha (↑)

4 - Prohibitin 1 (↑)

5 - cAMP-dependent protein kinase catalytic subunit alpha (↓)

6 - Gamma enolase (↓)

Following MS analysis, these bands' identities were further categorized (Table 3). In all, 6 differentially expressed proteins in the neocortex and 10 differentially expressed proteins in the hippocampus were found. Four of these proteins with differential expression exhibit similar alterations in both of the brain regions: Gamma-enolase and cAMP-dependent protein kinase catalytic subunit alpha are negatively regulated in the hippocampus and neocortex of $Mecp2^{-/y}$ animals compared to WT circumstances, but prohibitin 1 and cytochrome b-c1 complex subunit 1 are increased.

	Protein	Direction of changes as compared to WT	Gene	Uniprot ID	Molecular/biological functions of proteins
			HIPPOCAMPUS		
1	Pyruvate dehydrogenase E1 component subunit beta, mitochondrial	Upregulated	*Pdhb*	Q9D051 ODPB_MOUSE	Pyruvate dehydrogenase (acetyl-transferring) activity/ glucose metabolic process
2	NADH-ubiquinone oxidoreductase 75 kDa subunit, mitochondrial	Upregulated	*Ndufs1*	Q91VD9 NDUS1_MOUSE	2 iron, 2 sulfur cluster binding/electron transfer activity
3	NADH dehydrogenase [ubiquinone] iron-sulfur protein 8, mitochondrial	Upregulated	*Ndufs8*	Q8K3J1 NDUS8_MOUSE	NADH dehydrogenase (ubiquinone) activity/ mitochondrial electron transport, NADH to ubiquinone
4	NADH dehydrogenase [ubiquinone] flavoprotein 2, mitochondrial	Upregulated	*Ndufv2*	Q9D6J6 NDUV2_MOUSE	NADH dehydrogenase (ubiquinone) activity/ mitochondrial electron transport, NADH to ubiquinone
5	Cytochrome b-c1 complex subunit 1, mitochondrial	Upregulated	*Uqcrc1*	Q9CZ13 QCR1_MOUSE	Metal ion binding/ mitochondrial electron transport, ubiquinol to cytochrome c
6	ATP synthase subunit d	Upregulated	*Atp5pd*	Q9DCX2 ATP5H_MOUSE	Proton-transporting ATP synthase activity, rotational mechanism/proton motive force-driven mitochondrial ATP synthesis

7	Creatine kinase B-type	Upregulated	*Ckb*	Q04447 KCRB_MOUSE	Kinase activity/phosphocreatine biosynthetic process
8	Prohibitin-1	Upregulated	*Phb*	P67778 PHB1_MOUSE	Protein heterodimerization activity/ mitochondrial organization
9	Gamma-enolase	Downregulated	*Eno2*	P17183 ENOG_MOUSE	Lyase/glycolysis
10	cAMP-dependent protein kinase catalytic subunit alpha	Downregulated	*Prkaca*	P05132 KAPCA_MOUSE	Serine/threonine protein kinase activity
NEOCORTEX					
11	Cytochrome b-c1 complex subunit 1, mitochondrial	Upregulated	*Uqcrc1*	Q9CZ13 QCR1_MOUSE	Metal ion binding/ mitochondrial electron transport, ubiquinol to cytochrome c
12	Guanine nucleotide-binding protein G(o) subunit alpha	Upregulated	*Gnao1*	P18872 GNAO_MOUSE	G protein-coupled receptor binding/G protein coupled receptor signaling pathway
13	Prohibitin-1	Upregulated	*Phb*	P67778 PHB1_MOUSE	Protein heterodimerization activity/ mitochondrial organization
14	Gamma-enolase	Downregulated	*Eno2*	P17183 ENOG_MOUSE	Lyase/glycolysis
15	cAMP-dependent protein kinase catalytic subunit alpha	Downregulated	*Prkaca*	P05132 KAPCA_MOUSE	Serine/threonine protein kinase activity
16	14-3-3 protein theta	Downregulated	*Ywhag*	P61982 1433G_MOUSE	Protein domain specific binding/protein targeting

Table 3. Results of comparative 2-D electrophoresis and MS experiments. The identities of differentially expressed proteins are listed. The protein spots that showed at least a 2-fold change between *Mecp2$^{-/y}$* and WT mice were chosen from each series of studies. A two-tailed Student's t test was used to examine the data from various studies for the spots that coincided by location (pI and molecular weight). Protein identities were revealed by MS analysis. The significance level was set at 5%. The Uniprot identification and molecular biological function of each protein are also provided. Reproduced from Golubiani G, van Agen L, Tsverava L, Solomonia R, Müller M. (2023) Mitochondrial Proteome Changes in Rett Syndrome. *Biology*. 12(7), 956. Table 2.

4.4 Confirmatory Western blot analysis of differentially expressed proteins

Western immunoblotting tests were conducted on 2 chosen proteins to confirm the outcomes of the 2D electrophoresis. For this task, two candidate proteins were selected, one from the neocortex and one from the differentially expressed proteins in the hippocampus. Furthermore, proteins were chosen based on their (1) regional specificity, meaning that they should only exhibit differential expression in one of the examined regions, such as the hippocampus or neocortex, and (2) the availability of trustworthy commercial antibodies. Based on these criteria, 14-3-3 protein theta and creatine kinase were chosen. Creatine kinase B is increased in the hippocampus of $Mecp2^{-/y}$ mice, but was not observed to be expressed differently in the neocortex of these animals (Table 3). Creatine kinase B antibodies interacted with a 50 kDa protein (Figure 5A), and $Mecp2^{-/y}$ animals presented significantly more protein on average in their hippocampi than WT mice did (t=2.41, p=0.037, df=10, Figure 5B).
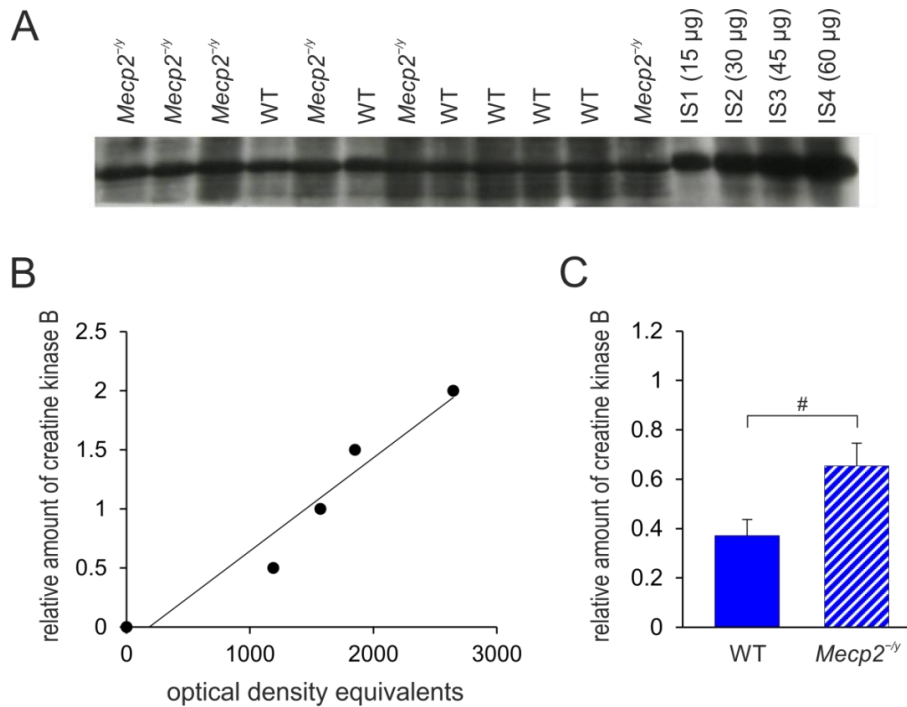
Figure 5. Expression levels of the creatine kinase B protein in the hippocampus of $Mecp2^{-/y}$ and WT mice. (A) Each lane represents a single sample. Internal standards, found in lanes IS1–IS4, contain 15, 30, 45, and 60 μg of protein, respectively. (B) A calibration plot that has been fitted using linear least-squares regression. (C) Comparison of the two groups of mice's mean levels of creatine kinase B (mean ± standard error of the mean) in the hippocampus. Crosshatches are used to show genotype-related RTT differences (# p < 0.05; unpaired, two-tailed Student's t-test). Modified from Golubiani G, van Agen L, Tsverava L, Solomonia R, Müller M. (2023) Mitochondrial Proteome Changes in Rett Syndrome. *Biology*.; 12(7), 956. Figure 7.

Additionally, according to our 2D electrophoresis (Table 3), *Mecp2^{-/y}* mice's neocortex appears to express less 14-3-3 protein theta. Western immunoblotting analysis confirmed this finding (Figure 6). The antibody against this protein responds with a band of 26 kDa molecular weight matching to 14-3-3 protein theta, and the mean expression level of the protein was considerably lower (45%) in *Mecp2^{-/y}* neocortex compared to WT ($t=2.35$, $p=0.04$, $df=10$). Heat shock protein 60 (HSP60) interacts with 14-3-3 protein and is engaged in neurodegeneration in addition to playing a role in the homeostasis of mitochondrial proteins (Satoh et al., 2005;Bross et al., 2012).
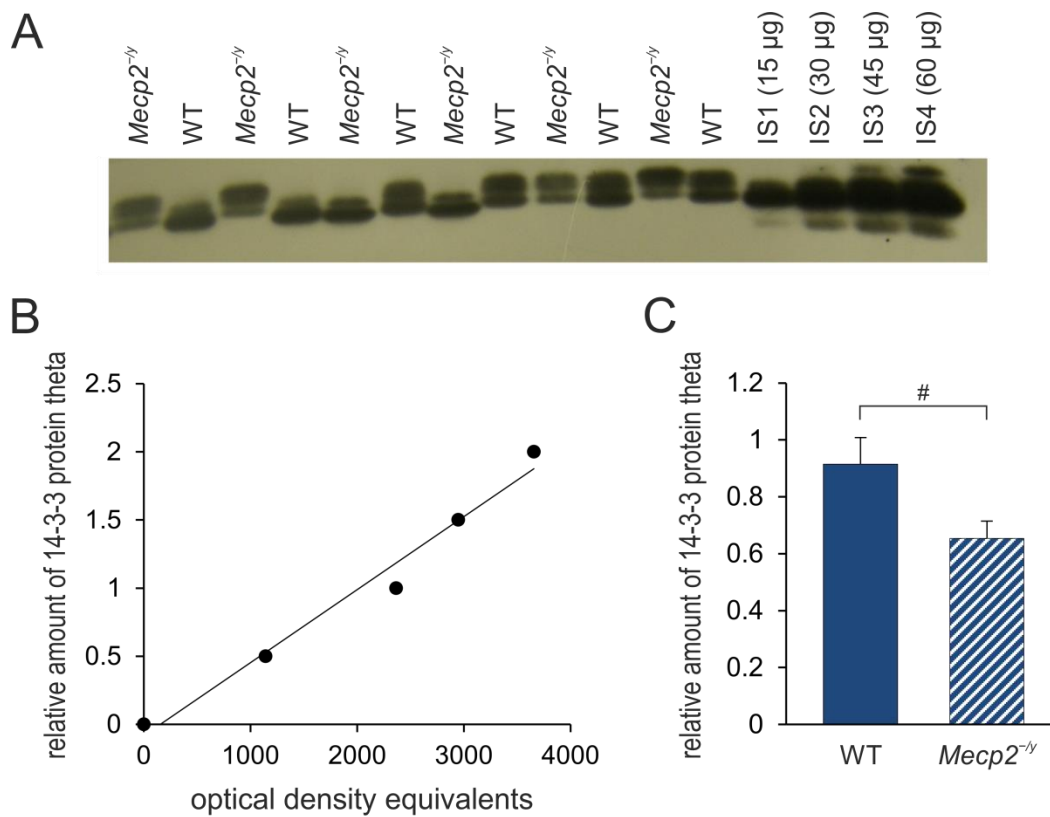
Figure 6. 14-3-3 protein theta expression in the neocortex of *Mecp2^{-/y}* and WT mouse. (**A**) Sample film; each lane contains an individual sample. Lanes IS1-IS4 are internal standards containing 15, 30, 45, and 60 µg of protein, respectively. (**B**) The calibration plot was fitted by a linear least-squares regression. (**C**) Mean levels of 14-3-3 protein theta (mean ± standard error of the mean) in the hippocampus of the two groups of mice. RTT-related differences among genotypes are identified by crosshatches (# *p* < 0.05; unpaired 2-tailed Student´s *t*-test). Modified from Golubiani G, van Agen L, Tsverava L, Solomonia R, Müller M. (2023) Mitochondrial Proteome Changes in Rett Syndrome. *Biology*. 12(7), 956. Figure 8.

Therefore, as a following step, it was investigated whether *Mecp2^{-/y}* and WT mice's neocortex and hippocampus had different expression levels of HSP60. Figure 7 shows that *Mecp2^{-/y}* animals have

considerably lower levels of HSP60 in their neocortex than WT mice (t=2.24, p=0.049, df=10, Figure 7), although there were no significant genotype-relate changes detected in the hippocampus (WT: 0.786 ± 0.092, *Mecp2*$^{-/y}$: 0.636 ± 0.100, n=6 each, p=0.3, data are presented as mean relative units ± SEM).
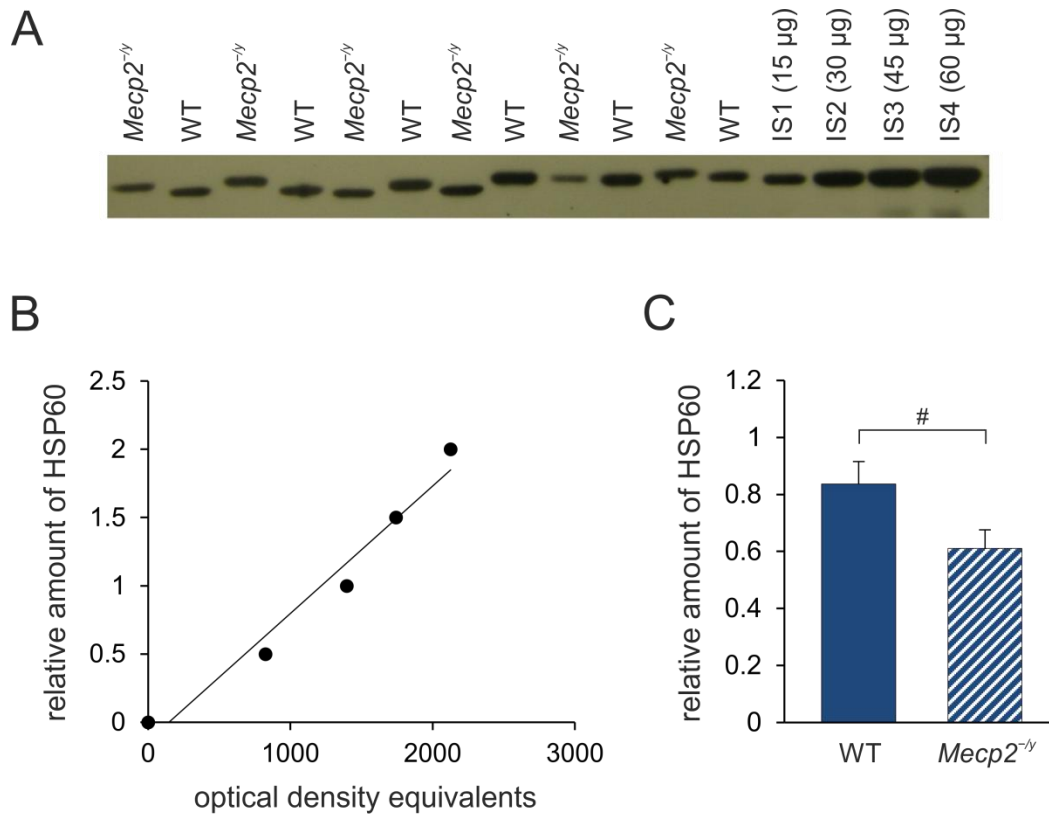
Figure 7. HSP60 expression levels in *Mecp2*$^{-/y}$ and WT mice's neocortex. (A) Sample film; Each lane represents a single sample. Internal standards, found in lanes IS1–IS4, contain 15, 30, 45, and 60 µg of protein, respectively. (B) A calibration plot that has been fitted using linear least-squares regression. (C) Mean levels of HSP60 (mean ± standard error of the mean) in the neocortex of the two groups of mice. RTT-related differences among genotypes are identified by crosshatches (# p < 0.05; unpaired 2-tailed Student´s t-test). Modified from Golubiani G, van Agen L, Tsverava L, Solomonia R, Müller M. (2023) Mitochondrial Proteome Changes in Rett Syndrome. *Biology*. 12,(7) 956. Figure 9.

4.5 Metabolomics results

To assess to whether the protein changes detected in the mitochondrial proteome may be accompanied also by alterations in the cellular metabolism, we ran a metabolomics screening on cortical tissue. This brain region was selected, as it provides sufficient tissue amounts for this kind of analyses. Hippocampus, due to its very small tissue amounts may not have fulfilled this condition.

The dissected cortices of adult WT and *Mecp2^-/y* mice were subjected to an untargeted metabolome study.

A total of 4143 distinct characteristics were found overall using metabolomics screening. Amongst them 2003 compounds were with hydrophilic characteristics in negative mode, 2037 were in positive mode, and 101 in GC mass traces. The MetaSysX database was used for their annotation, which resulted in 283 distinct features which were definitely identified (Supplementary Materials Table 2). From these 283 compounds 32 were matched to multiple reference compounds, and therefore have to be considered as co-eluting compounds. When only the identified metabolites are analyzed, principal component analysis reveals that the WT and *Mecp2^-/y* samples tend to settle within their respective categories (Figure 8A). This also becomes evident, when taking into account all measurements (Figure 8B).
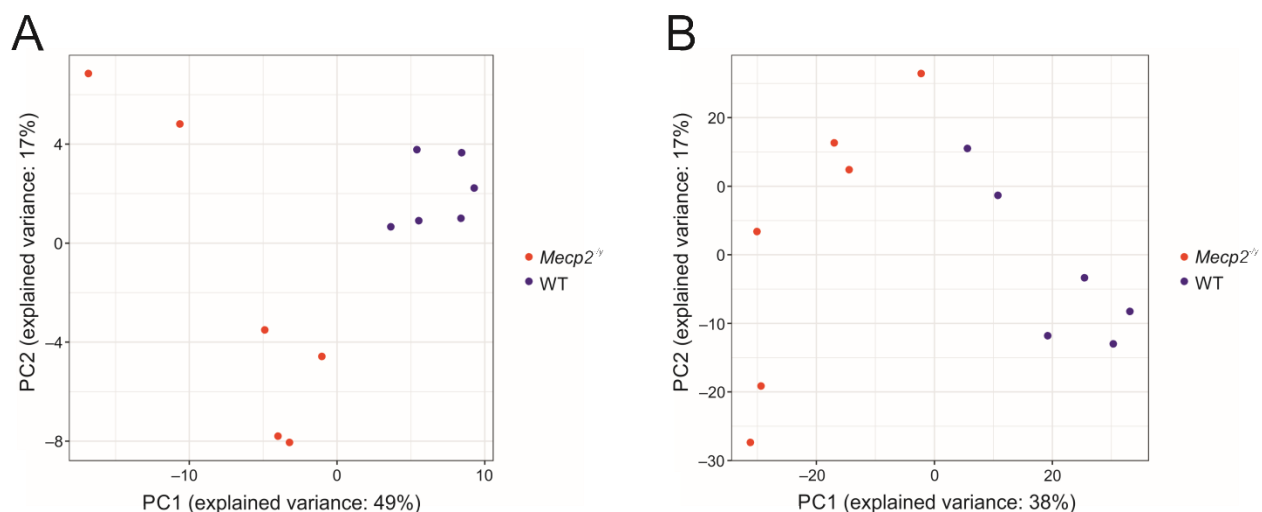
Figure 8. Principal component analysis (PCA) plots for *Mecp2^-/y* and WT mice cortices. *Mecp2^-/y* and WT cortices are shown in red and blue dots, respectively. Only the identified metabolites (A) are used to calculate PCA, and all measurements are taken into account in the neighboring panel (B). The percentage of explained variance for the x (first component) and y (second component) axes are both presented. Reproduced from Golubiani G, Lagani V, Solomonia R, Müller M. (2021). Metabolomic Fingerprint of *Mecp2*-Deficient Mouse Neocortex: Evidence for a Pronounced Multi-Facetted Metabolic Component in Rett Syndrome. *Cells*. 10: 2494. Figure 1.

WT and *Mecp2^-/y* neocortex showed distinct metabolic changes, with a total of 101 identified metabolites changing substantially between genotypes at an adjusted p-value of 0.05 (see Supplementary Materials Table 1). Specifically, 68 metabolites were significantly increased as compared to WT, while the remaining 33 metabolites were significantly lower in the *Mecp2^-/y*

neocortex. These variably regulated metabolites include amino acids, peptides, neurotransmitters, lipids, nucleosides/nucleotides, carbohydrates, and other chemically diverse substances. In the $Mecp2^{-/y}$ neocortex, cysteinylglycine, L-homocysteine, L-glutamyl-L-glutamine, gamma-glutamyl-tyrosine, and 3-methoxytyramine are those five metabolites that were most significantly downregulated (according tp log2 fold changes). Sucrose, D-glucose 6-phosphate, D-fructose 1,6-bisphosphate, glyceraldehyde 3-phosphate, and rutin are the five metabolites that are most significantly elevated (see Supplementary Materials Table 1).

The number of deregulated identified metabolites and the degree of their alteration are visualized using a volcano plot to show the results of the deregulation analysis and the complicated genotype-related differences (Figure 9A). In this plot, the non-significantly impacted metabolites are presented in blue, whereas red denotes significantly modified metabolites (FDR 0.05) for clear identification. Figure 9B displays an equivalent plot of all the measurements.
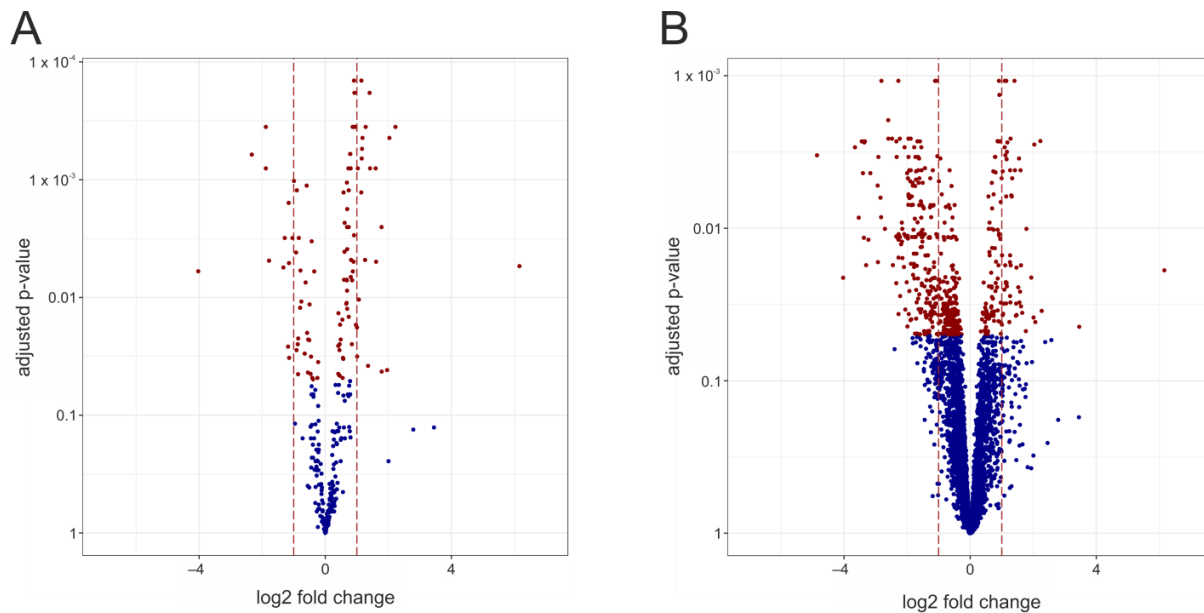
Figure 9. Volcano charts showing unregulated data from the $Mecp2^{-/y}$ and WT brain. One known metabolite is represented by each dot. The adjusted p-values for $Mecp2^{-/y}$ and WT are shown on the y-axis by the -log10 transformed log2 fold changes on the x-axis (as computed by a moderated t-test). Measurements having an adjusted p-value of less than 0.05 are represented by red dots, whereas measurements that are not substantially deregulated are represented by blue dots. The brown vertical lines denote a ±1 log2 fold shift, which translates to metabolites being present in the $Mecp2^{-/y}$ brain either twice as much (+1) or half as much (-1) as before. For all measurements and the identified metabolites (A), volcano graphs are displayed (B). Reproduced from Golubiani G, Lagani V, Solomonia R, Müller M. (2021). Metabolomic Fingerprint of $Mecp2$-Deficient Mouse Neocortex: Evidence for a Pronounced Multi-Facetted Metabolic Component in Rett Syndrome. *Cells*. 10: 2494. Figure 2.

For the sake of clear visualization, a heatmap of all the deregulated data, together with the concentration values of all the deregulated detected metabolites was assembled (Figure 10B). These heatmaps show a very distinct clustering of the tissue samples under study that is clearly genotype-dependent. Furthermore, both the WT and the $Mecp2^{-/y}$ cortices exhibit a different pattern of groupings of metabolites that are up- and down-regulated.
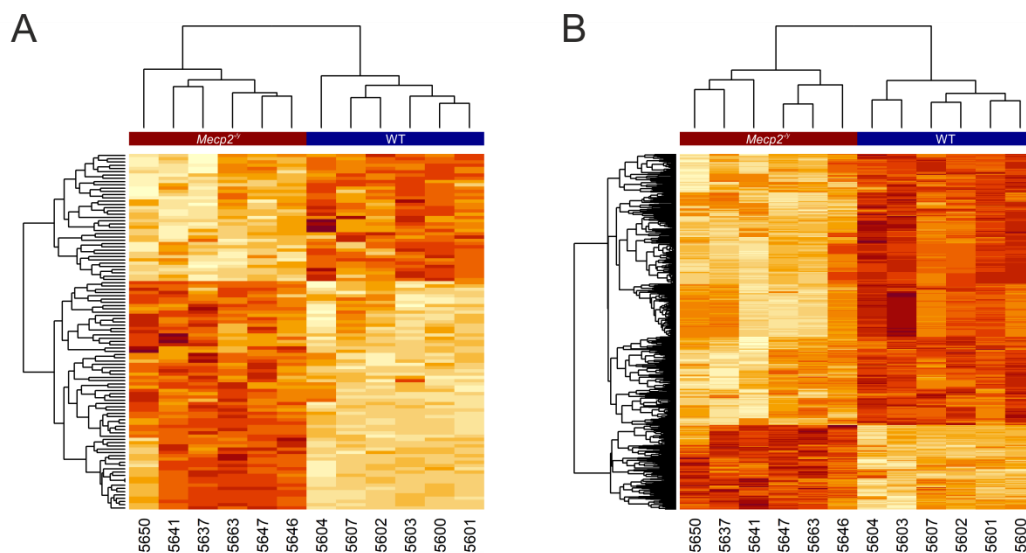
Figure 10. Heatmaps showing all deregulated recognized and unidentified metabolite concentration values. White values are lower and dark red values are higher. Rows of measurements are arranged, while columns are used to represent the tissue samples. A red and a blue banner, respectively, are used to identify the $Mecp2^{-/y}$ and WT samples at the top of the heatmap. The clustering of measurements and distinctive sample identifiers is displayed using dendrograms (individual mouse numbers). The identified metabolites (A) and all measurements were used to calculate the heatmaps (B). Reproduced from Golubiani G, Lagani V, Solomonia R, Müller M. (2021). Metabolomic Fingerprint of $Mecp2$-Deficient Mouse Neocortex: Evidence for a Pronounced Multi-Facetted Metabolic Component in Rett Syndrome. *Cells*. 10: 2494.

The $Mecp2^{-/y}$ and WT mouse brain metabolomes differ significantly and dramatically, as seen by the volcano plots and heatmaps. This specifically includes a number of amino acids, the majority of which showed increased levels in the $Mecp2^{-/y}$ neocortex (Figure 11).
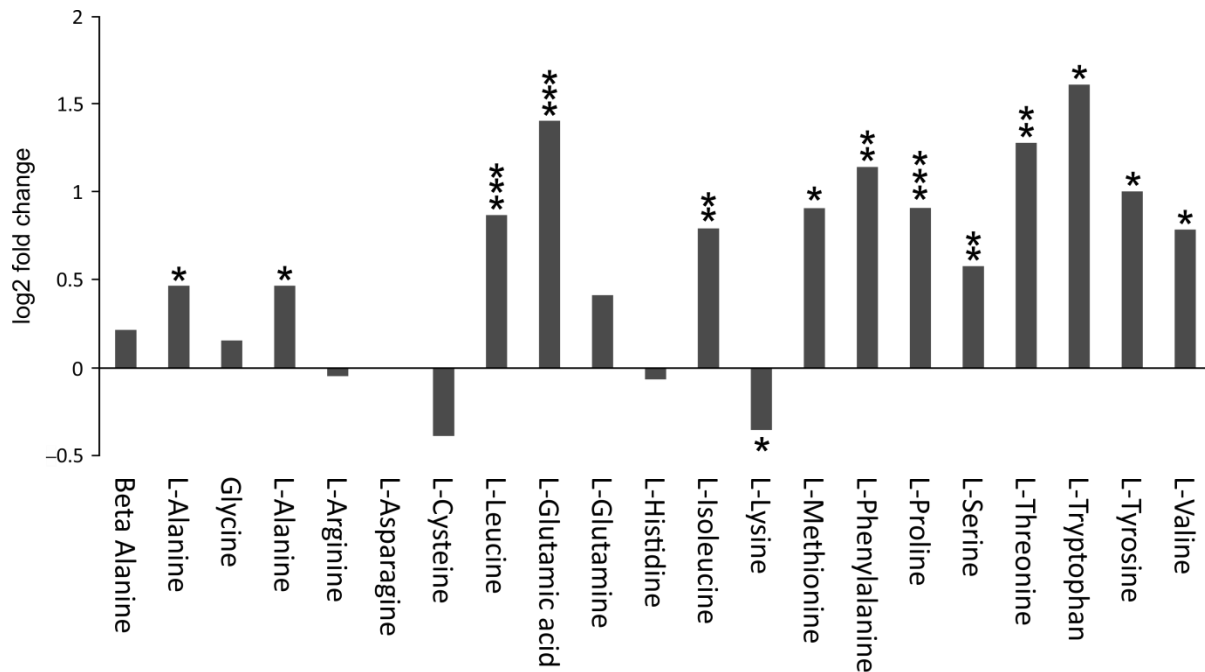
Figure 11. In the *Mecp2^{-/y}* and WT brain, many amino acids are present at distinctly different amounts. *Mecp2^{-/y}* mice had higher detection levels for the majority of these compounds. When compared to WT line, only lysine was reduced. The log2 fold changes of the various compounds are plotted. Significant deviations from WT are denoted by asterisks (***$p < 0.001$, ** $p < 0.01$,* $p < 0.05$). Reproduced from Golubiani G, Lagani V, Solomonia R, Müller M. (2021). Metabolomic Fingerprint of *Mecp2*-Deficient Mouse Neocortex: Evidence for a Pronounced Multi-Facetted Metabolic Component in Rett Syndrome. *Cells*. 10: 2494.

Amongst all amino acids only lysine displayed a markedly lower quantity in *Mecp2^{-/y}* neocortex when compared to WT mice. Furthermore, there were still a sizable number of unidentified metabolites. Some of these have a strong ability to distinguish across WT and *Mecp2^{-/y}* mice, and may therefore be suitable as possible biomarkers for the development of disease or the severity of symptoms.

Because of so many significantly changed metabolites, it is becoming obvious that the symptomatic *Mecp2^{-/y}* animals should have multiple altered cellular pathways. So, using all mouse metabolism-related pathways listed in the Kyoto Encyclopedia of Genes and Genomes, a deregulation analysis at the pathway level (KEGG) was performed (Kanehisa and Goto, 2000).

A total of 41 metabolic pathways had at least three defined metabolites in them, and in the *Mecp2^{-/y}* neocortex there were substantial alterations detected in 31 of these pathways (FDR 0.05, Figure 12, Table 4).

In general, amino acids and carbohydrates metabolism pathways are upregulated. However, there were some modifications in cofactor and vitamin metabolism, overall energy metabolism, lipid metabolism, and metabolism of lipids (Table 4). When compared to WT, the majority (30 of 31) of highly disrupted pathways were elevated in the *Mecp2$^{-/y}$* brain. This is clearly evident from the diagram of the pathway-enrichment analyses where red color tones indicates for upregulated pathways (Figure 12).
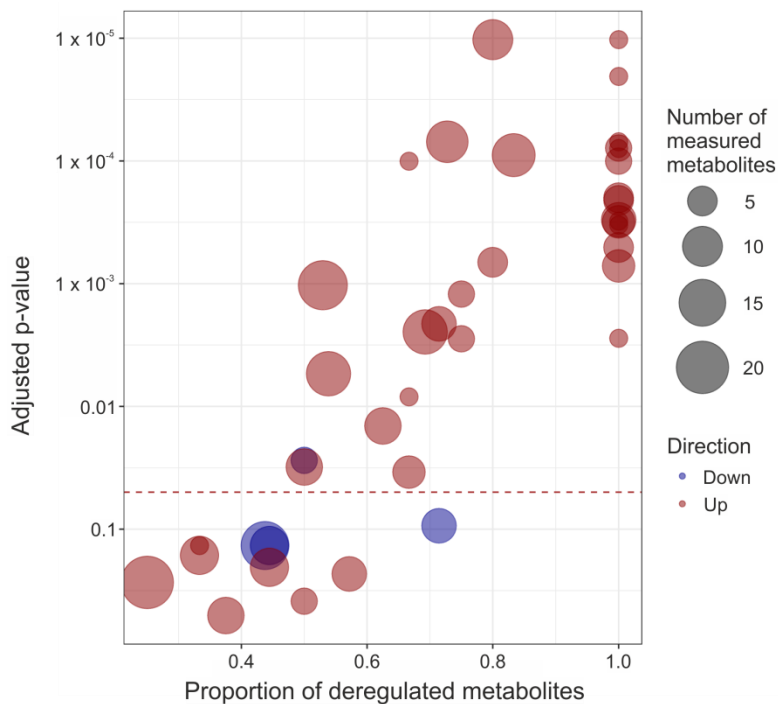
Figure 12. Results of the pathway enrichment are graphically presented. The fraction of unregulated metabolites is shown on the x-axis for each pathway, and the adjusted p-value is shown on the y-axis for each pathway. Each dot's size corresponds to the quantity of recognized metabolites that are present in that pathway, and its color denotes whether that pathway is being regulated up (red) or down (blue). Reproduced from Golubiani G, Lagani V, Solomonia R, Müller M. (2021). Metabolomic Fingerprint of *Mecp2*-Deficient Mouse Neocortex: Evidence for a Pronounced Multi-Facetted Metabolic Component in Rett Syndrome. *Cells*. 10: 2494.

In *Mecp2$^{-/y}$* brain, only glycerophospholipid metabolism was markedly downregulated. In addition to histidine, tyrosine, tryptophan, beta-alanine, and glutathione metabolism, changes in nucleotide (pyrimidine, purine) metabolism and lysine breakdown did not reach the threshold of significance (FDR > 0.05). Between the *Mecp2$^{-/y}$* and WT neocortex, there were no significant differences in the synthesis of vitamin B6, pantothenate, or CoA. (Table 4).

Pathway	Number of features	Number down	Number up	Direction	p-Value	Adjusted p-Value	Group
Starch and sucrose metabolism	3	0	3	Up	1.00×10^{-6}	1.02×10^{-5}	Carbohydrate metabolism
Glyoxylate and dicarboxylate metabolism	11	0	8	Up	8.00×10^{-6}	6.97×10^{-5}	
Galactose metabolism	4	0	4	Up	1.20×10^{-5}	7.86×10^{-5}	
Fructose and mannose metabolism	3	0	3	Up	1.40×10^{-5}	7.91×10^{-5}	
Glycolysis/gluconeogenesis	5	0	5	Up	5.40×10^{-5}	0.000199	
Citrate cycle (TCA cycle)	7	0	7	Up	9.60×10^{-5}	0.000301	
Pentose phosphate pathway	3	0	3	Up	0.000106	0.000309	
Butanoate metabolism	6	0	6	Up	0.000115	0.000313	
Ascorbate and aldarate metabolism	3	0	3	Up	0.00013	0.000332	
Pentose and glucuronate interconversions	5	0	5	Up	0.000211	0.000508	
Pyruvate metabolism	6	0	6	Up	0.000333	0.000717	
Propanoate metabolism	4	0	3	Up	0.000623	0.001215	
Oxidative phosphorylation	5	0	4	Up	0.000295	0.000671	Energy metabolism
Sulfur metabolism	6	2	4	Up	0.025918	0.034278	
Biosynthesis of unsaturated fatty acids	4	0	3	Up	0.001717	0.002815	Lipid metabolism
Primary bile acid biosynthesis	3	0	2	Up	0.00549	0.008336	
Glycerophospholipid metabolism	4	2	1	Down	0.01947	0.027526	
Pyrimidine metabolism	16	7	3	Down	0.116182	0.136098	Nucleotide metabolism
Purine metabolism	20	7	5	Up	0.257673	0.270886	

Arginine biosynthesis	10	0	8	Up	1.00×10^{-6}	1.02×10^{-5}	Amino acid metabolism
Valine, leucine, and isoleucine degradation	3	0	3	Up	9.00×10^{-6}	6.97×10^{-5}	
Alanine, aspartate, and glutamate metabolism	12	0	10	Up	1.80×10^{-5}	8.97×10^{-5}	
Valine, leucine, and isoleucine biosynthesis	4	0	4	Up	2.50×10^{-5}	0.0001	
Phenylalanine metabolism	5	0	5	Up	6.20×10^{-5}	0.00021	
Arginine and proline metabolism	17	3	9	Up	0.000503	0.00103	
Cysteine and methionine metabolism	13	4	9	Up	0.001386	0.00247	
Phenylalanine, tyrosine, and tryptophan biosynthesis	3	0	3	Up	0.00163	0.002784	
Glycine, serine, and threonine metabolism	13	4	7	Up	0.00343	0.005408	
Lysine degradation	7	5	1	Down	0.07318	0.093761	
Histidine metabolism	9	2	3	Up	0.143679	0.163634	
Tyrosine metabolism	7	2	4	Up	0.214087	0.230988	
Tryptophan metabolism	4	1	2	Up	0.377303	0.386735	
D-Glutamine and D-glutamate metabolism	3	0	3	Up	2.00×10^{-6}	2.05×10^{-5}	Metabolism of other amino acids
Taurine and hypotaurine metabolism	7	1	5	Up	0.001137	0.002118	
beta-Alanine metabolism	9	4	2	Down	0.113484	0.136098	
Glutathione metabolism	9	4	4	Up	0.184715	0.204683	
Porphyrin and chlorophyll metabolism	3	0	2	Up	2.30×10^{-5}	0.0001	Metabolism of cofactors and vitamins
Nicotinate and nicotinamide metabolism	8	1	5	Up	0.00984	0.014408	

Thiamine metabolism	8	3	4	Up	0.022741	0.031079	
Vitamin B6 metabolism	3	0	1	Up	0.110406	0.136098	
Pantothenate and CoA biosynthesis	8	3	3	Up	0.505619	0.505619	

Table 4. List of the 41 KEGG metabolic pathways tested on minimum of three identified metabolites. Name, number of down- and upregulated features, raw *p*-value, and adjusted *p*-value are all presented for each pathway. According to the adjusted *p*-value the *Mecp2$^{-/y}$* neocortex showed significant changes in 31 of the indicated metabolic pathways. Reproduced from Golubiani G, Lagani V, Solomonia R, Müller M. (2021). Metabolomic Fingerprint of *Mecp2*-Deficient Mouse Neocortex: Evidence for a Pronounced Multi-Facetted Metabolic Component in Rett Syndrome. *Cells*. 10: 2494.

It is becoming clear that the neocortex of *Mecp2$^{-/y}$* mice displays a variety of abnormal metabolic symptoms due to the pathways' significant cellular dysfunction. In view of the magnitude of metabolic changes detected, it certainly can be expected that proper brain functioning will most likely be significantly affected by these dysregulations. These metabolic alterations are fully explained in the following "Discussion" section, and a visual representation of the malfunctioning metabolism is shown in Figure 13.
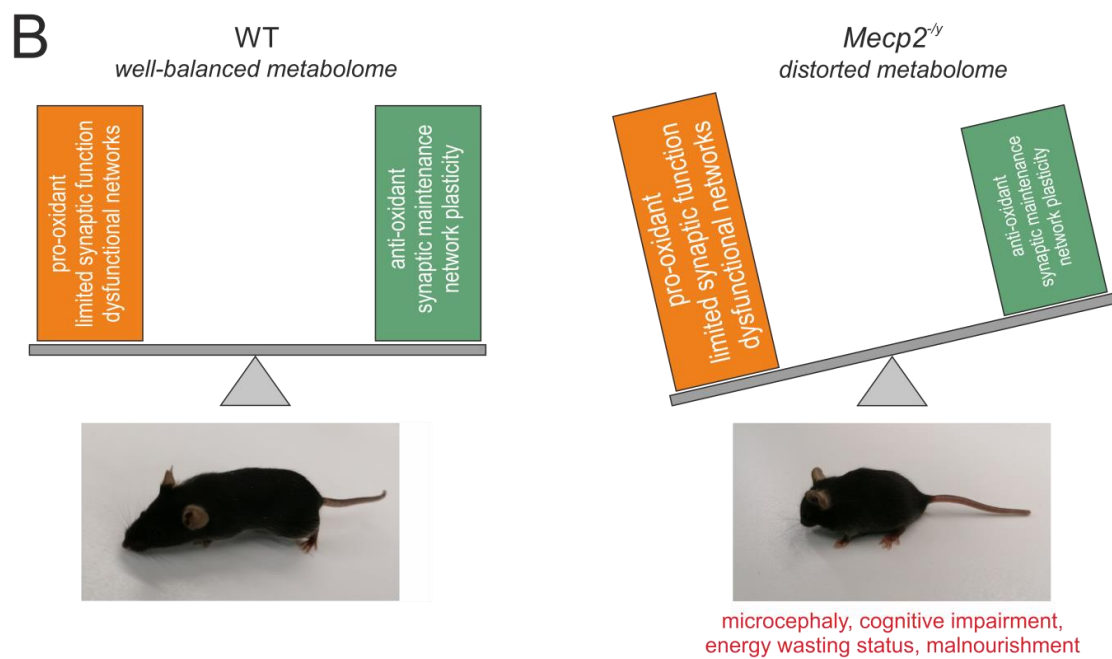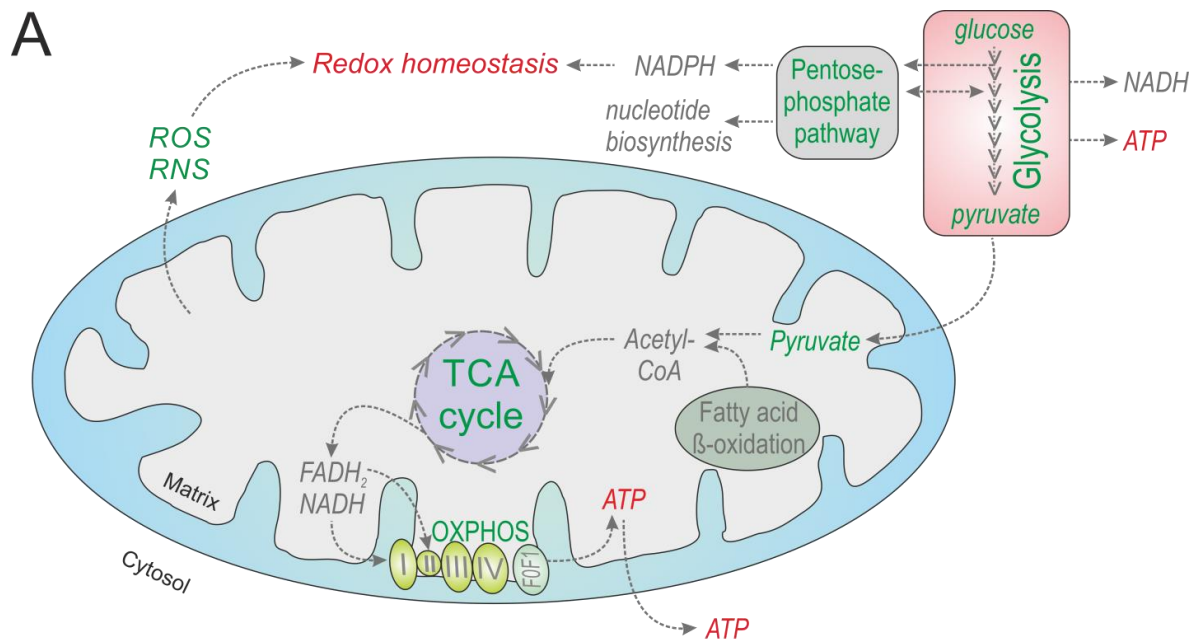
Figure 13. Multiple metabolic abnormalities in the brain of the *Mecp2*-deficient animal. Our unsupervised metabolomics research has revealed several key metabolic pathways that have been dramatically changed. Red font denotes downregulation and disruption, whereas green font represents upregulation (A). The entity of impacted metabolites is likely a contributor to the distinctive traits of RTT, which have been extensively described in a number of prior investigations. For instance, this can entail fostering pro-oxidant circumstances that cause a cellular redox imbalance, limiting synaptic function and network plasticity, and encouraging an energy-wasting state (B). Reproduced from Golubiani G, Lagani V, Solomonia R, Müller M. (2021). Metabolomic Fingerprint of *Mecp2*-Deficient Mouse Neocortex: Evidence for a Pronounced Multi-Facetted Metabolic Component in Rett Syndrome. *Cells*. 10: 2494.

4.6 ROS measurement

Mitochondrial ROS formation was rated based on the oxidation-sensitive dye H_2DCFDA. Upon oxidation, this dye is converted irreversibly into a fluorescent product. Therefore, in the experiments the oxidation becomes evident as an increase in fluorescence over time. Since the omitted fluorescence at the starting point of each individual RTT and WT sample does not differ from each other, the recorded ROS changes were normalized to that starting point, which allowed reducing data variability. Recordings show significant rises of overtime oxidation rates in RTT hippocampus and neocortex compared to WT, where hippocampus seems more prone to the intensified ROS release compared to neocortex (Figure 14).
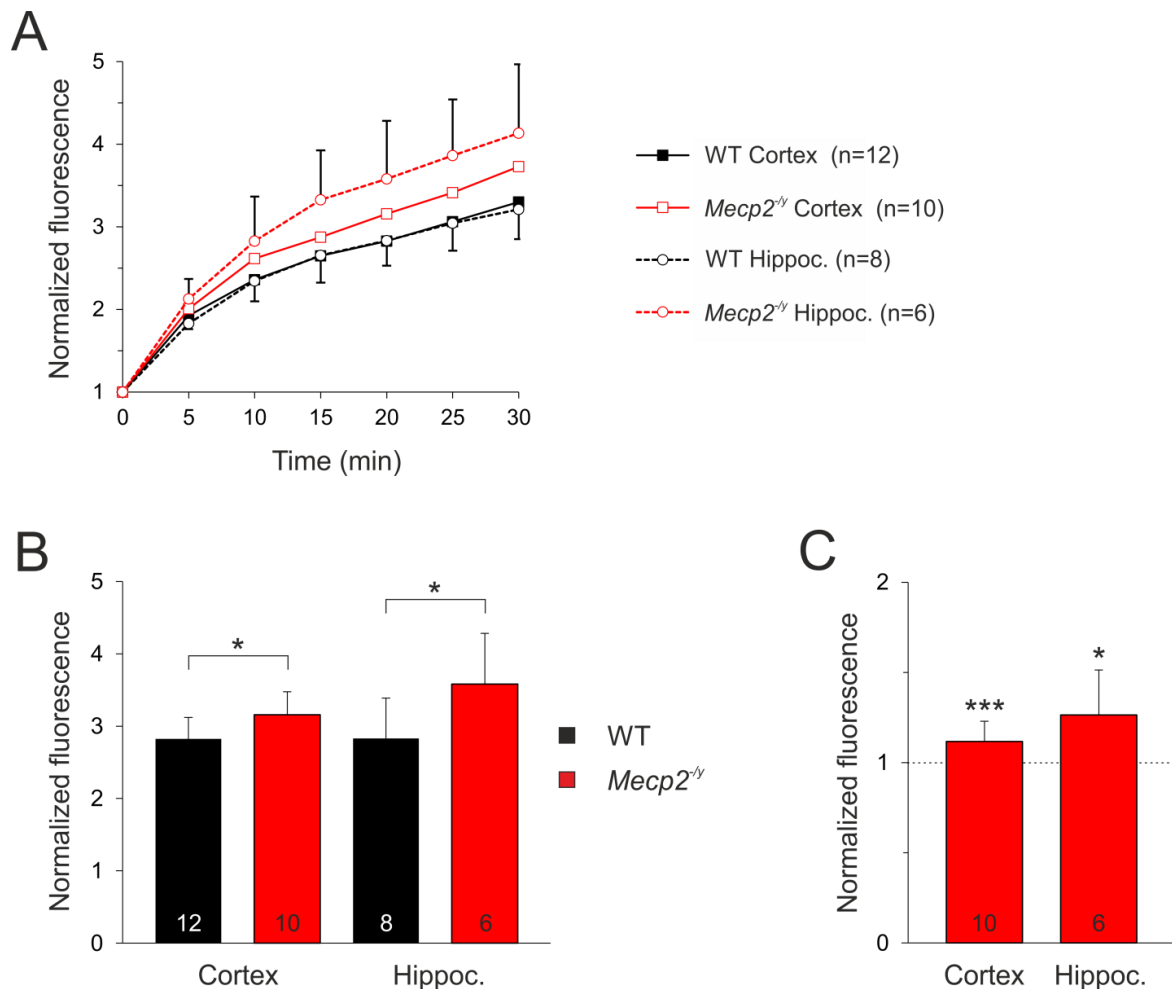
Figure 14: ROS generation measurements with H_2DCFDA: ***$p < 0.001$, * $p < 0.05$. "n" is the number of samples analyzed. A) build-up of H_2DCFDA fluorescence over time for the indicated WT and $Mecp2^{-/y}$ samples from hippocampus and neocortex. B) Summary at the 20 min time point. C) Fluorescence changes reached after 20 min, normalized to the mean of WT conditions.

5. Discussion

Range of data collected from Rett syndrome mice model by different experimental approaches provide proof of various changes in proteomic, metabolomic and physiological status in *Mecp2$^{-/y}$*. Although differences can clearly be seen, it is hard to say decisively which might be involved in developing the pathological impairments and which might be caused by compensatory response on presented challenges.

5.1 Proteomic results

Experimental findings demonstrate significant differences between the mitochondrial proteomes of *Mecp2$^{-/y}$* mice and their WT counterparts. These results were acquired by an *ad hoc* method, which included selecting proteins involved in mitochondrial dynamics, and additionally, we performed investigations using the proteomics approach of 2-D electrophoresis and subsequent MS analysis, which does not make any a priori assumptions about the involvement of specific proteins. The differences that had been noticed in 2-D, were further confirmed for particular proteins by using Western immunoblotting. It is interesting to note that all of the mitochondrial proteins that we detected and confirmed to be differentially expressed among the two genotypes, are nuclear-encoded proteins. In the neocortex and hippocampus of *Mecp2$^{-/y}$* mice, we discovered bidirectional alterations in the expression levels of mitochondrial proteins. Generally, the MeCP2 protein works as a transcriptional gene inhibitor, in specific circumstances it may also play a role as a transcriptional gene activator (Chahrour et al., 2008). This implies that protein integrity distorting mutations in the *MECP2* gene may cause both, the up-regulation and down-regulation of various genes, as was also seen in the current investigation. We also leave open the possibility that some of these variations are a result of the *Mecp2* knockout condition in the hemizygous mice.

5.2 Mitochondrial fusion/fission dynamics.

Anomalies in the general morphological appearance, including the size of the mitochondria are present in RTT patients and mouse models (Eeg-Olofsson et al., 1990;Dotti et al., 1993;Cornford et al., 1994;Bebensee et al., 2017). Mitochondrial mass as well as the present number of mitochondrial particles is increased in astrocyte cell cultures grown from *Mecp2$^{-/y}$* mice compared to WT cultures (Bebensee et al., 2017). Considering the given information, mitochondrial fission and

44

fusion as well as their precise regulation (mitochondrial dynamics) apparently are thrown off-balance during RTT pathology. Our findings showed that *Mecp2$^{-/y}$* mice have lower levels of mitofusin-1 in their neocortex. The hippocampus had a similar tendency, but the difference was not statistically significant. The increased numbers of mitochondria and their distorted shapes in RTT can be at least partially be attributed to decreased mitochondrial fusion. We propose that these flaws in the kinetics of mitochondrial fusion and fission may also contribute to aberrant mitochondrial functioning. It is widely known that altered mitochondrial dynamics are closely associated with quite a number of CNS disorders (Simmons et al., 2020). The abnormal fission and fusion of mitochondrial processes in glial cells is tightly related to the glia activation as part of inflammatory responses (Rahman and Suk, 2020). Preclinical research shows that restoring mitochondrial homeostasis - by boosting mitochondrial biogenesis - slows the course of injury and improves functional recovery (Simmons et al., 2020). Interestingly, learning and memory are crucially linked to higher levels of mitofusin-1 and DRP-1, and the higher levels of these two proteins do correspond with learning effectiveness (Margvelani et al., 2018). Since the progression of RTT gives rise also to poor memory performance (Samaco et al., 2013;He et al., 2022), decreased protein expression levels of mitofusin-1 protein might be part of the complex clinical manifestation of this disorder.

In 2-D electrophoresis experiments, we were not able to detect different levels of mitofusin-1 between the two groups of mice studied. As emphasized in the Methods section only spots, that were differing in intensity at least by two fold were targeted and analyzed by MS. For that reason, mitofusin-1 might not have fallen into the selected group of spots for subsequent MS analysis.

Mitochondria in dermal fibroblast obtained from RTT patients are characterized by obviously disordered morphological appearance of a hyper-fused condition. In addition, mitofusins 1 and 2 were proven to be upregulated, whereas dynamin related protein 1 and mitochondrial fission 1 protein were downregulated in these cells. Furthermore, these fibroblasts exhibited a defective PINK1/Parkin-mediated mitochondrial clearance (Crivellari et al., 2021).

5.3 Complex I components of the OXPHOS system

Within the mitochondrial respiratory chain, complex I is the biggest and the most elaborate enzyme structure (Janssen et al., 2006). In the hippocampus of the *Mecp2$^{-/y}$* mice - in comparison to WT

animals - three components of this complex, NADH-ubiquinone oxidoreductase 75 kDa subunit (NDUSF1), NADH dehydrogenase [ubiquinone] iron-sulfur protein 8 (NDUFS8), and NADH dehydrogenase [ubiquinone] flavoprotein 2 (NDUFV2), were upregulated. Measurement of NADH:ubiquinone oxidoreductase subunit B8 (NDUFB8) in the hippocampus and neocortex did not identify any genotype-related variations among the mouse strains though. An analogous situation seems to be present in the case cytochrome b-c1 complex subunit 1, which will be discussed in following subchapter.

Six and fifteen month old rats do not differ by cortical complex I activity, but still 2-D electrophoresis analysis showed a decrease in NDUFV2 and NDUFS1 subunits (Tatarkova et al., 2016). The binuclear Fe-S cluster, which is integral to the NDUFV2 protein, may serve as an antioxidant electron transporter. Yet it does not take part in the transfer of electrons from FMN to ubiquinone (Janssen et al., 2006). Given the oxidative burden brought on by the condition of RTT, this overexpression might act as a protective mechanism. In any event, the alterations seen for the chosen complex I subunits suggest that this very complex is flexible in terms of how mitochondria and cells function, and these alterations might therefore be considered potential compensatory responses under the neuropathological RTT conditions. In several brain regions from people affected by the disorders Down syndrome, Alzheimer's disease, and schizophrenia, there is a decrease in the protein levels of complex I subunits expressing genes NDUFV2 and NDUFS1 (Kim et al., 2001;Karry et al., 2004). Reduced NADH dehydrogenase enzyme activity was found in a patient with a severe clinical appearance of RTT (Coker and Melnyk, 1991). Potential alterations in complex I composition and/or activity have also been noted in a number of *Mecp2*-mutant mice models. Core complex I (NDUFS8) and complex II (SDHB sub) subunit protein expression levels are decreased in female *Mecp2*-mutant mice (De Filippis et al., 2015b). Prior to this, a somewhat diminished level of a complex I core subunit (NDUFB8) also was discovered in *Mecp2*$^{-/y}$ neocortex and hippocampus in comparison to WT (Can et al., 2018). However, it should be noted that, in the present thesis an internal protein standard was used, while the earlier study relied on GAPDH expression as the internal reference. On the genetic level, reduced mRNA levels of NADH dehydrogenase subunit 2 were seen in the mitochondria obtained from the whole brains of *Mecp2*-deficient animals, but not in those with mild symptoms at the early disease stage (Kriaucionis et al., 2006).

5.4 Complex III components of the OXPHOS system

Our 2D-gel studies reveal that cytochrome b-c1 complex subunit 1 is expressed more abundantly in the *Mecp2$^{-/y}$* neocortex and hippocampus. The ubiquinol-cytochrome c oxidoreductase, a multi-subunit transmembrane complex that is a member of the mitochondrial electron transport chain and promotes oxidative phosphorylation, contains this protein as one of its constituents (complex III).

Findings of a potential role of cytochrome b-c1 complex subunit 1 in RTT pathology are in line with an earlier differential display approach study which revealed only one upregulated gene, namely UQCRC1 in the whole brain of *Mecp2$^{-/y}$* mice (Kriaucionis et al., 2006). The mRNA coding for UQCRC1 was found to be upregulated 1.7 fold in mutant mice (Kriaucionis et al., 2006).

The cytochrome b-c1 complex subunit 2 was assessed as part of our Western-blot analysis of OXPHOS complexes, but no appreciable genotype-related changes were discovered in the hippocampus or neocortex. Along these lines, it was not possible to locate any published information on the equivalent effects of different treatments or pathological circumstances on these two subunits.

In the hippocampus of mice subjected to prolonged nicotine treatment, the protein cytochrome b-c1 complex subunit 1 was found to be increased (Matsuura et al., 2016). It is important to note that this increase was observed in precursor form of cytochrome b-c1 complex subunit 1 together with other proteins, which are generally located in the cytosol, indicating that this protein underwent compelling alterations after being exposed to pathology (Matsuura et al., 2016). In vitro peroxynitrite treatment of isolated beef heart mitochondria causes subunit 1 of the cytochrome b-c1 complex to become nitrosylated, whereas subunit 2 did not experience the same posttranslational alterations (Kohutiar et al., 2018). In a rat model of nonalcoholic fatty liver disease, proteomic analyses of the hepatic mitochondria indicated a decrease in cytochrome b-c1 complex subunit 1, but not a decline in subunit 2 expression (Lee et al., 2018). Cytochrome b-c1 complex subunit 1 alterations have also been detected as part of the ischemia-reperfusion mediated damage (Lin et al., 2012). Furthermore, high-litter size spermatozoa exhibited high levels of cytochrome b-c1 complex subunit 2, whereas low-litter size spermatozoa expressed high levels of cytochrome b-c1 complex subunit 1 (Kwon et al., 2015). Accordingly, subunit 2 expression was

positively connected with litter size, but subunit 1 expression was inversely correlated with litter size (Kwon et al., 2015). All of these findings suggest that these two cytochrome b-c1 complex subunits play distinct roles in the operation of complex III. Besides, alterations in any of them are not frequently linked with the corresponding changes in the other subunit.

Previously, our laboratory assessed the expression of yet another subunit, cytochrome b-c1 complex subunit 5. In these analyses, GAPDH was used as the internal reference, and no statistically significant differences among the hippocampi and cortices of WT and $Mecp2^{-/y}$ mice were detected (Can et al., 2018).

Our metabolomics findings show that the cortical tissue isolated from $Mecp2^{-/y}$ mouse brain has more OXPHOS metabolites than compared to the age-matched WT neocortex (Golubiani et al., 2021). This might be a way to make up for the mitochondrial dysfunction and for the obviously ineffective mitochondrial respiration that has been shown in RTT-syndrome mouse models (Kriaucionis et al., 2006;De Filippis et al., 2015b;Can et al., 2018;Golubiani et al., 2021). This suggestion is supported by the rise in cytochrome b-c1 complex subunit 1.

It is well described, that the distinct respiratory complexes I, III and IV can form various multicomponent supercomplex combinations, which can exist simultaneously with unbound complex III2 and complex IV (Cruciat et al., 2000). It is yet unknown how the structural remodeling of the mitochondrial respiratory chain can adapt OXPHOS function to various energy requirements through the regulatory mechanisms of supercomplex formation (Fernández-Vizarra and Ugalde, 2022). For human cells and postmitotic tissues is has recently been demonstrated that two distinct mitochondrial respiratory chain organizations, C-MRC and S-MRC, are present side-by-side. This coexistence appears to be characterized by the preferential expression of the three distinct COX7A subunit isoforms COX7A1, COX7A2, and SCAFI (Fernández-Vizarra et al., 2022). Chances are, that supramolecular assemblages in the mitochondria of $Mecp2$-deficient brains may crucially influence the unique characteristics of these organelles. Any gross changes in supercomplex construction do not appear to exist in adult $Mecp2^{-/y}$ animals, at least not in the hippocampus, the neocortex, and in heart tissue (Can et al., 2018). As mentioned before, assessment of the hippocampi and the cortices of WT and $Mecp2^{-/y}$ mice for altered cytochrome b-c1 complex subunit 5 expression in comparison to GAPDH has found no discernible changes (Can et al., 2018). At the transcript level (mRNA), the

whole-brain based transcriptome of the "Bird" mouse model was showing a 1.7 fold increase of cytochrome b-c1 complex subunit 1 in early and late symptomatic mice . However, Western blots were unable to identify any matching changes in protein expression (Kriaucionis et al., 2006). Complex II+III enzyme activity was shown to be reduced in the skeletal muscle of male *Mecp2*-mutant mice, but not in their whole brains, their cerebelli, or their hippocampi (Gold et al., 2014). This may also spark a discussion on the extents of brain-related mitochondrial alterations versus those arising in peripheral organs.

5.5 ATP synthase complex of the OXPHOS system

2D gels and subsequent MS analysis show that *Mecp2$^{-/y}$* hippocampal ATP-synthase subunit d is upregulated. Earlier, the ratio of ATP-synthase subunit beta (ATP5B) to GAPDH was found to be lower in *Mecp2$^{-/y}$* neocortex compared to WT neocortex. Additionally, a decreased activity of complex V was seen in symptomatic female *Mecp2*-mutant mice (De Filippis et al., 2015b;Valenti et al., 2017). Existing data display a range of findings about the *Mecp2*-deficient brain tissue´s metabolic status. Reduced brain ATP levels in *Mecp2*-null mice have been documented (Saywell et al., 2006), neurons of the neonatal *Mecp2$^{-/y}$* hippocampus produce more ATP, but they also have faster ATP turnover rates (Toloe et al., 2014), whereas comparable ATP tissue levels were found in *Mecp2$^{-/y}$* mouse hippocampal slices. Finally, female *Mecp2*-mutant mice had significantly lower ATP levels as well (Fischer et al., 2009). It appears that in order to address the problem of cellular ATP supply and energy consumption in *Mecp2*-deficient neural networks, more in-depth research with cell-type specific resolution would be necessary.

5.6 Modulatory and metabolic key players

In comparison to WT mice, *Mecp2$^{-/y}$* animals showed considerably higher levels of the protein prohibitin 1 in both their hippocampi us and their neocortices. Although prohibitin 1 and prohibitin 2 are found in the cytosol, mitochondria, and the nucleus, increasing evidence points to a crucial role for mitochondria (Signorile et al., 2019). These two proteins join together at the inner membrane of mitochondria to form a supramolecular structure and to control mitochondrial metabolism (Signorile et al., 2019). Prohibitins physically interact with respiratory complex subunits and modify their stability and translation, which contributes to their role in the regulation of OXPHOS system activity (Signorile et al., 2019). It was demonstrated that prohibitin 1

overexpression boosts complex I-dependent, NADH-fueled, mitochondrial respiration and thereby facilitates ATP synthesis (Liu et al., 2009;Li et al., 2015). Vice-versa, respiratory chain complexes express less and perform less well when prohibitin 1 is downregulated (Merkwirth et al., 2012;Supale et al., 2013). Our metabolomics data (see "Results" suggested that *Mecp2$^{-/y}$* mice's brain had higher OXPHOS activity levels. We therefore propose that this process may be aided by the elevated levels of prohibitin-1.

Creatine kinase B was found to be an increased protein in the mitochondrial fraction of the *Mecp2$^{-/y}$* hippocampus, and Western blotting further supported the observed changes. By activating the K$^+$/Cl$^-$ cotransporter KCC2, which is particular to neurons, creatine kinase B exerts critical effects on GABAergic neurons in addition to playing a significant role in maintaining brain energy balance (Inoue et al., 2006). Epigenomic analyses were performed in dermal fibroblasts from RTT monozygotic twins, which despite having the same *MECP2* mutation as well as identical X-chromosome inactivation patterns, showed varied illness manifestation and severity (Miyake et al., 2013). The upstream regions of genes essentially contributing to proper brain function, such as creatine kinase B, showed variations in DNA methylation between the twins´ fibroblasts. As expected, the degree of gene expression was inversely linked with the degree of methylation in these upstream areas (Miyake et al., 2013). No controls were employed in this investigation though: Hence, it is unclear whether creatine kinase B is elevated or depressed in comparison to healthy controls. However, the elevated levels of creatine kinase B seen in the hippocampus of our *Mecp2*-null mice may be a result of compensatory modifications intended to enhance brain energy homeostasis.

The protein 14-3-3 theta is downregulated in *Mecp2$^{-/y}$* neocortex, according to the 2-D electrophoresis assays performed. The additional Western immunoblotting tests confirmed this conclusion. A class of scaffolding proteins known as 14-3-3 proteins, which are found in all eukaryotes, regulate a wide range of other cellular proteins by fine-shaping their functions or activities (Obsilova and Obsil, 2022). Consequently, these proteins take part in important physiological functions like energy metabolism (Obsilova and Obsil, 2022). When the electron transport chain is compromised and the redox state is disrupted, upregulating the 14-3-3 protein enhances mitochondrial activity (Qiao et al., 2020). As a result, we propose that the observed downregulation of 14-3-3 theta in the neocortex of *Mecp2$^{-/y}$* mice may be a factor in the altered

mitochondrial functioning along the progression of RTT. *Mecp2$^{-/y}$* mice have decreased levels of gamma enolase in their neocortex and hippocampus. Enolases are cytosolic carbon-oxygen lyases that are highly expressed and involved in the metabolism of glucose. Alpha, beta, and gamma are the three isozymes of enolase that are produced by separate genes in vertebrates. Beta enolase is only found in muscles, gamma enolase is only found in neurons, and alpha enolase is present everywhere (Isgrò et al., 2015). Beyond glycolysis and gluconeogenesis, enolase has recently been demonstrated to perform a number of regulatory activities (Butterfield and Lange, 2009). Five substances involved in the glycolysis and gluconeogenesis processes were upregulated, according to our earlier metabolomics research (Golubiani et al., 2021). Therefore, it seems odd that one of the crucial enzymes involved in glycolysis processes has been downregulated. However, we must consider that the cytosolic fractions were not examined and that the downregulation of gamma enolase was seen in the mitochondrial fraction of the neocortex and hippocampus of *Mecp2$^{-/y}$* mice. Enolase is found in the intermembrane space/outer mitochondrial membrane fraction, according to published research (Giegé et al., 2003;Poon et al., 2005). Enolase may also play a distinct extra role in the operation of the mitochondria by transporting particular tRNAs. According to research on yeast, only around 3% of the total lysine transfer RNA acceptor 1 (tRK1) pool enters mitochondria, whereas the second isoacceptor, tRK2, stays in the cytosolic compartment. Under stressful circumstances, it is hypothesized that tRK1's regulation of mitochondria will increase mitochondrial translation. Enolase 2 facilitates the import of tRK1 into the mitochondria (Baleva et al., 2015). By analogy, we can hypothesize that gamma enolase downregulation contributes to another, as of yet unexplained, involvement of this enzyme in mitochondrial function despite the increase of glycolysis.

5.7 Linking the changes in mitochondrial proteome to functional alterations

Obtained data conclusively demonstrate significant abnormalities to the mitochondrial proteome in the brain and hippocampus of male *Mecp2*-deficient mice. These variations add important information to our understanding of the unique condition of brain mitochondria in RTT-related disease. The finding, that the two brain regions' changes in protein expression only partially overlap, highlights the significance of investigations that are carefully focused particular to each relevant brain region. Also, this demands a thorough cross-regional comparison to be performed.

Only then can the complete picture of mitochondrial changes along the various steps of RTT pathogenesis be clarified.

Transcriptional analysis on patient-derived peripheral blood samples revealed a number of mitochondria-relevant genes to be primarily elevated (Pecorelli et al., 2013). In addition, a review of the RTT-related modifications in human-derived tissues indicates mitochondria as one of the three primary targets impacted by RTT, along with dendritic/synaptic abnormalities and glial function (Shovlin and Tropea, 2018). Additionally, whole cell proteomic analyses of the dermal fibroblasts from controls and RTT patients revealed that the expression of proteins involved in the mitochondrial function and performance is subject to a multitude of changes (Cicaloni et al., 2020). RTT patients were shown to have elevated levels of ATP synthase subunit g, cytochrome c oxidase subunit 6B1, NADH-cytochrome b5 reductase 3, and mitochondrial peroxiredoxin-5 patients (Cicaloni et al., 2020). However, tissue specialization can be seen in the mitochondrial makeup and bioenergetic characteristics (Kappler et al., 2019), and variations seen in lymphocytes and fibroblasts may not also be found in brain tissue. However, the overexpression of distinct mitochondrial complexes in different tissues can be interpreted as a sign of diminished performance of mitochondrial respiration, perhaps coupled with abnormal ATP generation (Pecorelli et al., 2013;Shovlin and Tropea, 2018).

No doubt, other tissues also contribute to the clinical expression and severity of RTT, and the brain is not the only organ impacted by mitochondrial changes in this condition. However, given the high metabolic demand of the brain and the lack of cerebral energy stores, any mitochondrial changes are likely to have a particularly negative impact on brain metabolism. The only modification to the mitochondrial proteome in post-mortem brain tissue from RTT patients that has been detected thus far is a reduction in cytochrome c oxidase subunit I. However, rather than at the protein level, this downregulation was seen at the mRNA level (Gibson et al., 2010). Determining the specifics of these changes and identifying the functional effects in the various brain regions will therefore be challenging but highly interesting tasks.

5.8 Metabolomics fingerprinting

The metabolomes of the *Mecp2$^{-/y}$* and WT mouse neocortex are clearly and significantly different from one another, according to our results. These variations were found in mice raised in the same

environment and fed the same nutrients composition. According to our knowledge, this is the first study of its sort to pay particular attention to variations in the full metabolome between the neocortical tissue of an RTT mouse model and WT mice. Previous research on the changes in brain metabolites in postmortem patient tissue samples or in *Mecp2*-mutant mice was ad hoc and focused on a certain subset of chemicals, primarily neurotransmitters and the breakdown products of these compounds. Only one untargeted metabolome investigation, concentrating on the blood plasma of RTT patients and control people, has been carried out to date (Neul et al., 2020). It must be mentioned that we studied the most severe conditions arising in the adult male, hemizygous *Mecp2$^{-/y}$* mouse model. Whether the X-chromosomal mosaicism present in female heterozygous mice may be associated with less pronounced metabolic derangements remains to the clarified. Mutations in the transcriptional modulator MeCP2 are the cause of the neurodevelopmental synaptopathy RTT, and already existing information strongly supports its link to variations in the expression of several genes (Amir et al., 1999;Johnson et al., 2017;Osenberg et al., 2018). Finding out which of these alterations are causally responsible for the pathological states, which ones simply represent compensatory measures, and which ones do not meet neither one of the two criteria, is one of the biggest hurdles for RTT as well as other neuropathologies.

5.9 Carbohydrate Metabolism

The first two products of glycolysis, glucose and glucose-6-phosphate, are present at higher levels in the neocortex of *Mecp2$^{-/y}$* mice, which, in light of the changes in glycolysis, leads us to hypothesize that glucose metabolism is enhanced in this area of the brain. Fructose 1,6-bisphosphate, glyceraldehyde 3-phosphate, and pyruvic acid concentrations were also noticeably raised. It is also reasonable to suppose that an increased glycolytic rate will result in a greater absorption of glucose by the brain. These data sheds additional light on the earlier results of our laboratory, where it was shown that glucose transporter SLC2A4 was upregulated in the CA1 region off hippocampus of *Mecp2$^{-/y}$* mice (Großer et al., 2012). In the same mouse model blood sugar is decreased (Janc et al., 2016a). Additionally, the *Mecp2$^{-/y}$* neocortex exhibits an upregulation of the pentose phosphate pathway. Nicotinamide adenine dinucleotide phosphate (NADPH), which is produced by this pathway and fed into reductive biosynthesis processes, is a crucial component contributing to the cellular redox equilibrium. Therefore, its overexpression could be seen as compensatory in

supplying the neocortex under the disease-related conditions of oxidative stress with the sufficient reducing equivalents.

Erythritol is elevated in the neocortex of *Mecp2$^{-/y}$* mice. Recent research has demonstrated that erythritol, a reduced version of the monosaccharide erythrose and an intermediate of the reductive pentosephosphate pathway, can be produced endogenously from glucose (Hootman et al., 2017). The elevated amount of erythritol in the neocortex of *Mecp2$^{-/y}$* mice may be due to the enhanced glucose metabolism. It's interesting to note that patients with mental illness have brains with higher erythritol levels (Zhang et al., 2016). Further investigation is required to determine the significance of the elevated erythritol level, because significant cognitive impairment is one of the characteristic traits of RTT.

Seven metabolites of the tricarboxylic acid (TCA) cycle are increased in *Mecp2$^{-/y}$* neocortex. The following 5 metabolites, namely; succinic acid, L-malic acid, alpha-ketoglutaric acid, citric acid, and thiamine pyrophosphate (a cofactor in the in the pyruvate decarboxylation reaction catalyzed by the pyruvate dehydrogenase complex) are substantially elevated. This unequivocally demonstrates that this pathway is dysregulated in the *Mecp2$^{-/y}$* mouse brain. Our metabolomics data represents, as far as we are aware, the first concrete proof of alterations in the TCA cycle in the *Mecp2$^{-/y}$* brain. With seven identified and elevated metabolites, the TCA cycle is unquestionably one of the core metabolic pathways that has been most significantly altered. The cerebral fluid (CSF) of RTT patients was examined for lactate, pyruvate, and citric acid cycle intermediates (Matsuishi et al., 1994). Of the entity of citric acid cycle metabolites, only alpha ketoglutarate and malate were significantly increased in these individuals when compared to control subjects. . This data also indirectly suggests elevated levels of citric acid cycle metabolites in the brain tissue, because the CSF metabolome is a reflection of the brain metabolome. For many downstream metabolic pathways, the TCA cycle is crucial. Its primary tasks include producing NADH and FADH$_2$ for mitochondrial respiration and releasing energy through the oxidation of acetyl-CoA obtained from carbs, lipids, and proteins. Because of this, the TCA cycle is closely controlled, and ATP inhibits pyruvate dehydrogenase and isocitrate dehydrogenase by acting as an allosteric inhibitor. It is widely recognized that high consumption rates of ATP increases the cellular ADP/ATP ratio and AMP concentrations, which in turn activate the TCA cycle's regulating enzymes (Martínez-Reyes and Chandel, 2020). Consequently, we cannot rule out the possibility that the observed increase in TCA

cycle metabolites is due to aberrant regulation of the cycle itself and a compensatory effort by the *MeCP2*-deficient organism. The total quantity of energy produced would rise as a result of increased TCA-enhanced glycolytic activity. At the same time, there would be more reduced NADH available to feed into various systems, such as the mitochondrial respiratory chain. Recent studies suggest that TCA cycle intermediates play an extra, novel role in signaling molecules that regulate chromatin changes, DNA methylation, hypoxia responses, and immunology (Martínez-Reyes and Chandel, 2020). In particular in tumors and in activated macrophages, succinate itself stabilizes the transcription factor - hypoxia inducible factor (HIF)-1, activates dendritic cells via succinate receptor 1, and post-translationally changes proteins (Mills and O'Neill, 2014). It is unclear, however, whether such prolonged succinate-mediated signaling also applies to *Mecp2*-deficient brain tissues. In line with these data, our earlier observations about altered hypoxia responses and elevated levels of HIF-1 alpha throughout the brain in *Mecp2$^{-/y}$* mice (Fischer et al., 2009;Kron and Müller, 2010) may gain additional interest.

5.10 General energy metabolism

Mecp2$^{-/y}$ animals had significantly higher levels of ADP, AMP, and orthophosphate in their neocortex. The largest amount (80-90%) of the brain's energy is consumed by neurons (Yu et al., 2018). Therefore, it is reasonable to assume that these variations are mostly the result of alterations in neuronal energy metabolism. Highly intensive metabolic energy expenditure and replenishment are required for neuronal function. The well-known oxidative phosphorylation effector ADP is thought to be a proximal signal that coordinates metabolic reactions to high energy demands (Yellen, 2018). Glycolysis is regarded as being activated by AMP. It speeds up the activation of the major regulator of the glycolytic pathway, 6-phosphofructo-1-kinase, which is promptly triggered by the activation of 5'-AMP-dependent protein kinase (AMPK) (Bolaños et al., 2008). Therefore, the increased glycolysis and TCA cycle in the *Mecp2$^{-/y}$* neocortex may be partially explained by the reported increases in ADP and AMP. Unfortunately, metabolomics cannot provide a detailed assessment of the electron transport chain (ETC) activity in the mitochondria. Instead, high resolution respirometric techniques are required for this (Doerrier et al., 2018). However, pathway analysis carried by us revealed that the oxidative phosphorylation was elevated due to the increased substrate levels. More substrates go into the mitochondrial ETC as a result of increased glycolysis and TCA cycle activity. This might be a way to cope with diminished mitochondrial

function and ineffective mitochondrial respiration seen in RTT (De Filippis et al., 2015b). Additionally, the elevated substrate levels may result in a dysregulation of the mitochondrial ETC on their own. Increased energy expenditure and enhanced ATP turnover were discovered in neurons of the neonatal *Mecp2*$^{-/y}$ hippocampus , providing evidence for these hypotheses (Toloe et al., 2014), and it has been suggested that under the pathological impact of RTT, mitochondria may operate in a energy-wasting condition (Jin et al., 2015). This may help to explain why whole brain examinations of male and female *Mecp2*-mutant mice revealed lower ATP levels (Saywell et al., 2006;De Filippis et al., 2015b). Focusing on the adult *Mecp2*$^{-/y}$ hippocampus, however in our laboratory work, no evidence of lower ATP levels in that particular brain area was found (Fischer et al., 2009). This highlights the requirement for more in depth, region specific research on the brain's energetics in *Mecp2*-mutant mice. The complete picture can only be obtained after that.

5.11 Amino acid metabolism

The majority of amino acids exhibit clearly higher levels compared to WT, making amino acid metabolism one of the most seriously impacted aspects in *Mecp2*-deficient mouse neocortex. There is currently a dearth of knowledge on the changed amino acid levels in RTT. In one case report on *postmortem* brain tissue, it was discovered that the putamen, pallidum, white matter, caudatum, and thalamus tended to have lower levels of a number of amino acids, However, CSF did not show these concurrent alterations (Riederer et al., 1985). Aspartate, glutamate, cysteine, glycine, and serine levels in RTT patient-derived blood samples were found to have increased or were heading upward, while arginine, histidine, and phenylalanine levels were found to have decreased or were trending downward (Neul et al., 2020). On the contrary, an RTT mouse study using whole brain extracts only saw minor variations in amino acid levels (glutamine increased, GABA trend to decrease). This could be explained by the fact that only a few metabolites have been identified using magnetic resonance spectroscopic analysis, and the use of whole brain extracts may have obscured information particular to certain brain regions (Viola et al., 2007).

The majority of amino acids were found in higher concentrations in the mouse neocortex. Therefore, the frequently-mentioned condition of chronic undernutrition in RTT, which is also demonstrated by the noticeably lower body weights of the *Mecp2*$^{-/y}$ mice, cannot explain for these changes. Thirteen of the 20 proteinogenic amino acids (L-alanine, L-glutamic acid, L-leucine, L-

isoleucine, L-lysine, L-methionine, L-phenylalanine, L-proline, L-serine, L-threonine, L-tryptophan, L-tyrosine, and L-valine) had noticeably higher amounts in the neocortex of the $Mecp2^{-/y}$ mice. Significant alterations in four proteinogenic amino acids were found in the plasma of RTT patients after a metabolomics analysis. In detail, aspartate and glutamate were elevated, whereas arginine and histidine were found to be significantly downregulated (Neul et al., 2020). Only one of these four—L-glutamic acid—was shown to be considerably elevated in our study. These differences between two can be explained by different species (human against mouse) and different specimen sources (neocortex against blood plasma) of the examined metabolomes, the remaining three did not differ. The observed variations highlight the value of targeted, tissue-specific investigations of neuropathological diseases once more. The noticeable rise in more than half of the amino acids that are proteinogenic not only points to aberrant protein synthesis, but also to alterations in the cellular pathways that are connected to certain amino acids or groups of amino acids.

Early presymptomatic stages of RTT do, in fact, show decreased protein synthesis in a number of brain regions, including the neocortex (Ricciardi et al., 2011). L-leucine, L-isoleucine, and L-valine are the three amino acids that make up the class of branched amino acids (BAAs), and all three showed a noticeable increase in concentration in the $Mecp2^{-/y}$ neocortex. BAAs play a role in protein synthesis as well as other crucial brain processes like nitrogen regulation and the cycling of neurotransmitters. They can also be used as energy substrates in the TCA cycle (Sperringer et al., 2017). Neuropathological disorders are associated with variations in BAA concentrations. L-leucine incubation of cerebral neocortex homogenates causes an increase in thiobarbituric acid-reactive compounds, which causes oxidative stress (Bridi et al., 2005). Cultured cortical astrocytes' shape and cytoskeletal organization are changed when exposed to BAAs (Funchal et al., 2005). Thus, the oxidative burden in RTT and the increased TCA cycle activity suggested by our data may be caused by elevated BAA levels.

The non-proteinogenic amino acid L-homocysteine, is significantly reduced in the $Mecp2^{-/y}$ neocortex. L-homocysteine belongs to the Sulfur -containing amino acids group. It originates from S-adenosylmethionine, a crucial source of methyl groups for methylation processes like DNA methylation and catecholamine production (Kaplan et al., 2020). Methionine metabolism results in the formation of L-homocysteine, and the methionine level is increased in the $Mecp2^{-/y}$ neocortex (see above). L-homocysteine should thus also be increased. The reverse, however, shows that

additional regulatory pathways reduce its levels. As a result, the methylation of target molecules may be less prominent. The oxidative burden in RTT, which would force the oxidation of L-homocysteine, may be a contributing factor. L-cystin was elevated in the *Mecp2*^-/y neocortex, consistent with the sulfhydryl oxidation that is thought to have occurred. MeCP2, a transcriptional repressor/regulator that binds to methylated CA sites within lengthy genes, is functionally disrupted in RTT, which is the underlying cause of the condition (Guy et al., 2011). Decreased expression of lengthy genes attenuates the physiological abnormalities linked to RTT in neurons missing MeCP2. These lengthy genes are a group of genes that are specifically expressed in the brain tissue and which are essential for neuronal function (Gabel et al., 2015). It can be hypothesized that a lower DNA methylation potency - caused by downregulated L-homocysteine may represent an effort by MeCP2-deficient cells to partially balance vacant methylated DNA binding sites.

5.12 Dipeptides

The *Mecp2*^-/y and WT cortices have significantly different levels of thirteen dipeptides. They are the following compounds: L-glutamyl-L-glutamine, gamma-glutamyl-tyrosine, phenylalanyl-L-glutamic acid, cysteinyl-glycine, L-valyl-glycine, gamma-glutamyl-leucine, L-tryptophyl-L-glutamic acid, L-tyrosyl-glycine. Five of them namely; L-glutamyl-L-glutamine, gamma-glutamyl-tyrosine, cysteinyl-glycine, gamma glutamyl-leucine, and gamma-glutamyl-tryptophan were reduced significantly. Four of these five peptides also contain glutamate. Most of these differently regulated dipeptides have recognized physiological roles. Patients with major depressive disorder exhibit significantly lower plasma levels of gamma-glutamyl leucine (Du et al., 2021).. According to this paper, the low levels of gamma-glutamyl leucine are a result of inadequate glutathione turnover, the primary cellular antioxidant that is essential for maintaining a healthy balance between prooxidants and antioxidants (Dringen et al., 2000;Martin and Teismann, 2009). In fact, both RTT patients and mice have severely disturbed cellular redox equilibrium in their brains (De Felice et al., 2009;Großer et al., 2012;De Felice et al., 2014;Can et al., 2018;Festerling et al., 2020). Astrocytes provide cysteine-glycine for the neuronal production of glutathione (Dringen et al., 1999). The *Mecp2*^-/y mouse neocortex may experience a (partly) disrupted antioxidant capacity and decreased glutathione production as a result of the lower quantity of this dipeptide. Curiously, cysteinyl-glycine is the most drastically downregulated metabolite of all the substances found in the *Mecp2*^-/y neocortex (log2 fold decrease of 4.03). Reactive carbonyls, which result from oxidant-mediated tissue damage,

particularly the oxidation of sugars and polyunsaturated fatty acids, are detoxified by histidine-containing dipeptides, which operate as a cell-endogenous protective mechanism (Song et al., 2014). Histidine-dipeptides weren't among the metabolites that could only be found in our study. The histidine-containing peptides L-carnosine, L-histidylalanine, and L-alanyl-L-histidine, all of which are capable of detoxifying carbonyls, were all assigned to one of the significantly diminished characteristics in the *Mecp2*$^{-/y}$ neocortex. Accordingly, each of these peptides is anticipated to decrease as a result of the oxidative burden in RTT.

5.13 Urea

Urea cycle problems are linked to cognitive and motor impairments, and this metabolite is evidently elevated in the neocortex of *Mecp2*$^{-/y}$ mice (Gropman and Batshaw, 2004). In the urea cycle, arginine is broken down by arginase to produce urea. While other cell types are also involved in the urea cycle, the liver is where it is most concentrated. The two amino acids citrulline and arginine appear to be the primary targets of a partial urea cycle in the brain (Sadasivudu and Rao, 1976). We detected the following metabolites; ornithine, citrulline, arginosuccinate, fumarate, and arginine among the numerous urea cycle components; however, only arginosuccinate was significantly elevated. The urea cycle's rate-limiting phase is the production of carbamoyl phosphate. In our investigation, this particular metabolite was not found or annotated. Given that *Mecp2* deletion in mice also causes a fatty liver, the elevated urea levels in the *Mecp2*$^{-/y}$ neocortex should be seen from a mechanistic perspective as a result of liver failure. However, there was no difference in urea levels between the plasma of RTT patients and control subjects (Neul et al., 2020).

Alzheimer's and Huntington's disease patients, even those with mild Huntington's disease neuropathology, as well as a transgenic sheep model of the Huntington disease, had higher urea levels in their brains (Patassini et al., 2015;Xu et al., 2016;Handley et al., 2017). The urea transporter SLC14A1 was also found to be considerably overexpressed in the striatum of the sheep model of Huntington disease by RNA-Seq analysis (Handley et al., 2017). Astrocytes are main cerebral cells expressing SLC14A1 and this transporter is responsible for facilitated diffusion of urea (Sands et al., 1992;Zhang et al., 2014). As a result, it was believed that the increased SLC14A1 expression was a direct reaction to the raised brain urea levels in Huntington's disease (Handley et al., 2017).

5.14 Neurotransmitters

In the neocortex of *Mecp2*$^{-/y}$ mice, levels of the neurotransmitters dopamine, acetylcholine, and serotonin are noticeably decreased. Methoxytyramine, a metabolite of dopamine, and choline, a precursor and breakdown product of acetylcholine, are also diminished in the *Mecp2*$^{-/y}$ neocortex. The neocortex, according to early research on the *postmortem* brains of RTT patients, has lower amounts of dopamine (Brucke et al., 1987;Wenk et al., 1991). Another study, however, disputed this and asserted that dopamine and its metabolites were present in all areas of the brain at normal levels. A more recent study focused on dopamine transporters and receptors in both humans and mice lacking the *Mecp2* gene (Wenk, 1996;Wong et al., 2018). When it comes to dopamine transporters, there are just slight variations. RTT patients and hemizygous/heterozygous MeCP2-deficient mice had less D2 dopamine receptors in the striatum than normal animals (Wong et al., 2018). It is yet uncertain if the decreased levels of dopamine and methoxytyramine found in the present thesis could be connected to a change in dopamine receptor expression because the neocortex was excluded from study of Wong et al.(2018). Early research on the *postmortem* brains of RTT patients also suggested that the serotonergic system had been down regulated. The rate-limiting enzyme of serotonin production, tryptophan hydroxylase-2, was shown to have lower amounts in parallel with low levels of serotonin (Riederer et al., 1985). By precisely deleting the *Mecp2* gene in serotonergic neurons, a cell-autonomous reduction in brain serotonin levels was induced. As a result, it is possible that the lower serotonin levels are not caused by MeCP2 malfunction in other cell groups (Samaco et al., 2009). This could have a direct impact on the development or the further spread of the illness. A more recent study revealed that fluoxetine can restore motor coordination in *Mecp2* heterozygous mice by enhancing the brain serotonergic system, which raises the possibility that medications that stabilize 5-HT7R neurotransmission can lessen the motor symptoms of RTT (De Filippis et al., 2015a;Villani et al., 2020).

As far as we are aware, our study is the first to show that the brains of *Mecp2*-mutant mice have less acetylcholine than normal. Numerous research have examined the choline levels, cholinergic receptors, vesicular acetylcholine transporters, and enzyme expression in *postmortem* RTT human tissue or MeCP2-deficient mice and those studies report decreased performance of cholinergic system function (Wenk and Hauss-Wegrzyniak, 1999;Ward et al., 2009;Ricceri et al., 2011;Oginsky et al., 2014). *Mecp2* was recently specifically removed from mouse cholinergic neurons, impairing

recognition memory and significantly altering baseline firing in L5/6 neurons (Ballinger et al., 2019). By preventing acetylcholine breakdown, these behavioral and electrophysiological abnormalities were repaired. Together with our findings, this suggests that lower acetylcholine levels are not merely a consequence of *Mecp2* disruption, but rather play a role in the emergence of RTT related pathology (Ballinger et al., 2019).

Additionally, our data show that the *Mecp2*$^{-/y}$ neocortex contains higher levels of glutamate and glutamine. Numerous cellular processes critically rely on the availability of glutamate. In addition to being a neurotransmitter and a precursor to the neurotransmitter gamma-aminobutyric acid (GABA, it is a canonical amino acid utilized for protein synthesis). We cannot assess the differences between GABA and other substances in the *Mecp2*$^{-/y}$ neocortex since GABA was not clearly identified in our investigation. Inside of cells, glutamate can be found as a free amino acid, packaged as a neurotransmitter in synaptic vesicles, or released as a neurotransmitter into the synaptic cleft and extracellular space. It is difficult to determine which specific proportion was elevated because our trials report global glutamate quantities. Released glutamate is transformed into glutamine in astrocytes before being sent to neurons, where it is then turned back into glutamate. As a result, glutamine serves the same classical amino acid role as glutamate while both serving as a precursor to it and a byproduct of glutamate metabolism.

Glutamate levels in *Mecp2*-mutant and WT mice have been studied in two studies so far (Viola et al., 2007;El-Khoury et al., 2014). Genotype-related variations in glutamate content were not found in a whole-brain based study (Viola et al., 2007). According to more successful brain region specific investigations that included the motor neocortex, lower glutamate levels were found only in the *Mecp2*-null mouse hippocampus (El-Khoury et al., 2014). In MeCP2-deficient mice, the equilibrium between synaptic excitation and inhibition is disrupted (Dani et al., 2005;Chao et al., 2007), for that reason, observed higher glutamate and glutamine levels can be involved in those changes. However, cortical pathways in RTT-affected mice exhibit decreased excitation and increased inhibition, rendering them hypoactive (Dani et al., 2005). Determining the precise contribution of the elevated glutamate and glutamine contents to these circumstances is yet unclear.

Several RTT characteristics are replicated when *Mecp2* is specifically deleted in a subpopulation of GABAergic forebrain interneurons: reduced glutamic acid decarboxylase 1 and 2 levels and

decreased GABA immunoreactivity are found in *Mecp2*-deficient GABAergic neurons (Chao et al., 2010). According to these findings, we suggest that the higher glutamate levels in the neocortex are insufficient to compensate for the reduced GABA levels in *Mecp2*$^{-/y}$ mice.

Our metabolomic investigations did not reveal considerably lower cAMP levels in the MeCP2-deficient brain, but they did reveal significantly higher AMP levels. As a result, it is possible to suppose that the cAMP-homeostasis is somewhat altered, which may further contribute to the aberrant synaptic signaling in *Mecp2*-mutant brains.

5.15 Lipid metabolism

The *Mecp2*$^{-/y}$ neocortex has a marked reduction in the quaternary ammonium complex (3-carboxypropyl) trimethylammonium (butyrobetaine). Gamma-butyrobetaine dioxygenase catalyzes the conversion of the precursor butyrobetaine to carnitine in mammals. Additionally, there is a tendency for the *Mecp2*$^{-/y}$ neocortex to have less carnitine, but this difference is not statistically significant. For long-chain fatty acids to be transported into mitochondria for oxidation, carnitine is necessary (VAZ and WANDERS, 2002). Recent research has shown that astrocytes almost solely participate in the mitochondrial oxidation of fatty acids, which accounts for up to 20% of the brain's overall energy (Panov et al., 2014). In light of this, we hypothesize that the *Mecp2*$^{-/y}$ neocortex's energy deficit may be caused in part by the butyrobetaine levels that have dropped. A higher level of both, carnitine palmitoyltransferase 1 A/B and carnitine acylcarnitine translocase was shown to be associated with changes in the carnitine cycle in the heart tissue of female *Mecp2*$^{+/-}$ mice (Mucerino et al., 2017). In the brain of the *Mecp2*$^{-/y}$ mouse, the quantity of arachidonic acid; (5Z,8Z,11Z,14Z)-Icosatetra-5,8,11,14-enoic acid is also noticeably elevated. Arachidonic acid is a target of processes that are catalyzed by free radicals and produce isoprostanes. Isoprostanes are consequently thought of as byproducts of lipid peroxidation, and their levels are elevated in the brains of *Mecp2*-knockout mice and in human patient blood samples (De Felice et al., 2011;De Felice et al., 2014). We did not find any isoprostane metabolites. Arachidonic acid, however, might become more oxidized and lipid peroxidation products also should build up in the *Mecp2*$^{-/y}$ neocortex based on the more oxidizing conditions in RTT, as was shown for complete brain extracts of MeCP2-deficient mice (De Felice et al., 2014). Arachidonic acid may also influence to the pro-inflammatory circumstances in RTT because it is a pro-inflammatory agent (Valacchi et al., 2018).

The brain and liver of male *Mecp2*-null mice were also shown to have altered cholesterol metabolism, and furthermore plasma cholesterol levels are elevated (Buchovecky et al., 2013). Our research supports these findings by confirming that the *Mecp2*$^{-/y}$ neocortex has much higher cholesterol levels.

5.16 Markers of oxidative stress

The analyses conducted as part of this thesis unveiled a number of dysregulated metabolites, which show the effect of the oxidative stress caused by the RTT on the cortical tissue. This includes the decreased quantities of cysteinyl-glycine and L-homocysteine stated above, as well as the higher concentrations of rutin, branched amino acids, and L-cystin. The flavonoid glycoside rutin, which is present in foods like apples and buckwheat, is a potent antioxidant. The microbiota in the intestines metabolize it (Jaganath et al., 2006). According to the clinical severity score in RTT, the gut microbiome has been shown to change toward a less varied and pro-inflammatory composition (Strati et al., 2016;Thapa et al., 2021). In *Mecp2*$^{-/y}$ mice, this could lead to altered bioavailability of unmetabolized rutin. The increased supply of decreased reduction equivalents produced by the accelerated glycolysis and pentose phosphate pathway may also be a response to the oxidative stress. In addition, the *Mecp2*$^{-/y}$ neocortex had higher levels of L-dihydroascorbic acid, an oxidized form of ascorbic acid. Ascorbic acid itself was not changed in content. But the buildup of its oxidized state in the *Mecp2*$^{-/y}$ brain seems to be another effect of the oxidative load. According to this theory, earlier investigations of *postmortem* brain tissue from an RTT patients found that the neocortex and other regions of the brain had lower levels of ascorbic acid (Sofić et al., 1987).

6. Conclusions

- The mitochondrial proteome of the MeCP2-deficient mouse brain differs from that of WT mice.

- The observed mitochondrial proteome differences are brain-region specific and at least involve neocortex and hippocampus.

- On the molecular level, the mitochondrial proteome differences include proteins of the oxidative phosphorylation system as well as other mitochondrial regulatory proteins.

- Untargeted metabolomic analyses identified a plethora of affected metabolites in the neocortex of $Mecp2^{-/y}$ mice, which convincingly demonstrates that RTT is associated with a highly complex and critical metabolic component.

- The pathology of RTT starting from one gene mutation includes nearly all levels of cellular activities including the metabolome - the ultimate product of gene, mRNA, and protein activities.

- Quantitative ROS measurement studies on isolated mitochondria confirm that the oxidative burden is significantly increased in $Mecp2^{-/y}$ hippocampal and cortical tissue.

- All these and other well-documented changes should be considered when evaluating therapeutic approaches in RTT and/or when developing further treatment concepts.

7. References

Adams, V.H., Mcbryant, S.J., Wade, P.A., Woodcock, C.L., and Hansen, J.C. (2007). Intrinsic disorder and autonomous domain function in the multifunctional nuclear protein, MeCP2. *J Biol Chem* 282**,** 15057-15064.

Amir, R.E., Van Den Veyver, I.B., Wan, M., Tran, C.Q., Francke, U., and Zoghbi, H.Y. (1999). Rett syndrome is caused by mutations in X-linked MECP2, encoding methyl-CpG-binding protein 2. *Nat Genet* 23**,** 185-188.

Anderson, A., Wong, K., Jacoby, P., Downs, J., and Leonard, H. (2014). Twenty years of surveillance in Rett syndrome: what does this tell us? *Orphanet J Rare Dis* 9**,** 87.

Baker, S.A., Chen, L., Wilkins, A.D., Yu, P., Lichtarge, O., and Zoghbi, H.Y. (2013). An AT-hook domain in MeCP2 determines the clinical course of Rett syndrome and related disorders. *Cell* 152**,** 984-996.

Baleva, M., Gowher, A., Kamenski, P., Tarassov, I., Entelis, N., and Masquida, B. (2015). A moonlighting human protein is involved in mitochondrial import of tRNA. *Int J Mol Sci* 16**,** 9354-9367.

Ballas, N., Lioy, D.T., Grunseich, C., and Mandel, G. (2009). Non-cell autonomous influence of MeCP2-deficient glia on neuronal dendritic morphology. *Nat Neurosci* 12**,** 311-317.

Ballinger, E.C., Schaaf, C.P., Patel, A.J., De Maio, A., Tao, H., Talmage, D.A., Zoghbi, H.Y., and Role, L.W. (2019). Mecp2 Deletion from Cholinergic Neurons Selectively Impairs Recognition Memory and Disrupts Cholinergic Modulation of the Perirhinal Cortex. *eNeuro* 6.

Bebensee, D.F., Can, K., and Muller, M. (2017). Increased Mitochondrial Mass and Cytosolic Redox Imbalance in Hippocampal Astrocytes of a Mouse Model of Rett Syndrome: Subcellular Changes Revealed by Ratiometric Imaging of JC-1 and roGFP1 Fluorescence. *Oxid Med Cell Longev* 2017**,** 3064016.

Belichenko, P.V., Wright, E.E., Belichenko, N.P., Masliah, E., Li, H.H., Mobley, W.C., and Francke, U. (2009). Widespread changes in dendritic and axonal morphology in Mecp2-mutant mouse models of Rett syndrome: evidence for disruption of neuronal networks. *J Comp Neurol* 514**,** 240-258.

Benjamini, Y., and Hochberg, Y. (1995). Controlling the False Discovery Rate: A Practical and Powerful Approach to Multiple Testing. *Journal of the Royal Statistical Society. Series B (Methodological)* 57**,** 289-300.

Bienvenu, T., Carrié, A., De Roux, N., Vinet, M.C., Jonveaux, P., Couvert, P., Villard, L., Arzimanoglou, A., Beldjord, C., Fontes, M., Tardieu, M., and Chelly, J. (2000). MECP2 mutations account for most cases of typical forms of Rett syndrome. *Hum Mol Genet* 9**,** 1377-1384.

Bolaños, J.P., Delgado-Esteban, M., Herrero-Mendez, A., Fernandez-Fernandez, S., and Almeida, A. (2008). Regulation of glycolysis and pentose-phosphate pathway by nitric oxide: impact on neuronal survival. *Biochim Biophys Acta* 1777**,** 789-793.

Bridi, R., Latini, A., Braum, C.A., Zorzi, G.K., Moacir, W., Lissi, E., and Dutra-Filho, C.S. (2005). Evaluation of the mechanisms involved in leucine-induced oxidative damage in cerebral cortex of young rats. *Free Radic Res* 39**,** 71-79.

Bross, P., Magnoni, R., and Bie, A.S. (2012). Molecular chaperone disorders: defective Hsp60 in neurodegeneration. *Curr Top Med Chem* 12**,** 2491-2503.

Brucke, T., Sofic, E., Killian, W., Rett, A., and Riederer, P. (1987). Reduced concentrations and increased metabolism of biogenic amines in a single case of Rett-syndrome: a postmortem brain study. *J Neural Transm* 68**,** 315-324.

Buchovecky, C.M., Turley, S.D., Brown, H.M., Kyle, S.M., Mcdonald, J.G., Liu, B., Pieper, A.A., Huang, W., Katz, D.M., Russell, D.W., Shendure, J., and Justice, M.J. (2013). A suppressor screen in *Mecp2* mutant mice implicates cholesterol metabolism in Rett syndrome. *Nat Genet* 45**,** 1013-1020.

Butterfield, D.A., and Lange, M.L. (2009). Multifunctional roles of enolase in Alzheimer's disease brain: beyond altered glucose metabolism. *J Neurochem* 111**,** 915-933.

Calfa, G., Hablitz, J.J., and Pozzo-Miller, L. (2011). Network hyperexcitability in hippocampal slices from Mecp2 mutant mice revealed by voltage-sensitive dye imaging. *J Neurophysiol* 105**,** 1768-1784.

Can, K., Menzfeld, C., Rehling, P., Kügler, S., Dudek, J., and Müller, M. (2018). Neuronal redox-imbalance in Rett Syndrome affects mitochondria as well as cytosol, and is accompanied by intensified mitochondrial O_2 consumption and ROS release. *Neuroscience Meeting Planner: Society for Neuroscience***,** Program No. 554.502.

Cappuccio, G., Donti, T., Pinelli, M., Bernardo, P., Bravaccio, C., Elsea, S.H., and Brunetti-Pierri, N. (2019). Sphingolipid Metabolism Perturbations in Rett Syndrome. *Metabolites* 9.

Chahrour, M., Jung, S.Y., Shaw, C., Zhou, X., Wong, S.T., Qin, J., and Zoghbi, H.Y. (2008). MeCP2, a key contributor to neurological disease, activates and represses transcription. *Science* 320**,** 1224-1229.

Chao, H.T., Chen, H., Samaco, R.C., Xue, M., Chahrour, M., Yoo, J., Neul, J.L., Gong, S., Lu, H.C., Heintz, N., Ekker, M., Rubenstein, J.L., Noebels, J.L., Rosenmund, C., and Zoghbi, H.Y. (2010). Dysfunction in GABA signalling mediates autism-like stereotypies and Rett syndrome phenotypes. *Nature* 468**,** 263-269.

Chao, H.T., Zoghbi, H.Y., and Rosenmund, C. (2007). MeCP2 controls excitatory synaptic strength by regulating glutamatergic synapse number. *Neuron* 56**,** 58-65.

Chen, R.Z., Akbarian, S., Tudor, M., and Jaenisch, R. (2001). Deficiency of methyl-CpG binding protein-2 in CNS neurons results in a Rett-like phenotype in mice. *Nat Genet* 27**,** 327-331.

Cicaloni, V., Pecorelli, A., Tinti, L., Rossi, M., Benedusi, M., Cervellati, C., Spiga, O., Santucci, A., Hayek, J., Salvini, L., Tinti, C., and Valacchi, G. (2020). Proteomic profiling reveals mitochondrial alterations in Rett syndrome. *Free Radic Biol Med* 155**,** 37-48.

Clarke, A. (1996). Rett syndrome. *J Med Genet* 33**,** 693-699.

Claveria-Gimeno, R., Lanuza, P.M., Morales-Chueca, I., Jorge-Torres, O.C., Vega, S., Abian, O., Esteller, M., and Velazquez-Campoy, A. (2017). The intervening domain from MeCP2 enhances the DNA affinity of the methyl binding domain and provides an independent DNA interaction site. *Sci Rep* 7**,** 41635.

Coker, S.B., and Melnyk, A.R. (1991). Rett syndrome and mitochondrial enzyme deficiencies. *J Child Neurol* 6**,** 164-166.

Cornford, M.E., Philippart, M., Jacobs, B., Scheibel, A.B., and Vinters, H.V. (1994). Neuropathology of Rett syndrome: case report with neuronal and mitochondrial abnormalities in the brain. *J Child Neurol* 9**,** 424-431.

Crivellari, I., Pecorelli, A., Cordone, V., Marchi, S., Pinton, P., Hayek, J., Cervellati, C., and Valacchi, G. (2021). Impaired mitochondrial quality control in Rett Syndrome. *Arch Biochem Biophys* 700**,** 108790.

Cruciat, C.M., Brunner, S., Baumann, F., Neupert, W., and Stuart, R.A. (2000). The cytochrome bc1 and cytochrome c oxidase complexes associate to form a single supracomplex in yeast mitochondria. *J Biol Chem* 275**,** 18093-18098.

Cui, J., Yang, Y., Zhang, C., Hu, P., Kan, W., Bai, X., Liu, X., and Song, H. (2011). FBI-1 functions as a novel AR co-repressor in prostate cancer cells. *Cell Mol Life Sci* 68**,** 1091-1103.

Dani, V.S., Chang, Q., Maffei, A., Turrigiano, G.G., Jaenisch, R., and Nelson, S.B. (2005). Reduced cortical activity due to a shift in the balance between excitation and inhibition in a mouse model of Rett syndrome. *Proc Natl Acad Sci U S A* 102**,** 12560-12565.

De Felice, C., Ciccoli, L., Leoncini, S., Signorini, C., Rossi, M., Vannuccini, L., Guazzi, G., Latini, G., Comporti, M., Valacchi, G., and Hayek, J. (2009). Systemic oxidative stress in classic Rett syndrome. *Free Radic Biol Med* 47**,** 440-448.

De Felice, C., Della Ragione, F., Signorini, C., Leoncini, S., Pecorelli, A., Ciccoli, L., Scalabri, F., Marracino, F., Madonna, M., Belmonte, G., Ricceri, L., De Filippis, B., Laviola, G., Valacchi, G., Durand, T., Galano, J.M., Oger, C., Guy, A., Bultel-Ponce, V., Guy, J., Filosa, S., Hayek, J., and D'esposito, M. (2014). Oxidative brain damage in Mecp2-mutant murine models of Rett syndrome. *Neurobiol Dis* 68**,** 66-77.

De Felice, C., Signorini, C., Durand, T., Oger, C., Guy, A., Bultel-Ponce, V., Galano, J.M., Ciccoli, L., Leoncini, S., D'esposito, M., Filosa, S., Pecorelli, A., Valacchi, G., and Hayek, J. (2011). F2-dihomo-isoprostanes as potential early biomarkers of lipid oxidative damage in Rett syndrome. *J Lipid Res* 52**,** 2287-2297.

De Filippis, B., Chiodi, V., Adriani, W., Lacivita, E., Mallozzi, C., Leopoldo, M., Domenici, M.R., Fuso, A., and Laviola, G. (2015a). Long-lasting beneficial effects of central serotonin receptor 7 stimulation in female mice modeling Rett syndrome. *Front Behav Neurosci* 9**,** 86.

De Filippis, B., Valenti, D., De Bari, L., De Rasmo, D., Musto, M., Fabbri, A., Ricceri, L., Fiorentini, C., Laviola, G., and Vacca, R.A. (2015b). Mitochondrial free radical overproduction due to respiratory chain impairment in the brain of a mouse model of Rett syndrome: protective effect of CNF1. *Free Radic Biol Med* 83**,** 167-177.

Dittmer, A., and Dittmer, J. (2006). Beta-actin is not a reliable loading control in Western blot analysis. *Electrophoresis* 27**,** 2844-2845.

Doerrier, C., Garcia-Souza, L.F., Krumschnabel, G., Wohlfarter, Y., Mészáros, A.T., and Gnaiger, E. (2018). High-resolution fluorespirometry and OXPHOS protocols for human cells, permeabilized fibers from small biopsies of muscle, and isolated mitochondria. *Methods Mol Biol* 1782**,** 31-70.

Dotti, M.T., Manneschi, L., Malandrini, A., De Stefano, N., Caznerale, F., and Federico, A. (1993). Mitochondrial dysfunction in Rett syndrome. An ultrastructural and biochemical study. *Brain Dev* 15**,** 103-106.

Dringen, R., Gutterer, J.M., and Hirrlinger, J. (2000). Glutathione metabolism in brain metabolic interaction between astrocytes and neurons in the defense against reactive oxygen species. *Eur J Biochem* 267**,** 4912-4916.

Dringen, R., Pfeiffer, B., and Hamprecht, B. (1999). Synthesis of the antioxidant glutathione in neurons: supply by astrocytes of CysGly as precursor for neuronal glutathione. *J Neurosci* 19**,** 562-569.

Du, Y., Wei, J., Yang, X., Dou, Y., Zhao, L., Qi, X., Yu, X., Guo, W., Wang, Q., Deng, W., Li, M., Lin, D., Li, T., and Ma, X. (2021). Plasma metabolites were associated with spatial working memory in major depressive disorder. *Medicine (Baltimore)* 100**,** e24581.

Eeg-Olofsson, O., Al-Zuhair, A.G., Teebi, A.S., Daoud, A.S., Zaki, M., Besisso, M.S., and Al-Essa, M.M. (1990). Rett syndrome: a mitochondrial disease? *J Child Neurol* 5**,** 210-214.

El-Khoury, R., Panayotis, N., Matagne, V., Ghata, A., Villard, L., and Roux, J.C. (2014). GABA and glutamate pathways are spatially and developmentally affected in the brain of Mecp2-deficient mice. *PLoS One* 9**,** e92169.

Ellaway, C., and Christodoulou, J. (2001). Rett syndrome: clinical characteristics and recent genetic advances. *Disabil Rehabil* 23**,** 98-106.

Fernández-Vizarra, E., López-Calcerrada, S., Sierra-Magro, A., Pérez-Pérez, R., Formosa, L.E., Hock, D.H., Illescas, M., Penas, A., Brischigliaro, M., Ding, S., Fearnley, I.M., Tzoulis, C., Pitceathly, R.D.S., Arenas, J., Martin, M.A., Stroud, D.A., Zeviani, M., Ryan, M.T., and Ugalde, C. (2022). Two independent respiratory chains adapt OXPHOS performance to glycolytic switch. *Cell Metab* 34**,** 1792-1808.

Fernández-Vizarra, E., and Ugalde, C. (2022). Cooperative assembly of the mitochondrial respiratory chain. *Trends Biochem Sci* 47**,** 999-1008.

Festerling, K., Can, K., Kügler, S., and Müller, M. (2020). Overshooting Subcellular Redox-Responses in Rett-Mouse Hippocampus during Neurotransmitter Stimulation. *Cells* 9.

Fischer, M., Reuter, J., Gerich, F.J., Hildebrandt, B., Hägele, S., Katschinski, D., and Müller, M. (2009). Enhanced hypoxia susceptibility in hippocampal slices from a mouse model of Rett syndrome. *J Neurophysiol* 101**,** 1016-1032.

Funchal, C., Gottfried, C., De Almeida, L.M., Dos Santos, A.Q., Wajner, M., and Pessoa-Pureur, R. (2005). Morphological alterations and cell death provoked by the branched-chain alpha-amino acids accumulating in maple syrup urine disease in astrocytes from rat cerebral cortex. *Cell Mol Neurobiol* 25**,** 851-867.

Gabel, H.W., Kinde, B., Stroud, H., Gilbert, C.S., Harmin, D.A., Kastan, N.R., Hemberg, M., Ebert, D.H., and Greenberg, M.E. (2015). Disruption of DNA-methylation-dependent long gene repression in Rett syndrome. *Nature* 522**,** 89-93.

Ghosh, R., Gilda, J.E., and Gomes, A.V. (2014). The necessity of and strategies for improving confidence in the accuracy of western blots. *Expert Rev Proteomics* 11**,** 549-560.

Ghosh, R.P., Horowitz-Scherer, R.A., Nikitina, T., Shlyakhtenko, L.S., and Woodcock, C.L. (2010). MeCP2 binds cooperatively to its substrate and competes with histone H1 for chromatin binding sites. *Mol Cell Biol* 30**,** 4656-4670.

Gibson, J.H., Slobedman, B., K, N.H., Williamson, S.L., Minchenko, D., El-Osta, A., Stern, J.L., and Christodoulou, J. (2010). Downstream targets of methyl CpG binding protein 2 and their abnormal expression in the frontal cortex of the human Rett syndrome brain. *BMC Neurosci* 11**,** 53.

Giegé, P., Heazlewood, J.L., Roessner-Tunali, U., Millar, A.H., Fernie, A.R., Leaver, C.J., and Sweetlove, L.J. (2003). Enzymes of glycolysis are functionally associated with the mitochondrion in Arabidopsis cells. *Plant Cell* 15**,** 2140-2151.

Gold, W.A., Krishnarajy, R., Ellaway, C., and Christodoulou, J. (2018). Rett Syndrome: A Genetic Update and Clinical Review Focusing on Comorbidities. *ACS Chem Neurosci* 9**,** 167-176.

Gold, W.A., Williamson, S.L., Kaur, S., Hargreaves, I.P., Land, J.M., Pelka, G.J., Tam, P.P., and Christodoulou, J. (2014). Mitochondrial dysfunction in the skeletal muscle of a mouse model of Rett syndrome (RTT): implications for the disease phenotype. *Mitochondrion* 15**,** 10-17.

Golubiani, G., Lagani, V., Solomonia, R., and Müller, M. (2021). Metabolomic fingerprint of Mecp2-deficient mouse cortex: evidence for a pronounced multi-facetted metabolic component in Rett syndrome. *Cells* 10.

Golubiani G, van Agen L, Tsverava L, Solomonia R, Müller M. (2023) Mitochondrial Proteome Changes in Rett Syndrome. *Biology*.; 12(7)

Gropman, A.L., and Batshaw, M.L. (2004). Cognitive outcome in urea cycle disorders. *Mol Genet Metab* 81 Suppl 1**,** S58-62.

Großer, E., Hirt, U., Janc, O.A., Menzfeld, C., Fischer, M., Kempkes, B., Vogelgesang, S., Manzke, T.U., Opitz, L., Salinas-Riester, G., and Müller, M. (2012). Oxidative burden and mitochondrial dysfunction in a mouse model of Rett syndrome. *Neurobiol Dis* 48**,** 102-114.

Guy, J., Cheval, H., Selfridge, J., and Bird, A. (2011). The role of MeCP2 in the brain. *Annu Rev Cell Dev Biol* 27**,** 631-652.

Guy, J., Gan, J., Selfridge, J., Cobb, S., and Bird, A. (2007). Reversal of neurological defects in a mouse model of Rett syndrome. *Science* 315**,** 1143-1147.

Guy, J., Hendrich, B., Holmes, M., Martin, J.E., and Bird, A. (2001). A mouse Mecp2-null mutation causes neurological symptoms that mimic Rett syndrome. *Nat Genet* 27**,** 322-326.

Haas, R.H., Light, M., Rice, M., and Barshop, B.A. (1995). Oxidative metabolism in Rett syndrome: 1. Clinical studies. *Neuropediatrics* 26**,** 90-94.

Hagberg, B. (2002). Clinical manifestations and stages of Rett syndrome. *Ment Retard Dev Disabil Res Rev* 8**,** 61-65.

Handley, R.R., Reid, S.J., Brauning, R., Maclean, P., Mears, E.R., Fourie, I., Patassini, S., Cooper, G.J.S., Rudiger, S.R., Mclaughlan, C.J., Verma, P.J., Gusella, J.F., Macdonald, M.E., Waldvogel, H.J., Bawden, C.S., Faull, R.L.M., and Snell, R.G. (2017). Brain urea increase is an early Huntington's disease pathogenic event observed in a prodromal transgenic sheep model and HD cases. *Proc Natl Acad Sci U S A* 114**,** E11293-e11302.

He, L., Caudill, M.S., Jing, J., Wang, W., Sun, Y., Tang, J., Jiang, X., and Zoghbi, H.Y. (2022). A weakened recurrent circuit in the hippocampus of Rett syndrome mice disrupts long-term memory representations. *Neuron* 110**,** 1689-1699.e1686.

Hendrich, B., and Tweedie, S. (2003). The methyl-CpG binding domain and the evolving role of DNA methylation in animals. *Trends Genet* 19**,** 269-277.

Hootman, K.C., Trezzi, J.P., Kraemer, L., Burwell, L.S., Dong, X., Guertin, K.A., Jaeger, C., Stover, P.J., Hiller, K., and Cassano, P.A. (2017). Erythritol is a pentose-phosphate pathway metabolite and associated with adiposity gain in young adults. *Proc Natl Acad Sci U S A* 114**,** E4233-e4240.

Inoue, K., Yamada, J., Ueno, S., and Fukuda, A. (2006). Brain-type creatine kinase activates neuron-specific K$^+$-Cl$^-$ co-transporter KCC2. *J Neurochem* 96**,** 598-608.

Isgrò, M.A., Bottoni, P., and Scatena, R. (2015). Neuron-specific enolase as a biomarker: biochemical and clinical aspects. *Adv Exp Med Biol* 867**,** 125-143.

Jaganath, I.B., Mullen, W., Edwards, C.A., and Crozier, A. (2006). The relative contribution of the small and large intestine to the absorption and metabolism of rutin in man. *Free Radic Res* 40**,** 1035-1046.

Janc, O.A., Huser, M.A., Dietrich, K., Kempkes, B., Menzfeld, C., Hulsmann, S., and Muller, M. (2016a). Systemic Radical Scavenger Treatment of a Mouse Model of Rett Syndrome: Merits and Limitations of the Vitamin E Derivative Trolox. *Front Cell Neurosci* 10**,** 266.

Janc, O.A., Hüser, M.A., Dietrich, K., Kempkes, B., Menzfeld, C., Hülsmann, S., and Müller, M. (2016b). Systemic radical scavenger treatment of a mouse model of Rett syndrome: merits and limitations of the vitamin E derivative Trolox. *Front Cell Neurosci* 10**,** 266.

Janc, O.A., and Müller, M. (2014). The free radical scavenger Trolox dampens neuronal hyperexcitability, reinstates synaptic plasticity, and improves hypoxia tolerance in a mouse model of Rett syndrome. *Front Cell Neurosci* 8**,** 56.

Janssen, R.J., Nijtmans, L.G., Van Den Heuvel, L.P., and Smeitink, J.A. (2006). Mitochondrial complex I: structure, function and pathology. *J Inherit Metab Dis* 29**,** 499-515.

Jin, L.W., Horiuchi, M., Wulff, H., Liu, X.B., Cortopassi, G.A., Erickson, J.D., and Maezawa, I. (2015). Dysregulation of glutamine transporter SNAT1 in Rett syndrome microglia: a mechanism for mitochondrial dysfunction and neurotoxicity. *J Neurosci* 35**,** 2516-2529.

Johnson, B.S., Zhao, Y.T., Fasolino, M., Lamonica, J.M., Kim, Y.J., Georgakilas, G., Wood, K.H., Bu, D., Cui, Y., Goffin, D., Vahedi, G., Kim, T.H., and Zhou, Z. (2017). Biotin tagging of MeCP2 in mice reveals contextual insights into the Rett syndrome transcriptome. *Nat Med* 23**,** 1203-1214.

Justice, M.J., Buchovecky, C.M., Kyle, S.M., and Djukic, A. (2013). A role for metabolism in Rett syndrome pathogenesis: New clinical findings and potential treatment targets. *Rare Dis* 1**,** e27265.

Kanehisa, M., and Goto, S. (2000). KEGG: kyoto encyclopedia of genes and genomes. *Nucleic Acids Res* 28**,** 27-30.

Kaplan, P., Tatarkova, Z., Sivonova, M.K., Racay, P., and Lehotsky, J. (2020). Homocysteine and Mitochondria in Cardiovascular and Cerebrovascular Systems. *Int J Mol Sci* 21.

Kappler, L., Hoene, M., Hu, C., Von Toerne, C., Li, J., Bleher, D., Hoffmann, C., Böhm, A., Kollipara, L., Zischka, H., Königsrainer, A., Häring, H.U., Peter, A., Xu, G., Sickmann, A., Hauck, S.M., Weigert, C., and Lehmann, R. (2019). Linking bioenergetic function of mitochondria to tissue-specific molecular fingerprints. *Am J Physiol Endocrinol Metab* 317**,** E374-e387.

Karry, R., Klein, E., and Ben Shachar, D. (2004). Mitochondrial complex I subunits expression is altered in schizophrenia: a postmortem study. *Biol Psychiatry* 55**,** 676-684.

Katz, D.M., Berger-Sweeney, J.E., Eubanks, J.H., Justice, M.J., Neul, J.L., Pozzo-Miller, L., Blue, M.E., Christian, D., Crawley, J.N., Giustetto, M., Guy, J., Howell, C.J., Kron, M., Nelson, S.B., Samaco, R.C., Schaevitz, L.R., St Hillaire-Clarke, C., Young, J.L., Zoghbi, H.Y., and Mamounas, L.A. (2012). Preclinical research in Rett syndrome: setting the foundation for translational success. *Dis Model Mech* 5**,** 733-745.

Kaufmann, W.E., Stallworth, J.L., Everman, D.B., and Skinner, S.A. (2016). Neurobiologically-based treatments in Rett syndrome: opportunities and challenges. *Expert Opin Orphan Drugs* 4**,** 1043-1055.

Kee, S.E., Mou, X., Zoghbi, H.Y., and Ji, D. (2018). Impaired spatial memory codes in a mouse model of Rett syndrome. *Elife* 7.

Kerr, B., Soto, C.J., Saez, M., Abrams, A., Walz, K., and Young, J.I. (2012). Transgenic complementation of MeCP2 deficiency: phenotypic rescue of Mecp2-null mice by isoform-specific transgenes. *Eur J Hum Genet* 20**,** 69-76.

Kilbaugh, T.J., Lvova, M., Karlsson, M., Zhang, Z., Leipzig, J., Wallace, D.C., and Margulies, S.S. (2015). Peripheral Blood Mitochondrial DNA as a Biomarker of Cerebral Mitochondrial Dysfunction following Traumatic Brain Injury in a Porcine Model. *PLoS One* 10**,** e0130927.

Kim, S.H., Vlkolinsky, R., Cairns, N., Fountoulakis, M., and Lubec, G. (2001). The reduction of NADH ubiquinone oxidoreductase 24- and 75-kDa subunits in brains of patients with Down syndrome and Alzheimer's disease. *Life Sci* 68**,** 2741-2750.

Kishi, N., and Macklis, J.D. (2004). MECP2 is progressively expressed in post-migratory neurons and is involved in neuronal maturation rather than cell fate decisions. *Mol Cell Neurosci* 27**,** 306-321.

Kohutiar, M., Eckhardt, A., Miksik, I., Santorova, P., and Wilhelm, J. (2018). Proteomic analysis of peroxynitrite-induced protein nitration in isolated beef heart mitochondria. *Physiol Res* 67**,** 239-250.

Kriaucionis, S., and Bird, A. (2004). The major form of MeCP2 has a novel N-terminus generated by alternative splicing. *Nucleic Acids Res* 32**,** 1818-1823.

Kriaucionis, S., Paterson, A., Curtis, J., Guy, J., Macleod, N., and Bird, A. (2006). Gene expression analysis exposes mitochondrial abnormalities in a mouse model of Rett syndrome. *Mol Cell Biol* 26**,** 5033-5042.

Kron, M., and Müller, M. (2010). Impaired Ca^{2+} homeostasis and concomitant K^+ channel dysfunction in MeCP2-deficient hippocampus during anoxia. *Acta Physiologica* 198 (Suppl 677)**,** P-Tue-132.

Kruusvee, V., Lyst, M.J., Taylor, C., Tarnauskaitė, Ž., Bird, A.P., and Cook, A.G. (2017). Structure of the MeCP2-TBLR1 complex reveals a molecular basis for Rett syndrome and related disorders. *Proc Natl Acad Sci U S A* 114**,** E3243-e3250.

Kwon, W.S., Rahman, M.S., Ryu, D.Y., Park, Y.J., and Pang, M.G. (2015). Increased male fertility using fertility-related biomarkers. *Sci Rep* 5**,** 15654.

Kyle, S.M., Vashi, N., and Justice, M.J. (2018). Rett syndrome: a neurological disorder with metabolic components. *Open Biol* 8.

Lappalainen, R., and Riikonen, R.S. (1996). High levels of cerebrospinal fluid glutamate in Rett syndrome. *Pediatr Neurol* 15**,** 213-216.

Lee, K., Haddad, A., Osme, A., Kim, C., Borzou, A., Ilchenko, S., Allende, D., Dasarathy, S., Mccullough, A., Sadygov, R.G., and Kasumov, T. (2018). Hepatic mitochondrial defects in a nonalcoholic fatty liver disease mouse model are associated with increased degradation of oxidative phosphorylation subunits. *Mol Cell Proteomics* 17**,** 2371-2386.

Lee, S.S., Wan, M., and Francke, U. (2001). Spectrum of MECP2 mutations in Rett syndrome. *Brain Dev* 23 Suppl 1**,** S138-143.

Leonard, H., Bower, C., and English, D. (1997). The prevalence and incidence of Rett syndrome in Australia. *Eur Child Adolesc Psychiatry* 6 Suppl 1**,** 8-10.

Leonard, H., Cobb, S., and Downs, J. (2017). Clinical and biological progress over 50 years in Rett syndrome. *Nat Rev Neurol* 13**,** 37-51.

Lewis, J.D., Meehan, R.R., Henzel, W.J., Maurer-Fogy, I., Jeppesen, P., Klein, F., and Bird, A. (1992). Purification, sequence, and cellular localization of a novel chromosomal protein that binds to methylated DNA. *Cell* 69**,** 905-914.

Li, L., Guo, J.D., Wang, H.D., Shi, Y.M., Yuan, Y.L., and Hou, S.X. (2015). Prohibitin 1 gene delivery promotes functional recovery in rats with spinal cord injury. *Neuroscience* 286**,** 27-36.

Li, R., and Shen, Y. (2013). An old method facing a new challenge: re-visiting housekeeping proteins as internal reference control for neuroscience research. *Life Sci* 92**,** 747-751.

Lin, H.B., Cadete, V.J., Sawicka, J., Wozniak, M., and Sawicki, G. (2012). Effect of the myosin light chain kinase inhibitor ML-7 on the proteome of hearts subjected to ischemia-reperfusion injury. *J Proteomics* 75**,** 5386-5395.

Liput, D.J. (2018). Cre-Recombinase Dependent Germline Deletion of a Conditional Allele in the Rgs9cre Mouse Line. *Front Neural Circuits* 12**,** 68.

Liu, S., Pei, P., Li, L., Wu, H., Zheng, X., Wang, S., Xiao, Y., Pan, H., Bao, X., Qi, Y., and Ma, Y. (2022). Mitochondrial DNA Copy Number in Rett Syndrome Caused by Methyl-CpG-Binding Protein-2 Variants. *J Pediatr* 241**,** 154-161.

Liu, X., Ren, Z., Zhan, R., Wang, X., Wang, X., Zhang, Z., Leng, X., Yang, Z., and Qian, L. (2009). Prohibitin protects against oxidative stress-induced cell injury in cultured neonatal cardiomyocyte. *Cell Stress Chaperones* 14**,** 311-319.

Liyanage, V.R., and Rastegar, M. (2014). Rett syndrome and MeCP2. *Neuromolecular Med* 16**,** 231-264.

Lu, H., Ash, R.T., He, L., Kee, S.E., Wang, W., Yu, D., Hao, S., Meng, X., Ure, K., Ito-Ishida, A., Tang, B., Sun, Y., Ji, D., Tang, J., Arenkiel, B.R., Smirnakis, S.M., and Zoghbi, H.Y. (2016). Loss and Gain of MeCP2 Cause Similar Hippocampal Circuit Dysfunction that Is Rescued by Deep Brain Stimulation in a Rett Syndrome Mouse Model. *Neuron* 91**,** 739-747.

Lyst, M.J., and Bird, A. (2015). Rett syndrome: a complex disorder with simple roots. *Nat Rev Genet* 16**,** 261-275.

Lyst, M.J., Ekiert, R., Guy, J., Selfridge, J., Koerner, M.V., Merusi, C., De Sousa, D., and Bird, A. (2018). Affinity for DNA Contributes to NLS Independent Nuclear Localization of MeCP2. *Cell Rep* 24**,** 2213-2220.

Margvelani, G., Meparishvili, M., Tevdoradze, E., Mccabe, B.J., and Solomonia, R. (2018). Mitochondrial fusion and fission proteins and the recognition memory of imprinting in domestic chicks. *Neuroreport* 29**,** 128-133.

Martin, H.L., and Teismann, P. (2009). Glutathione--a review on its role and significance in Parkinson's disease. *Faseb j* 23**,** 3263-3272.

Martínez-Reyes, I., and Chandel, N.S. (2020). Mitochondrial TCA cycle metabolites control physiology and disease. *Nat Commun* 11**,** 102.

Matsuishi, T., Urabe, F., Percy, A.K., Komori, H., Yamashita, Y., Schultz, R.S., Ohtani, Y., Kuriya, N., and Kato, H. (1994). Abnormal carbohydrate metabolism in cerebrospinal fluid in Rett syndrome. *J Child Neurol* 9**,** 26-30.

Matsuura, K., Otani, M., Takano, M., Kadoyama, K., and Matsuyama, S. (2016). The influence of chronic nicotine treatment on proteins expressed in the mouse hippocampus and cortex. *Eur J Pharmacol* 780**,** 16-25.

Meehan, R.R., Lewis, J.D., Mckay, S., Kleiner, E.L., and Bird, A.P. (1989). Identification of a mammalian protein that binds specifically to DNA containing methylated CpGs. *Cell* 58**,** 499-507.

Mellén, M., Ayata, P., Dewell, S., Kriaucionis, S., and Heintz, N. (2012). MeCP2 binds to 5hmC enriched within active genes and accessible chromatin in the nervous system. *Cell* 151**,** 1417-1430.

Meparishvili, M., Nozadze, M., Margvelani, G., Mccabe, B.J., and Solomonia, R.O. (2015). A proteomic study of memory after imprinting in the domestic chick. *Front Behav Neurosci* 9**,** 319.

Merkwirth, C., Martinelli, P., Korwitz, A., Morbin, M., Brönneke, H.S., Jordan, S.D., Rugarli, E.I., and Langer, T. (2012). Loss of prohibitin membrane scaffolds impairs mitochondrial architecture and leads to tau hyperphosphorylation and neurodegeneration. *PLoS Genet* 8**,** e1003021.

Mills, E., and O'neill, L.A. (2014). Succinate: a metabolic signal in inflammation. *Trends Cell Biol* 24**,** 313-320.

Miyake, K., Yang, C., Minakuchi, Y., Ohori, K., Soutome, M., Hirasawa, T., Kazuki, Y., Adachi, N., Suzuki, S., Itoh, M., Goto, Y., Andoh, T., Kurosawa, H., Oshimura, M., Sasaki, M., Toyoda, A., and Kubota, T. (2013). Comparison of genomic and epigenomic expression in monozygotic twins discordant for Rett syndrome. *PLoS One* 8**,** e66729.

Moore, L.D., Le, T., and Fan, G. (2013). DNA methylation and its basic function. *Neuropsychopharmacology* 38**,** 23-38.

Motil, K.J., Caeg, E., Barrish, J.O., Geerts, S., Lane, J.B., Percy, A.K., Annese, F., Mcnair, L., Skinner, S.A., Lee, H.S., Neul, J.L., and Glaze, D.G. (2012). Gastrointestinal and nutritional problems occur frequently throughout life in girls and women with Rett syndrome. *J Pediatr Gastroenterol Nutr* 55**,** 292-298.

Mucerino, S., Di Salle, A., Alessio, N., Margarucci, S., Nicolai, R., Melone, M.A., Galderisi, U., and Peluso, G. (2017). Alterations in the carnitine cycle in a mouse model of Rett syndrome. *Sci Rep* 7**,** 41824.

Na, E.S., Nelson, E.D., Kavalali, E.T., and Monteggia, L.M. (2013). The impact of MeCP2 loss- or gain-of-function on synaptic plasticity. *Neuropsychopharmacology* 38**,** 212-219.

Neul, J.L., Fang, P., Barrish, J., Lane, J., Caeg, E.B., Smith, E.O., Zoghbi, H., Percy, A., and Glaze, D.G. (2008). Specific mutations in methyl-CpG-binding protein 2 confer different severity in Rett syndrome. *Neurology* 70**,** 1313-1321.

Neul, J.L., Skinner, S.A., Annese, F., Lane, J., Heydemann, P., Jones, M., Kaufmann, W.E., Glaze, D.G., and Percy, A.K. (2020). Metabolic signatures differentiate Rett syndrome from unaffected siblings. *Front Integr Neurosci* 14**,** 7.

Obsilova, V., and Obsil, T. (2022). Structural insights into the functional roles of 14-3-3 proteins. *Front Mol Biosci* 9**,** 1016071.

Oginsky, M.F., Cui, N., Zhong, W., Johnson, C.M., and Jiang, C. (2014). Alterations in the cholinergic system of brain stem neurons in a mouse model of Rett syndrome. *Am J Physiol Cell Physiol* 307**,** C508-520.

Olson, C.O., Zachariah, R.M., Ezeonwuka, C.D., Liyanage, V.R., and Rastegar, M. (2014). Brain region-specific expression of MeCP2 isoforms correlates with DNA methylation within Mecp2 regulatory elements. *PLoS One* 9**,** e90645.

Osenberg, S., Karten, A., Sun, J., Li, J., Charkowick, S., Felice, C.A., Kritzer, M., Nguyen, M.V.C., Yu, P., and Ballas, N. (2018). Activity-dependent aberrations in gene expression and alternative splicing in a mouse model of Rett syndrome. *Proc Natl Acad Sci U S A* 115**,** E5363-E5372.

Panov, A., Orynbayeva, Z., Vavilin, V., and Lyakhovich, V. (2014). Fatty acids in energy metabolism of the central nervous system. *Biomed Res Int* 2014**,** 472459.

Patassini, S., Begley, P., Reid, S.J., Xu, J., Church, S.J., Curtis, M., Dragunow, M., Waldvogel, H.J., Unwin, R.D., Snell, R.G., Faull, R.L., and Cooper, G.J. (2015). Identification of elevated urea as a severe, ubiquitous metabolic defect in the brain of patients with Huntington's disease. *Biochem Biophys Res Commun* 468**,** 161-166.

Pecorelli, A., Leoni, G., Cervellati, F., Canali, R., Signorini, C., Leoncini, S., Cortelazzo, A., De Felice, C., Ciccoli, L., Hayek, J., and Valacchi, G. (2013). Genes related to mitochondrial functions, protein degradation, and chromatin folding are differentially expressed in lymphomonocytes of Rett syndrome patients. *Mediators Inflamm* 2013**,** 137629.

Pejhan, S., and Rastegar, M. (2021). Role of DNA Methyl-CpG-Binding Protein MeCP2 in Rett Syndrome Pathobiology and Mechanism of Disease. *Biomolecules* 11.

Pelka, G.J., Watson, C.M., Christodoulou, J., and Tam, P.P. (2005). Distinct expression profiles of Mecp2 transcripts with different lengths of 3'UTR in the brain and visceral organs during mouse development. *Genomics* 85**,** 441-452.

Poon, H.F., Frasier, M., Shreve, N., Calabrese, V., Wolozin, B., and Butterfield, D.A. (2005). Mitochondrial associated metabolic proteins are selectively oxidized in A30P α-synuclein transgenic mice--a model of familial Parkinson's disease. *Neurobiol Dis* 18**,** 492-498.

Qiao, Y., Hu, T., Yang, B., Li, H., Chen, T., Yin, D., He, H., and He, M. (2020). Capsaicin alleviates the deteriorative mitochondrial function by upregulating 14-3-3η in anoxic or anoxic/reoxygenated cardiomyocytes. *Oxid Med Cell Longev* 2020**,** 1750289.

Quaderi, N.A., Meehan, R.R., Tate, P.H., Cross, S.H., Bird, A.P., Chatterjee, A., Herman, G.E., and Brown, S.D. (1994). Genetic and physical mapping of a gene encoding a methyl CpG binding protein, Mecp2, to the mouse X chromosome. *Genomics* 22**,** 648-651.

Rahman, M.H., and Suk, K. (2020). Mitochondrial dynamics and bioenergetic alteration during inflammatory activation of astrocytes. *Front Aging Neurosci* 12**,** 614410.

Rett, A. (1966). Über ein eigenartiges hirnatrophisches Syndrom bei Hyperammonämie im Kindesalter. *Wien Med Wochenschr* 116**,** 723-726.

Ricceri, L., De Filippis, B., Fuso, A., and Laviola, G. (2011). Cholinergic hypofunction in MeCP2-308 mice: beneficial neurobehavioural effects of neonatal choline supplementation. *Behav Brain Res* 221**,** 623-629.

Ricciardi, S., Boggio, E.M., Grosso, S., Lonetti, G., Forlani, G., Stefanelli, G., Calcagno, E., Morello, N., Landsberger, N., Biffo, S., Pizzorusso, T., Giustetto, M., and Broccoli, V. (2011). Reduced AKT/mTOR signaling and protein synthesis dysregulation in a Rett syndrome animal model. *Hum Mol Genet* 20**,** 1182-1196.

Riederer, P., Brücke, T., Sofic, E., Kienzl, E., Schnecker, K., Schay, V., Kruzik, P., Killian, W., and Rett, A. (1985). Neurochemical aspects of the Rett syndrome. *Brain Dev* 7**,** 351-360.

Rodrigues, D.C., Mufteev, M., and Ellis, J. (2020). Regulation, diversity and function of MECP2 exon and 3'UTR isoforms. *Hum Mol Genet* 29**,** R89-r99.

Sadasivudu, B., and Rao, T.I. (1976). Studies on functional and metabolic role of urea cycle intermediates in brain. *J Neurochem* 27**,** 785-794.

Salem, M.A., Jüppner, J., Bajdzienko, K., and Giavalisco, P. (2016). Protocol: a fast, comprehensive and reproducible one-step extraction method for the rapid preparation of polar and semi-polar metabolites, lipids, proteins, starch and cell wall polymers from a single sample. *Plant Methods* 12**,** 45.

Samaco, R.C., Fryer, J.D., Ren, J., Fyffe, S., Chao, H.T., Sun, Y., Greer, J.J., Zoghbi, H.Y., and Neul, J.L. (2008). A partial loss of function allele of methyl-CpG-binding protein 2 predicts a human neurodevelopmental syndrome. *Hum Mol Genet* 17**,** 1718-1727.

Samaco, R.C., Mandel-Brehm, C., Chao, H.T., Ward, C.S., Fyffe-Maricich, S.L., Ren, J., Hyland, K., Thaller, C., Maricich, S.M., Humphreys, P., Greer, J.J., Percy, A., Glaze, D.G., Zoghbi, H.Y., and Neul, J.L. (2009). Loss of MeCP2 in aminergic neurons causes cell-autonomous defects in neurotransmitter synthesis and specific behavioral abnormalities. *Proc Natl Acad Sci U S A* 106**,** 21966-21971.

Samaco, R.C., Mcgraw, C.M., Ward, C.S., Sun, Y., Neul, J.L., and Zoghbi, H.Y. (2013). Female *Mecp2*$^{+/-}$ mice display robust behavioral deficits on two different genetic backgrounds providing a framework for pre-clinical studies. *Hum Mol Genet* 22**,** 96-109.

Sands, J.M., Gargus, J.J., Fröhlich, O., Gunn, R.B., and Kokko, J.P. (1992). Urinary concentrating ability in patients with Jk(a-b-) blood type who lack carrier-mediated urea transport. *J Am Soc Nephrol* 2**,** 1689-1696.

Satoh, J., Onoue, H., Arima, K., and Yamamura, T. (2005). The 14-3-3 protein forms a molecular complex with heat shock protein Hsp60 and cellular prion protein. *J Neuropathol Exp Neurol* 64**,** 858-868.

Saywell, V., Viola, A., Confort-Gouny, S., Le Fur, Y., Villard, L., and Cozzone, P.J. (2006). Brain magnetic resonance study of Mecp2 deletion effects on anatomy and metabolism. *Biochem Biophys Res Commun* 340**,** 776-783.

Shahbazian, M.D., Antalffy, B., Armstrong, D.L., and Zoghbi, H.Y. (2002). Insight into Rett syndrome: MeCP2 levels display tissue- and cell-specific differences and correlate with neuronal maturation. *Hum Mol Genet* 11**,** 115-124.

Shovlin, S., and Tropea, D. (2018). Transcriptome level analysis in Rett syndrome using human samples from different tissues. *Orphanet J Rare Dis* 13**,** 113.

Signorile, A., Sgaramella, G., Bellomo, F., and De Rasmo, D. (2019). Prohibitins: a critical role in mitochondrial functions and implication in diseases. *Cells* 8.

Simmons, E.C., Scholpa, N.E., and Schnellmann, R.G. (2020). Mitochondrial biogenesis as a therapeutic target for traumatic and neurodegenerative CNS diseases. *Exp Neurol* 329**,** 113309.

Smyth, G.K. (2005). "Limma: linear models for microarray data," in *Bioinformatics and Computational Biology Solutions using R and Bioconductor,* eds. R. Gentleman, V. Carey, S. Dudoit, R. Irizarry & W. Huber. (New York: Springer), 397-420.

Sofić, E., Riederer, P., Killian, W., and Rett, A. (1987). Reduced concentrations of ascorbic acid and glutathione in a single case of Rett syndrome: a postmortem brain study. *Brain Dev* 9**,** 529-531.

Song, B.C., Joo, N.S., Aldini, G., and Yeum, K.J. (2014). Biological functions of histidine-dipeptides and metabolic syndrome. *Nutr Res Pract* 8**,** 3-10.

Sperringer, J.E., Addington, A., and Hutson, S.M. (2017). Branched-Chain Amino Acids and Brain Metabolism. *Neurochem Res* 42**,** 1697-1709.

Stauch, K.L., Purnell, P.R., and Fox, H.S. (2014). Quantitative proteomics of synaptic and nonsynaptic mitochondria: insights for synaptic mitochondrial vulnerability. *J Proteome Res* 13**,** 2620-2636.

Stettner, G.M., Huppke, P., Gärtner, J., Richter, D.W., and Dutschmann, M. (2008). Disturbances of breathing in Rett syndrome: Results from patients and animal models. *Adv Exp Biol Med* 605**,** 503-507.

Strati, F., Cavalieri, D., Albanese, D., De Felice, C., Donati, C., Hayek, J., Jousson, O., Leoncini, S., Pindo, M., Renzi, D., Rizzetto, L., Stefanini, I., Calabrò, A., and De Filippo, C. (2016). Altered gut microbiota in Rett syndrome. *Microbiome* 4**,** 41.

Supale, S., Thorel, F., Merkwirth, C., Gjinovci, A., Herrera, P.L., Scorrano, L., Meda, P., Langer, T., and Maechler, P. (2013). Loss of prohibitin induces mitochondrial damages altering β-cell function and survival and is responsible for gradual diabetes development. *Diabetes* 62**,** 3488-3499.

Tatarkova, Z., Kovalska, M., Timkova, V., Racay, P., Lehotsky, J., and Kaplan, P. (2016). The effect of aging on mitochondrial complex I and the extent of oxidative stress in the rat brain cortex. *Neurochem Res* 41**,** 2160-2172.

Taverna, F., Goveia, J., Karakach, T.K., Khan, S., Rohlenova, K., Treps, L., Subramanian, A., Schoonjans, L., Dewerchin, M., Eelen, G., and Carmeliet, P. (2020). BIOMEX: an interactive workflow for (single cell) omics data interpretation and visualization. *Nucleic Acids Res* 48**,** W385-w394.

Thapa, S., Venkatachalam, A., Khan, N., Naqvi, M., Balderas, M., Runge, J.K., Haag, A., Hoch, K.M., Glaze, D.G., Luna, R.A., and Motil, K.J. (2021). Assessment of the gut bacterial microbiome and metabolome of girls and women with Rett Syndrome. *PLoS One* 16**,** e0251231.

Toloe, J., Mollajew, R., Kügler, S., and Mironov, S.L. (2014). Metabolic differences in hippocampal 'Rett' neurons revealed by ATP imaging. *Mol Cell Neurosci* 59C**,** 47-56.

Tosto, G., and Reitz, C. (2016). "Chapter 6 - Use of "omics" technologies to dissect neurologic disease," in *Handbook of Clinical Neurology,* eds. M.J. Aminoff, F. Boller & D.F. Swaab. Elsevier), 91-106.

Valacchi, G., Virgili, F., Cervellati, C., and Pecorelli, A. (2018). OxInflammation: from subclinical condition to pathological biomarker. *Front Physiol* 9**,** 858.

Valenti, D., De Bari, L., Vigli, D., Lacivita, E., Leopoldo, M., Laviola, G., Vacca, R.A., and De Filippis, B. (2017). Stimulation of the brain serotonin receptor 7 rescues mitochondrial dysfunction in female mice from two models of Rett syndrome. *Neuropharmacology* 121**,** 79-88.

Vaz, F.M., and Wanders, R.J.A. (2002). Carnitine biosynthesis in mammals. *Biochemical Journal* 361**,** 417-429.

Villani, C., Sacchetti, G., Carli, M., and Invernizzi, R.W. (2020). Fluoxetine rescues rotarod motor deficits in Mecp2 heterozygous mouse model of Rett syndrome via brain serotonin. *Neuropharmacology* 176**,** 108221.

Villemagne, P.M., Naidu, S., Villemagne, V.L., Yaster, M., Wagner, H.N., Jr., Harris, J.C., Moser, H.W., Johnston, M.V., Dannals, R.F., and Wong, D.F. (2002). Brain glucose metabolism in Rett Syndrome. *Pediatr Neurol* 27**,** 117-122.

Viola, A., Saywell, V., Villard, L., Cozzone, P.J., and Lutz, N.W. (2007). Metabolic fingerprints of altered brain growth, osmoregulation and neurotransmission in a rett syndrome model. *PLoS ONE* 2**,** e157.

Ward, B.C., Kolodny, N.H., Nag, N., and Berger-Sweeney, J.E. (2009). Neurochemical changes in a mouse model of Rett syndrome: changes over time and in response to perinatal choline nutritional supplementation. *J Neurochem* 108**,** 361-371.

Warren, Z., Mcpheeters, M.L., Sathe, N., Foss-Feig, J.H., Glasser, A., and Veenstra-Vanderweele, J. (2011). A systematic review of early intensive intervention for autism spectrum disorders. *Pediatrics* 127**,** e1303-1311.

Weese-Mayer, D.E., Lieske, S.P., Boothby, C.M., Kenny, A.S., Bennett, H.L., Silvestri, J.M., and Ramirez, J.M. (2006). Autonomic nervous system dysregulation: breathing and heart rate perturbation during wakefulness in young girls with Rett syndrome. *Pediatr Res* 60**,** 443-449.

Wenk, G.L. (1996). Rett syndrome: evidence for normal dopaminergic function. *Neuropediatrics* 27**,** 256-259.

Wenk, G.L., and Hauss-Wegrzyniak, B. (1999). Altered cholinergic function in the basal forebrain of girls with Rett syndrome. *Neuropediatrics* 30**,** 125-129.

Wenk, G.L., Naidu, S., Casanova, M.F., Kitt, C.A., and Moser, H. (1991). Altered neurochemical markers in Rett's syndrome. *Neurology* 41**,** 1753-1756.

Wong, D.F., Blue, M.E., Brašić, J.R., Nandi, A., Valentine, H., Stansfield, K.H., Rousset, O., Bibat, G., Yablonski, M.E., Johnston, M.V., Gjedde, A., and Naidu, S. (2018). Are dopamine receptor and transporter changes in Rett syndrome reflected in Mecp2-deficient mice? *Exp Neurol* 307**,** 74-81.

Wu, D., Lim, E., Vaillant, F., Asselin-Labat, M.L., Visvader, J.E., and Smyth, G.K. (2010). ROAST: rotation gene set tests for complex microarray experiments. *Bioinformatics* 26**,** 2176-2182.

Xu, J., Begley, P., Church, S.J., Patassini, S., Hollywood, K.A., Jüllig, M., Curtis, M.A., Waldvogel, H.J., Faull, R.L., Unwin, R.D., and Cooper, G.J. (2016). Graded perturbations of metabolism in multiple regions of human brain in Alzheimer's disease: Snapshot of a pervasive metabolic disorder. *Biochim Biophys Acta* 1862**,** 1084-1092.

Yellen, G. (2018). Fueling thought: Management of glycolysis and oxidative phosphorylation in neuronal metabolism. *J Cell Biol* 217**,** 2235-2246.

Yu, Y., Herman, P., Rothman, D.L., Agarwal, D., and Hyder, F. (2018). Evaluating the gray and white matter energy budgets of human brain function. *J Cereb Blood Flow Metab* 38**,** 1339-1353.

Zhang, L., He, J., Jugloff, D.G., and Eubanks, J.H. (2008). The MeCP2-null mouse hippocampus displays altered basal inhibitory rhythms and is prone to hyperexcitability. *Hippocampus* 18**,** 294-309.

Zhang, Q., Zhao, Y., Bao, X., Luo, J., Zhang, X., Li, J., Wei, L., and Wu, X. (2017). Familial cases and male cases with MECP2 mutations. *Am J Med Genet B Neuropsychiatr Genet* 174**,** 451-457.

Zhang, R., Zhang, T., Ali, A.M., Al Washih, M., Pickard, B., and Watson, D.G. (2016). Metabolomic Profiling of Post-Mortem Brain Reveals Changes in Amino Acid and Glucose Metabolism in Mental Illness Compared with Controls. *Comput Struct Biotechnol J* 14**,** 106-116.

Zhang, Y., Chen, K., Sloan, S.A., Bennett, M.L., Scholze, A.R., O'keeffe, S., Phatnani, H.P., Guarnieri, P., Caneda, C., Ruderisch, N., Deng, S., Liddelow, S.A., Zhang, C., Daneman, R., Maniatis, T., Barres, B.A., and Wu, J.Q. (2014). An RNA-sequencing transcriptome and splicing database of glia, neurons, and vascular cells of the cerebral cortex. *J Neurosci* 34**,** 11929-11947.

8. Supplemental materials

Supplementary Table 1. List of the 101 metabolites that were shown to be significantly different between *Mecp2*[-/y] and WT cortices (FDR ≤0.05). Each metabolite's common name, log2 fold change, raw p-value, and corrected p-value are presented. Only the metabolites that could be clearly identified (annotated) in the database are listed. Reproduced from Golubiani G, Lagani V, Solomonia R, Müller M. (2021). Metabolomic Fingerprint of Mecp2-Deficient Mouse Neocortex: Evidence for a Pronounced Multi-Facetted Metabolic Component in Rett Syndrome. Cells. 10: 2494.

Metabolite	Log Fold Change	Average Expression	*p*-Value	Adjusted *p*-Value
L-Proline	0.910	19.269	1.02×10^{-6}	0.00014
L-Glutamic acid	1.406	19.899	2.04×10^{-6}	0.00018
N-Acetylglutamic acid	1.146	13.495	7.33×10^{-7}	0.00014
Adenosine monophosphate	0.925	20.923	3.23×10^{-6}	0.00018
Adenosine diphosphate	0.925	20.923	3.23×10^{-6}	0.00018
L-Threonine	1.281	18.628	9.24×10^{-6}	0.00036
L-Leucine	0.870	17.672	1.18×10^{-5}	0.00036
D-Glucose 6-phosphate	2.226	12.018	1.23×10^{-5}	0.00036
Citric acid	0.872	18.512	1.38×10^{-5}	0.00036
Inositol 1-phosphate	0.959	13.174	1.45×10^{-5}	0.00036
(S)-Methyl-3-hydroxybutanoate	0.935	16.364	1.51×10^{-5}	0.00036
Putrescine	1.179	14.878	2.05×10^{-5}	0.00044
D-Fructose 1,6-bisphosphate	2.035	12.807	2.18×10^{-5}	0.00044
D-Fructose	1.167	15.985	2.89×10^{-5}	0.00055
L-Valine	0.787	18.180	$3.55E \times 10^{-5}$	0.00060
L-Isoleucine	0.794	16.510	3.63×10^{-5}	0.00060
L-Homocysteine	−2.332	19.231	3.89×10^{-5}	0.00061
Inosine 5prime-monophosphate	1.158	15.513	4.43×10^{-5}	0.00066
D-Glucose	1.418	14.891	5.85×10^{-5}	0.00080
Urea	1.599	18.093	6.27×10^{-5}	0.00080
L-Glutamyl-L-glutamine	−1.885	27.116	6.07×10^{-5}	0.00080
5prime-Deoxy-5prime-(methylthio)adenosine	0.732	12.146	6.81×10^{-5}	0.00080
(5Z,8Z,11Z,14Z)-Icosatetra-5,8,11,14-enoic acid	1.032	12.834	6.63×10^{-5}	0.00080
L-Rhamnose	0.805	15.911	7.07×10^{-5}	0.00080
S-Adenosyl methionine	−0.994	23.740	9.39×10^{-5}	0.00102
L-Threonic acid	0.685	16.744	0.00010	0.00106
Xanthine	−0.590	24.310	0.00011	0.00112
Glycerol	0.743	19.067	0.00013	0.00123
Uracil	−0.903	21.188	0.00013	0.00123
L-Serine	0.580	20.901	0.00014	0.00128
L-Phenylalanine	1.143	16.688	0.00014	0.00128
Riboflavin	−1.161	20.071	0.00018	0.00157
Erythritol	0.696	13.022	0.00021	0.00178
Orthophosphate	0.612	20.971	0.00029	0.00232
L-Dehydroascorbic acid	0.691	21.847	0.00032	0.00252

alpha-Ketoglutaric acid	1.783	12.766	0.00033	0.00252
Succinic acid	0.743	17.429	0.00034	0.00252
L-Methionine	0.909	16.361	0.00041	0.00296
1-Methyl-4-Imidazoleacetic acid	−0.837	21.803	0.00044	0.00312
Dopamine	−1.285	21.788	0.00046	0.00312
Choline	−0.431	26.902	0.00051	0.00333
L-Malic acid	0.695	17.421	0.00060	0.00389
alpha-D-Glucose 1-phosphate	0.608	16.334	0.00065	0.00409
Acetylcholine	−0.927	23.071	0.00067	0.00415
Guanidineacetic acid	0.821	20.099	0.00080	0.00480
Cholesterol	1.261	19.067	0.00081	0.00480
gamma-Glutamyl-tyrosine	−1.785	19.524	0.00084	0.00487
L-Phenylalanyl-L-glutamic acid	0.898	18.323	0.00089	0.00497
L-Tryptophan	1.611	14.883	0.00090	0.00497
Sucrose	6.158	13.392	0.00101	0.00541
3-Methoxytyramine	−1.329	19.231	0.00106	0.00555
Hydroxymethylphosphonic acid	−0.787	23.679	0.00115	0.00590
Cysteinylglycine	−4.028	21.772	0.00118	0.00598
L-Cystine	0.874	11.928	0.00123	0.00601
L-Lysine	−0.351	24.204	0.00123	0.00601
Xylitol	0.809	14.890	0.00140	0.00671
L-Valylglycine	0.679	18.356	0.00151	0.00707
myo-Inositol 2-phosphate	0.595	12.668	0.00152	0.00707
Quinic acid	0.856	11.418	0.00157	0.00714
Pantothenic acid	0.685	13.364	0.00159	0.00714
gamma-Glutamyl-leucine	−0.625	20.675	0.00168	0.00745
L-Homoserine	0.690	13.175	0.00201	0.00876
L-Tryptophyl-L-glutamic acid	1.067	17.063	0.00243	0.01042
O-Acetyl-L-homoserine	−0.758	25.057	0.00256	0.01082
2-Hydroxypyridine	0.676	18.513	0.00267	0.01111
L-Tyrosylglycine	0.669	17.228	0.00276	0.01131
Cytidine	−0.498	24.940	0.00283	0.01144
3-Ureidopropanoic acid	−0.797	16.984	0.00307	0.01222
L-Tyrosyl-L-glutamine	0.694	16.728	0.00317	0.01246
Pyroglutamic acid	0.419	23.178	0.00351	0.01361
sn-Glycerol 3-phosphate	0.544	19.750	0.00409	0.01542
L-Alanine	0.468	21.447	0.00456	0.01700
Thiaminpyrophosphate	0.972	17.802	0.00465	0.01708
L-Tyrosine	1.005	18.152	0.00495	0.01796
Serotonin	−0.856	19.538	0.00630	0.02227
5-Hydroxy-D,L-lysine	−0.541	16.762	0.00655	0.02274
L-Argininosuccinic acid	0.489	20.133	0.00659	0.02274
Uric acid	−0.872	20.411	0.00739	0.02490
L-Prolyl-L-threonine	0.456	17.391	0.00754	0.02491
Caffeic acid	0.846	11.955	0.00757	0.02491
L-Glutamine	0.415	23.021	0.00793	0.02579

gamma-Glutamyl-tryptophan	−1.178	18.306	0.00813	0.02614
S-(2-Carboxyethyl)cysteine	−0.912	19.479	0.00890	0.02799
Cytidine monophosphate	0.449	24.217	0.00890	0.02799
Uridine	−0.650	23.353	0.00964	0.02996
L-Valyl-L-alanine	1.011	18.636	0.01030	0.03168
Spermidine	−0.449	22.564	0.01043	0.03174
Spermine	−1.144	20.609	0.01090	0.03252
Pyruvic acid	0.570	16.746	0.01126	0.03319
(3-Carboxypropyl) trimethylammonium	−0.226	25.234	0.01211	0.03533
Urocanic acid	1.357	20.985	0.01319	0.03809
Glyceraldehyde 3-phosphate	1.960	19.691	0.01448	0.04138
Rutin	1.789	11.194	0.01504	0.04256
Guanosine	−0.551	26.262	0.01548	0.04336
Stearic acid (FA 18:0)	0.412	17.346	0.01606	0.04447
L-Lysyl-L-glutamic acid	−0.465	17.413	0.01619	0.04447
Xanthosine	−0.864	18.294	0.01649	0.04486
Palmitic acid (FA 16:0)	0.457	17.561	0.01711	0.04611
Cytidine 5prime-diphosphoethanolamine	−0.249	23.064	0.01821	0.04817
L-Phenylalanyl-L-threonine	0.550	16.795	0.01842	0.04826
1-Methylnicotinamide	−0.390	19.488	0.01907	0.04951

Supplementary Table 2. List of all annotated metabolites. Reproduced from Golubiani G, Lagani V, Solomonia R, Müller M. (2021). Metabolomic Fingerprint of *Mecp2*-Deficient Mouse Neocortex: Evidence for a Pronounced Multi-Facetted Metabolic Component in Rett Syndrome. Cells. 10: 2494

Metabolite	Log.fold.change	Average.expression	Pvalue	Adjusted.pvalue
L-Proline	0.910364847	19.268619	1.02E-06	0.000143678
L-Glutamic_acid	1.405947697	19.8986119	2.04E-06	0.000182672
N-Acetylglutamic_acid	1.14608971	13.49508312	7.33E-07	0.000143678
Adenosine_monophosphate	0.925431723	20.92283765	3.23E-06	0.000182672
Adenosine_diphosphate	0.925431723	20.92283765	3.23E-06	0.000182672
L-Threonine	1.280944045	18.62842653	9.24E-06	0.000355332
L-Glutamylglycine_|_L-Aspartyl-L-alanine_|_Glycyl-L-glutamic_acid_|_L-Alanyl-L-aspartic_acid	-1.884776605	20.42198275	8.92E-06	0.000355332
L-Leucine	0.869859403	17.67189279	1.18E-05	0.000355332
D-Glucose_6-phosphate	2.225577112	12.01816324	1.23E-05	0.000355332
Citric_acid	0.872324355	18.51228499	1.38E-05	0.000355332
Inositol_1-phosphate	0.959271973	13.17443792	1.45E-05	0.000355332
(S)-Methyl-3-hydroxybutanoate	0.934581762	16.36377358	1.51E-05	0.000355332
Putrescine	1.178846798	14.87831494	2.05E-05	0.000441438
D-Fructose_1,6-bisphosphate	2.035249928	12.80678239	2.18E-05	0.000441438
D-Fructose	1.167056757	15.98535056	2.89E-05	0.000546067
L-Valine	0.787206983	18.17950115	3.55E-05	0.00060476
L-Isoleucine	0.79431364	16.5102761	3.63E-05	0.00060476
L-Homocysteine	-2.331632788	19.23053362	3.89E-05	0.000611821
Inosine_5prime-monophosphate	1.157600877	15.51293914	4.43E-05	0.000659335
D-Glucose	1.418283415	14.89091169	5.85E-05	0.000800649
Urea	1.598661908	18.09257677	6.27E-05	0.000800649
L-Glutamyl-L-glutamine	-1.884904713	27.11648733	6.07E-05	0.000800649
5prime-Deoxy-5prime-(methylthio)adenosine	0.732141245	12.14648557	6.81E-05	0.000800649
(5Z,8Z,11Z,14Z)-Icosatetra-5,8,11,14-enoic_acid	1.031702338	12.83350372	6.63E-05	0.000800649
L-Rhamnose	0.805086123	15.91103464	7.07E-05	0.000800649
S-Adenosyl_methionine	-0.993747197	23.74037586	9.39E-05	0.001021811
L-Threonic_acid	0.684850562	16.7441406	0.000100839	0.001056943
Xanthine	-0.590421827	24.31018454	0.000111038	0.001122275
Glycerol	0.74255619	19.06670092	0.000130275	0.001228923
Uracil	-0.903421442	21.18827062	0.000127396	0.001228923
L-Serine	0.579756565	20.90098081	0.000144906	0.001281509
L-Phenylalanine	1.142606217	16.6882559	0.000143034	0.001281509
Riboflavin	-1.160626938	20.07087316	0.000183039	0.001569698
Erythritol	0.69635314	13.02246792	0.000213423	0.001776433
Orthophosphate	0.611876768	20.97105837	0.000287398	0.002323819

L-Dehydroascorbic_acid	0.691235622	21.84685323	0.000323978	0.002522096
alpha-Ketoglutaric_acid	1.782703728	12.7661811	0.000331765	0.002522096
Succinic_acid	0.742693312	17.42949611	0.000338656	0.002522096
L-Methionine	0.908894628	16.36105358	0.000407954	0.002960279
1-Methyl-4-Imidazoleacetic_acid	-0.837075378	21.80343026	0.000443631	0.003119355
Dopamine	-1.284697775	21.78807503	0.000462943	0.003119355
D-Mannose_|_D-Tagatose_|_D-Galactose_|_myo-Inositol_|_allo-Inositol_|_alpha-D-Talose_|_D-chiro-Inositol	-1.039213853	25.74456344	0.000456768	0.003119355
Choline	-0.431043703	26.90171757	0.000505721	0.00332835
L-Malic_acid	0.694670848	17.42147725	0.00060495	0.003890931
alpha-D-Glucose_1-phosphate	0.608475547	16.33371138	0.000649924	0.004087301
Acetylcholine	-0.927272907	23.07065289	0.000673763	0.004145105
Guanidineacetic_acid	0.820712568	20.09857657	0.000800676	0.004799821
Cholesterol	1.26134407	19.0671946	0.000814104	0.004799821
gamma-Glutamyl-tyrosine	-1.785159912	19.52425254	0.000842754	0.004867336
L-Phenylalanyl-L-glutamic_acid	0.897985638	18.32305035	0.000890862	0.004972086
L-Tryptophan	1.611387398	14.88326519	0.00089603	0.004972086
L-Glutamyl-L-Serine_|_L-Aspartyl-L-threonine_|_L-Seryl-L-glutamic_acid_|_L-Threonyl-L-aspartic_acid	-1.150295438	19.73175287	0.000937591	0.005102657
Sucrose	6.158042428	13.3923006	0.001012537	0.005406564
3-Methoxytyramine	-1.329118853	19.23131033	0.001059866	0.005554481
Hydroxymethylphosphonic_acid	-0.787341612	23.67877477	0.001146676	0.005900169
Cysteinylglycine	-4.027560695	21.77167408	0.001183926	0.005983054
L-Cystine	0.873750312	11.92833169	0.00122662	0.00600919
L-Lysine	-0.351196902	24.20427702	0.001231565	0.00600919
Xylitol	0.808853428	14.89013391	0.001398548	0.006708289
L-Valylglycine	0.679369707	18.35627748	0.001506708	0.00706882
myo-Inositol_2-phosphate	0.595473178	12.66808989	0.001523668	0.00706882
Quinic_acid	0.855868818	11.41828108	0.001572353	0.007144912
Pantothenic_acid	0.684616238	13.36373728	0.001590564	0.007144912
gamma-Glutamyl-leucine	-0.625316557	20.67488703	0.001683805	0.007445575
L-Homoserine	0.68975963	13.17477756	0.002011208	0.008756489
L-Tryptophyl-L-glutamic_acid	1.066921912	17.06268455	0.002429858	0.010418938
O-Acetyl-L-homoserine	-0.757940773	25.05720935	0.00256228	0.010822766
2-Hydroxypyridine	0.676439085	18.51302151	0.002669588	0.011110195
L-Tyrosylglycine	0.668551912	17.22759761	0.002757835	0.01131112
Cytidine	-0.498261918	24.93982939	0.002828586	0.011435569
3-Ureidopropanoic_acid	-0.797498453	16.98390769	0.003066315	0.012222074
L-Tyrosyl-L-glutamine	0.694020544	16.72809727	0.003170807	0.012463033
Pyroglutamic_acid	0.419081783	23.17766854	0.00350977	0.013606368
Homoserine_lactone_|_1-	0.74211736	23.15446502	0.00381263	0.014580734

Aminocyclopropanecarboxylic_acid				
sn-Glycerol_3-phosphate	0.543551875	19.7500315	0.004085449	0.01541576
L-Alanine	0.468433877	21.44703378	0.004564538	0.016996897
Thiaminpyrophosphate	0.971660353	17.80216496	0.004646168	0.017076178
L-Tyrosine	1.004840045	18.15237569	0.004949104	0.017956364
D-Gluconic_acid_|_D-Galactonic_acid	-0.57716358	21.82861582	0.005566274	0.019939945
Serotonin	-0.856307127	19.53843285	0.006295366	0.022269858
5-Hydroxy-D,L-lysine	-0.540744435	16.76212247	0.006548181	0.022737002
L-Argininosuccinic_acid	0.488731305	20.13284785	0.006588107	0.022737002
L-Carnosine_|_L-Histidylalanine_|_L-Alanyl-L-histidine	-0.510078428	23.84237731	0.006742973	0.022991102
Uric_acid	-0.871941502	20.41143074	0.007390704	0.024899634
L-Prolyl-L-threonine	0.456035648	17.39143136	0.007544332	0.024909985
Caffeic_acid	0.846467135	11.9550661	0.007569819	0.024909985
L-Glutamine	0.414533575	23.02109404	0.007928206	0.025789453
gamma-Glutamyl-tryptophan	-1.177923893	18.30634829	0.008127535	0.026137415
S-(2-Carboxyethyl)cysteine	-0.91157588	19.47881657	0.008900643	0.027987579
Cytidine_monophosphate	0.4489582	24.21657427	0.008898191	0.027987579
Uridine	-0.649567915	23.35256602	0.009635198	0.029964406
L-Valyl-L-alanine	1.01063017	18.6355412	0.01029879	0.031679973
Spermidine	-0.449078377	22.56408946	0.010430484	0.031740074
D-Fructose_1-phosphate_|_D-Fructose-6-phosphate_|_myo-Inositol_2-phosphate_|_alpha-D-Mannose_1-phosphate_|_alpha-D-Glucose_1-phosphate_|_alpha-D-Glucose_6-phosphate_|_alpha-D-Galactose_1-phosphate	0.558820403	22.05377729	0.01091753	0.032522746
Spermine	-1.143593858	20.60944719	0.010896321	0.032522746
Pyruvic_acid	0.570419873	16.74637866	0.011257659	0.033186641
(3-Carboxypropyl)trimethylammonium	-0.226471368	25.23419337	0.012109628	0.035330153
Urocanic_acid	1.356715892	20.98518796	0.013189	0.038086602
Glyceraldehyde_3-phosphate	1.960244427	19.69145219	0.014475453	0.041379325
Rutin	1.788608378	11.19429253	0.015037426	0.042555916
Guanosine	-0.55096833	26.26155349	0.015475131	0.04336101
Stearic_acid_(FA_18:0)	0.41242329	17.34639851	0.016057562	0.044469661
L-Lysyl-L-glutamic_acid	-0.464667625	17.41251084	0.016185071	0.044469661
Xanthosine	-0.864172112	18.29395621	0.01648527	0.044858955
Palmitic_acid_(FA_16:0)	0.457120538	17.56149856	0.01710802	0.046110188
N-Acetyl-D-glucosamine_|_N-Acetyl-D-mannosamine_|_N-Acetyl-D-galactosamine	-0.412035985	18.02620754	0.018034925	0.048149846
Cytidine_5prime-diphosphoethanolamine	-0.248695498	23.06352172	0.018211465	0.048166773

L-Phenylalanyl-L-threonine	0.549963989	16.79472457	0.018417025	0.048259427
1-Methylnicotinamide	-0.389940475	19.48795031	0.019070126	0.049512345
L-Tyrosyl-L-Threonine	0.78708422	18.58742469	0.019937919	0.051294828
alpha-L-Fucose_1-phosphate	0.43322505	18.82915783	0.021782108	0.055194714
L-Tyrosyl-L-glutamic_acid	0.325103968	17.19357652	0.021843844	0.055194714
Nicotinic_acid	0.758012388	20.2361408	0.022382698	0.056055784
N-epsilon-Acetyl-L-lysine	-0.432392877	20.49597802	0.022892564	0.056829787
Inosine	-0.317629925	28.07012108	0.024738424	0.060878034
L-Isoleucyl-L-glutamine	0.408583998	18.67223619	0.026528608	0.064720656
Cytosine	-0.379539169	18.84250837	0.027579068	0.066334106
S-Adenosyl-L-homocysteine	0.791297963	21.7158033	0.027720531	0.066334106
O-Phospho-L-serine	-0.377281948	21.56297239	0.02789314	0.066334106
L-Ornithine	0.716137403	19.14741915	0.028297154	0.066639605
(2S)-2-amino-3-(1-Methyl-1H-imidazol-5-yl)propanoic_acid	-0.435924287	20.76259687	0.028492552	0.066639605
Pyridoxal-5prime-monophosphate	0.575858427	19.11444236	0.02931851	0.068009331
Suberic_acid	0.739782503	16.71331223	0.029887359	0.068765225
Glycyl-L-phenylalanine	-0.374836698	18.53844512	0.030537511	0.069694482
Cystathionine	0.619857418	22.28752207	0.033281649	0.075349652
Adenine	-0.224482767	25.29713844	0.037077221	0.083276616
N-epsilon,N-epsilon,N-epsilon-Trimethyllysine	-0.210268312	24.21061457	0.049981248	0.111375536
L-Prolylglycine	0.36533213	18.89061966	0.053364919	0.117825334
Cytidine_diphosphate	-0.958696578	18.33000485	0.053708368	0.117825334
5-(2-Hydroxyethyl)-4-methylthiazole	-0.309122134	16.61242141	0.054746399	0.1191787
Betaine	-0.426471245	24.25424968	0.055950079	0.120869255
3-Hydroxy-3-methylglutaric_acid	-0.464477942	18.44493994	0.058394456	0.125194174
Azelaic_acid	0.757162352	18.9047093	0.059179291	0.125922852
Sorbitol	3.448546223	13.67641652	0.060048797	0.126819475
Benzoic_acid	0.591421583	15.037138	0.060626132	0.126986652
4-Guanidinobutyric_acid	0.443544658	20.49088725	0.061025387	0.126986652
D-Maltose_|_D-Trehalose	2.790938455	19.70644242	0.064000538	0.13220549
L-Lysyl-L-serine_|_L-Seryl-L-lysine	0.370505672	16.91285605	0.066391527	0.13615074
D-Ribose_5-phosphate	0.414422035	13.65919217	0.0674557	0.136504507
L-Threonyl-L-valine	0.775123767	17.77678373	0.068171048	0.136504507
4-Aminobutanoic_acid	0.24786664	22.31316696	0.068439641	0.136504507
(S)-Lactate	0.228093765	23.79639063	0.068493428	0.136504507
Uridine_5-diphosphoglucose_|_Uridine_5prime-diphosphogalactose	-0.239379808	24.9095793	0.069478064	0.137498546
L-Glutamyl-L-threonine	0.302300685	18.44118959	0.070974493	0.139484593
2-aminoadipate	0.800863145	15.31156504	0.079029569	0.154243917
L-Seryl-L-leucine	0.507236279	17.31328703	0.080826953	0.156671423
(S)-Piperidine-2-carboxylic_acid	-0.454693462	21.40476645	0.081496688	0.156894984
L-Kynurenine	0.621790223	18.69611315	0.08235143	0.156991328

N-Acetyl-L-methionine	-0.720368362	18.78402303	0.08307763	0.156991328
Deoxyguanosine	-0.357037316	16.85451565	0.083210951	0.156991328
L-Methionyl-L-glutamic_acid	0.274872002	16.74667274	0.0858921	0.160976585
L-Alanyl-L-leucine	0.490342713	17.15252343	0.08684978	0.161700577
D-Ribose_1-phosphate_|_D-Ribulose_5-phosphate_|_alpha-D-Xylose_1-phosphate	0.355405053	21.99715189	0.093031023	0.17207699
Fumaric_acid	0.370239998	17.56798248	0.095677251	0.175822481
Uridine_diphosphate	-0.205964832	22.19805715	0.097170764	0.177415008
Panose_|_Maltotriose_|_D-Melezitose	-0.39428218	18.18038869	0.098059572	0.177890122
Taurine	0.251256092	21.62100626	0.101238925	0.182487998
Tetronic_acid	-0.281660618	20.82036732	0.109560352	0.196237846
Cytidine_3prime-phosphate	-0.2037424	20.86691334	0.110263807	0.196255706
L-Cycloserine	-0.21864199	18.90000514	0.116639615	0.206306319
L-Leucyl-L-glutamic_acid	0.222366043	19.08364456	0.123818511	0.217643718
Saccharopine	-0.426239362	21.28423647	0.132098064	0.229672035
L-Cysteine	-0.38604679	16.9879281	0.1322846	0.229672035
Allantoin	-0.25628377	18.58204082	0.140543664	0.242523517
L-Prolyl-L-serine	0.486899265	17.88428183	0.143067518	0.24538247
Thiamine	-0.234791328	18.44618401	0.144611556	0.245483696
2-Methylcitric_acid	-0.305009885	16.9187475	0.145075223	0.245483696
Mannitol_|_Sorbitol_|_Galactitol	2.002549017	19.77159292	0.145728837	0.245483696
6-Phosphogluconic_acid	0.347349115	19.85087911	0.150129365	0.251400061
O-Acetyl-L-carnitine	-0.141578918	28.24508256	0.155731921	0.259247846
L-Seryl-L-aspartic_acid	0.271594752	16.73033434	0.158157217	0.261745569
Adenosine_5prime-diphosphoglucose	-0.277176755	17.20260742	0.166179913	0.273423927
L-Isoleucyl-L-arginine	-0.446784308	18.05843498	0.169988453	0.278073596
L-Lysylglycine	0.257015302	17.3295692	0.175414066	0.285299889
Glycyl-L-valine	-0.25532188	17.05209613	0.178605212	0.288830143
Thymidine	-0.272594763	17.30096348	0.180317258	0.289941955
1-Methylhistamine_|_3-Methylhistamine	-0.341831945	18.61035738	0.181401284	0.290037081
L-Alanyl-L-threonine_|_L-Threonyl-L-alanine	-0.216994242	19.7337492	0.184213091	0.292878117
Glycyl-L-tyrosine	-0.264798088	19.1262099	0.185869669	0.293860984
Glycerol-3-phosphate_|_beta-Glycerophosphate	-0.121939528	24.44080082	0.199042619	0.312939229
5-Aminolevulinic_acid_|_cis-4-Hydroxy-D-proline_|_trans-3-Hydroxy-L-proline_|_trans-4-Hydroxy-L-proline	-0.273002058	20.58611923	0.207912842	0.325079194
Nonanoic_acid	0.321176343	11.63150154	0.213054657	0.331288285
Oxalate	0.221267312	16.88292015	0.237289785	0.366956334
2-Aminoethyl-dihydrogen_phosphate	0.388049553	25.44811468	0.243597951	0.374664239

Thymidine_5prime-phosphate	0.132874713	17.61013028	0.250409932	0.383059517
N-Acetylneuraminic_acid	-0.127697747	24.03802202	0.252638078	0.384390193
Deoxyuridine	-0.19656435	17.19592557	0.256509658	0.38819376
L-Aspartylglycine	0.254090233	18.37873498	0.261684722	0.393919023
N,N-Dimethylglycine_|_3-Aminoisobutyric_acid_|_(R)-2-Aminobutanoic_acid	0.240180163	27.43599785	0.267219642	0.398016625
N-Acetyl-L-cysteine	-0.554378058	17.32169002	0.267209223	0.398016625
Stachyose_|_Maltotetraose	-0.306227958	17.26257436	0.27412469	0.406163807
Adenosine_3prime,5prime-cyclic_phosphate	-0.5090874	19.6299343	0.279465236	0.410763816
Creatine	-0.107361217	32.08303922	0.280132214	0.410763816
Glycine	0.157526417	21.21737034	0.286478802	0.417904644
Hypoxanthine	0.371336537	25.77080639	0.2935553	0.426031538
L-Valyl-L-asparagine	0.246238065	16.7975536	0.298468244	0.430951597
L-Carnitine	-0.114893328	28.46279473	0.301372709	0.432936429
L-Leucylglycine	0.559558567	19.25290275	0.314710374	0.449813312
Lignoceric_acid_(FA_24:0)	0.287638793	10.76693625	0.31650514	0.450105299
2-[[Amino(imino)methyl]amino]ethane-1-sulfonic_acid	0.164176855	18.62501903	0.327624525	0.46167277
L-Seryl-L-isoleucine	0.209295507	18.27821313	0.328891416	0.46167277
[(3aS,4S,5S,6E,10E,11aR)-6-formyl-5-methoxy-10-methyl-3-methylidene-2-oxo-3a,4,5,8,9,11a-hexahydrocyclodeca[b]furan-4-yl]_2-methylpropanoate	0.197472753	17.40360234	0.330114489	0.46167277
L-Phenylalanyl-L-glutamine	0.220418978	16.87019526	0.331164566	0.46167277
L-Aspartic_acid_|_Iminodiacetic_acid	-0.119727602	27.93348998	0.33693424	0.467413676
L-Alanyl-L-isoleucine	0.182288852	17.15324193	0.34990719	0.483042609
beta-Alanine	0.217722758	14.10682074	0.367332595	0.504636527
Phosphocreatine	0.140266642	23.77139433	0.376821285	0.511049118
Hexacosanoic_acid	0.175616915	12.9437497	0.377347303	0.511049118
Pyridoxal	0.347706888	18.40045789	0.378158032	0.511049118
Nobiletin	0.14347851	19.22033348	0.379223727	0.511049118
2prime-Deoxycytidine-5prime-monophosphate	0.145182583	18.43209072	0.392123443	0.525928599
Ascorbic_acid	-0.099171523	27.94229016	0.396346491	0.529085174
L-Glutamyl-L-alanine_|_L-Alanyl-L-glutamic_acid	0.287383178	19.95252448	0.406885184	0.540603319
Glycyl-L-isoleucine	0.223383035	16.6444878	0.416671462	0.551018803
L-Alanyl-L-valine	-0.31406529	19.26137989	0.422242005	0.555788313
Maleamic_acid	-0.06879747	22.60856983	0.427301208	0.559525313
p-Hydroxyphenyllactic_acid	0.27287364	20.56651076	0.42903531	0.559525313
Sedoheptulose-7-phosphate_|_(D-	0.111447815	19.1681878	0.444219317	0.574036834

	Glycero-alpha-D-Manno-Heptopyranosyl)-Dihydrogenphosphate			
L-Alanyl-L-glutamine	-0.207188794	17.60715722	0.44391952	0.574036834
Allantoic_acid	0.24635466	13.07021586	0.447274272	0.575357359
Sorbitol-6-phosphate	0.295087782	17.91562592	0.4600889	0.589163614
L-Isoleucyl-L-serine	0.200925562	18.3470923	0.470028255	0.599180163
myo-Inositol	0.182975533	20.91555376	0.486289259	0.617129419
Histamine	0.146385397	16.34509258	0.49194699	0.621522313
Anserine	-0.181563823	23.59572665	0.495673649	0.6234473
5,6-Dihydrothymine	-0.224879488	17.26050037	0.499171966	0.62506932
Guanosine_diphosphate	0.21777941	22.69904781	0.510691852	0.636677507
L-Alanyl-L-alanine_|_Gly-gamma-aminobutyric_acid	-0.079968801	20.24646151	0.517940688	0.642882521
L-Valyl-L-glutamine	0.087451776	18.52988981	0.525407519	0.648619195
Benzophenone	0.097047613	17.61253914	0.528296157	0.648619195
L-Alanyl-L-tyrosine_|_L-Phenylalanyl-L-serine	0.224084115	17.78636549	0.529438283	0.648619195
N-Acetyl-D-phenylalanine	0.28269008	16.8647516	0.538934165	0.656956186
L-Isoleucyl-L-alanine	-0.266186107	19.33500414	0.5446054	0.656956186
Guanine	-0.08556109	18.02553266	0.546826021	0.656956186
L-Seryl-L-valine	0.192702903	19.14474587	0.546870536	0.656956186
L-beta-Imidazolelactic_acid	0.209643963	19.10859778	0.547850388	0.656956186
Geraniol_|_Fenchyl_alcohol	0.11687557	21.19447782	0.562977834	0.672247793
Creatinine	0.047433208	24.43087274	0.576468403	0.685464529
N-Acetyltyrosine	-0.15975452	16.22813998	0.606162019	0.7177567
Ergothioneine	0.072955258	22.09382041	0.621211881	0.732279232
L-Isoleucyl-L-aspartic_acid	-0.102294241	17.40200217	0.628338401	0.732279232
L-Valyl-L-histidine	0.132541948	16.49600753	0.628269178	0.732279232
Pyridoxamine-5prime-phosphate	0.110000037	20.01350748	0.629110288	0.732279232
Tangeretin	0.080246118	19.12312298	0.631364426	0.732279232
Nicotinamide	0.05197329	28.86532817	0.637856422	0.736789255
L-Histidine	-0.063566577	24.42788823	0.654229165	0.752629487
L-Valyl-L-lysine	-0.036907908	21.86901084	0.673616257	0.771795145
L-Leucyl-L-alanine	0.111360405	16.93668639	0.678295359	0.774022527
L-Isoleucyl-L-threonine	0.056888057	17.42436146	0.704701429	0.792312209
L-Isoleucyl-L-isoleucine	-0.102214095	16.71705052	0.707152581	0.792312209
L-Glutamyl-L-valine_|_L-Leucyl-L-aspartic_acid	-0.060355131	17.8925777	0.708309945	0.792312209
beta-Nicotinamide-adenine_dinucleotide	0.100652088	17.10216725	0.709180583	0.792312209
Deoxycytidine	0.048201747	19.194098	0.711084108	0.792312209
L-Aspartyl-L-glutamine_|_L-Asparaginyl-L-glutamic_acid	-0.072020438	19.28502195	0.711121205	0.792312209
5-Hydroxyindole-3-acetic_acid	0.070323523	19.53104177	0.72124195	0.800437145

L-Isoleucyl-L-lysine	0.068316414	16.62637454	0.727835673	0.803147187
L-Valyl-L-serine	-0.104640942	18.41354809	0.729359813	0.803147187
L-Prolyl-L-glutamic_acid	0.042081428	19.8964025	0.752536558	0.825456767
L-Leucyl-L-threonine	0.10189654	17.18343701	0.758964084	0.829292802
L-Arginine	-0.045078635	26.08503146	0.779394761	0.848341221
trans-4-Hydroxy-L-proline	0.094319125	13.91254925	0.788708359	0.855189523
D-Saccharic_acid	0.064947098	23.28066932	0.806169823	0.870786489
D-Panthenol	-0.233323028	19.27129437	0.826433082	0.889279704
L-Glutamyl-L-aspartic_acid	0.032933153	18.30391916	0.836559484	0.896766416
4-Pregnene-11-beta-17-alpha-diol-3-20-dione_|_(9xi,11beta,14xi)-11,21-Dihydroxypregn-4-ene-3,20-dione	-0.041279007	16.93100044	0.864817922	0.923560271
L-Citrulline	0.024327373	21.06589883	0.869914755	0.925510811
Phosphoglycolic_acid	0.028960261	16.66548934	0.879497897	0.931289502
Hypotaurine	-0.031148133	20.28218628	0.881927868	0.931289502
2-Deoxyadenosine_5-phosphate	0.02375839	18.07875758	0.889021997	0.935290799
L-Isoleucyl-L-glutamic_acid	-0.014868483	17.76992983	0.901587172	0.944996925
Nerolidol	0.017408927	18.73242769	0.907819996	0.948018667
L-Valyl-L-aspartic_acid	-0.016311975	18.73588535	0.930616698	0.968251933
D-Galactose_|_myo-Inositol_|_allo-Inositol_|_muco-Inositol_|_alpha-D-Talose_|_D-chiro-Inositol	-0.015170368	24.65683218	0.935056563	0.969307719
5-Aminoimidazole-4-carboxamide-1-beta-D-ribofuranosyl	0.017776888	18.38152973	0.943904694	0.972917594
N-Methylnicotinic_acid	-0.016113135	22.60709829	0.94544463	0.972917594
L-Threonyl-L-isoleucine	0.019577629	16.82985874	0.948852494	0.972917594
D-2-Aminoadipic_acid_|_N-Methyl-L-glutamic_acid	0.018391918	24.25602673	0.960639228	0.981447298
L-Asparagine	-7.25E-16	20.26068609	1	1
N-Acetyl-L-aspartic_acid	0.001246033	29.29685449	0.988965369	1
2-Aminophenol	-6.01E-18	17.31210201	1	1
L-Valyl-L-glutamic_acid	-0.001462613	19.15888345	0.99457281	1
L-Phenylalanyl-L-valine	-4.85E-15	16.96386906	1	1
D-Trehalose_|_D-Gentiobiose	-2.67E-15	19.29362673	1	1

9. Acknowledgements

I want to express my strongest gratitude towards those people, who stood beside me along this way. Guided, supported and cheered for me when I needed it most.

Especially, I want to thank my supervisors, Prof. Dr. Michael Müller and Prof. Dr. Revaz Solomonia, who entrusted me with this hard task and helped me to overcome it together. I had a lot to learn from them and feel extremely lucky to have them as a mentor not only in science, but in life as well. They have done for me more than just being thesis supervisors. Also I would like to thank Prof. Dr. Peter Rehling, for sharing his time, resources, views and experience with us.

I cannot go without mentioning our technician, Belinda Kempkes for her assistance at the University of Göttingen. Her tireless effort and dedication made each experiment run smooth and safe.

I want to thank my colleague, Dr. Lia Tsverava at Ilia State University for sharing her experience and physically helping me with many laboratory associated works.

I want to mention all the efforts spent by our program coordinators, Aleksandra Bovt and Vakhtang Pataridze, who helped us to deal with excruciating bureaucracy and paperwork.

Special thanks to Shota Rustaveli National Scientific Foundation of Georgia and to the Volkswagen Foundation for supporting the Lehmann-Haupt International Doctoral Program and its participants.

10. CV

Name: Gocha Golubiani
Address: 9 dzma kherkheulidze 4/6 Rustavi, Georgia. 3700
E-mail: gocha.golubiani.1@iliauni.edu.ge

Education_____

10/09/2011- 20/07/2015:   Ilia State University Tbilisi. Faculty of Natural Sciences and Engineering.
                          Degree of Bachelor in Natural Sciences in Biology

01/10/2015 – 12/07/2017: Ilia State University Tbilisi. Faculty of Natural Sciences and Engineering.
                          Degree of Master of Molecular Biosciences. Experimental Diploma:
                          "Study of Cognin interactome in chick brain"

10/05/2018 – till present: Ph.D. student at Ilia state university Tbilisi – Molecular Biosciences and
                          Georg-August University of Göttingen: - Molecular Medicine.

Work Experience_____

09/11/2016- 1/05/2018:   Ilia State University, Institute of Chemical Biology, Laboratory assistance

01/08/2015 - 01/07.2016: Ilia State University, laboratory of Molecular Genetics, Laboratory
                          assistance

Scientific publications and activities _____

Gocha Golubiani, Laura van Agen, Lia Tsverava, L.; Revaz Solomonia, Michael Müller. Mitochondrial
Proteome Changes in Rett Syndrome. *Biology.* 2023, 12(7), 956.

Gocha Golubiani, Vincenzo Lagani, Revaz Solomonia, Michael Müller. (2021) Metabolomic
Fingerprint of *Mecp2*-Deficient Mouse Cortex: Evidence for a Pronounced Multi-Facetted Metabolic
Component in Rett Syndrome. *Cells*. 2021 Sep 21;10(9):2494.

Karolina Can, Christiane Menzfeld, Lena Rinne, Peter Rehling, Sebastian Kügler, Gocha Golubiani,
Jan Dudek, Michael Müller. (2019). Neuronal Redox-Imbalance in Rett Syndrome Affects
Mitochondria as Well as Cytosol, and Is Accompanied by Intensified Mitochondrial O_2 Consumption
and ROS Release. *Front Physiol.* 2019 Apr 30;10:479.

Conference: International virtual meeting NeuroFrance2021. 19-21 May. Poster presentation:
Gocha Golubiani, Revaz Solomonia, Michael Müller. (2021) Rett syndrome mouse model
mitochondrial proteomic comparative analysis.